



*Trademark of General Electric Company. Image Credit: Humza Deas

A comparative analysis of the vortex model and the blade element momentum (BEM) model for wind turbine design

Rohit Phadke

A comparative analysis of the vortex model and the blade element momentum (BEM) model for wind turbine design

by

Rohit Phadke

to obtain the degree of Master of Science
at the Delft University of Technology,
to be defended publicly on Tuesday October 29, 2019 at 11:00 AM.

Student number: 4712080
Project duration: January 15, 2019 – October 15, 2019
Thesis committee: Prof. dr. ir. CJ. Simao Ferreira, TU Delft, supervisor
Ir. W. A. Timmer, TU Delft, committee
Dr. Ir. A. H. van Zuijlen, TU Delft, committee
Dr. Ir. K. Boorsma, TNO, company supervisor

An electronic version of this thesis is available at <http://repository.tudelft.nl/>.



Preface

"Renewable energy will help end our dependence on the fossil fuels and fight a serious threat that climate changes pose to living beings."

The battle against climate change begins with maximizing the share of renewable energy in the total energy mix, such that the cost of energy will be minimum. Wind energy will play a vital role in maximizing the share of renewables in the total energy mix. In order to reach the LCOE projection of 0.09€/KWh [18], a decrease in the material cost involved in the manufacturing of blades should play an important role.

The drive to make wind energy cheaper pushed me to dive deeper into the subject of wind turbine aerodynamics and thus, I chose to work on this thesis project. The research will help the wind energy community to make the wind turbine design process robust, safe and cost-optimal. The thesis focuses on improving the general practice (based on the IEC standard) for wind turbine blade design by incorporating a more advanced aerodynamic model, called as the vortex wake model. The thesis report begins with introducing both of the aerodynamic models, followed by a comparative analysis of the traditional blade element momentum theory model (BEM) with the vortex wake model. The report includes a number of interesting observations and shortcomings involved in the state-of-art wind turbine design procedure.

In truth, I could not have achieved my current level of success without a strong support group. Firstly, I would like to thank my family, this would have not been possible without your support. The credit of success of this thesis goes to my supervisors, Koen and Carlos. Their wisdom, depth of knowledge and valuable remarks guided this thesis to the right path. Special gratitude to Mr. Koert Lindenburg, the chief developer of Focus6 software for providing me with valuable insights and suggestions along the course of the thesis. I would also like to thank Wouter Engels for resolving the technical issues related to FOCUS6 software. A special thanks to my colleagues at ECN who never made me feel away from the university.

A year at remotely located Alkmaar would never have been enjoyable without the company of my friends. I fall short of words to show my appreciation to my wall, Shreeya, for always being there throughout the journey. Her support and encouragement helped me to achieve this accomplishment. A special thanks to Kunal, for having demanding debates, political discussions and fact checks. A final thanks to Stephano, Marco, and Bose for the amazing dinners and parties.

*Rohit Phadke
Delft, October 2019*

Summary

A wind turbine is a complex machine that includes a number of mechanical and electrical components. The rotor is one of the most important components which is responsible for energy extraction. With the quest to extract maximum available energy, the size, cost and effort involved in the manufacturing of the rotor is increasing exponentially. Such exponential growth involves greater stakes and bigger risks. Ultimately, this calls for a safe, robust and cost-optimal design.

The current state of the art design process involves the implementation of the blade element momentum (BEM) model rather than a more accurate vortex wake model for aerodynamic load calculations. The popularity of the BEM model lies in the attractive computation time of few seconds involved in this method while the later method involves computation time of several days. Essentially, the development of an aerodynamic model with high accuracy and a considerable aerodynamic effort is vital.

The project begins with understanding both of the aerodynamic models and tools. Focus6 software by WMC in coupling with AeroModule by ECN is used as an aeroelastic load calculation tool for this project. AeroModule by ECN features both of the aerodynamic load calculation models. The BEM model is comparatively easier to understand and implement compared to the vortex wake model. In this thesis project, AVATAR 10 MW turbine is operated as a test turbine.

As of now, results obtained from both of the models were tested, analyzed and validated with the experimental results for certain specific load situations. However, the wind turbine design procedure is based on the IEC standard and thus, it is very important to compare the results obtained from both of the models as per the guidelines of the IEC standard. As part of the project, few critical IEC design load cases are selected on the basis of the violation of the assumptions involved in the BEM model. The selected load cases involve various inflow conditions, which are- axial inflow with a gust, yawed inflow and turbulent inflow.

All of the selected load cases are evaluated next. The evaluation process starts with simulating the load cases with both of the models in the Focus6 environment. Later, the results obtained from both of the models were analysed to understand the cause behind the variations in the results. Several parameter variations, for example- yaw misalignment angle, the magnitude of induction, etc. are made such that the causes of the variations in the results obtained from both of the models are enlightened.

The primary reason for the variations in the results is attributed to the violation of the assumptions involved in the BEM model. However, further analyses of the results proved that the root cause for the variations in the results obtained from both of them come from the dissimilarities in the prediction of the induced velocities (axial and tangential).

The important result for this wind turbine model can be regarded as the higher fatigue load prediction by the vortex model wake than that by the BEM model in the case of a misaligned inflow condition. The higher fatigue load prediction by the vortex wake model can be attributed to a larger variation of the axially induced velocity by the vortex wake model.

The load cases with a higher magnitude of the induced velocity and with a significant difference in the induced velocity calculation by both of the models tend to show variations in the load calculations. Such load cases could be simulated with the vortex wake model. Therefore, a more robust wind turbine design and certification procedure with a reasonable computational effort could be achieved.

Contents

Summary	v
List of Figures	ix
List of Tables	xi
1 Introduction	1
1.1 Overview	1
1.2 Background information	2
1.3 Theory	2
1.3.1 Blade Element Momentum (BEM) model	2
1.3.2 Vortex wake models	5
1.4 Research questions and objectives	9
1.4.1 Research questions	9
1.4.2 Research objectives	9
1.5 Research methodology	9
1.6 Report outline	10
2 Aerodynamic models and the test turbine	11
2.1 Aerodynamic load calculation models	11
2.1.1 FOCUS6	11
2.1.2 ECN Aeromodule	12
2.1.3 Comparison of the BEM and vortex wake approach on the basis of different parameters and results	14
2.2 Test Wind turbine	17
2.2.1 AVATAR Project	17
2.2.2 The AVATAR Wind turbine	17
3 IEC Design Load Cases	19
3.1 Sources of unsteady loading	19
3.2 IEC Design Load Case overview	20
3.3 DLC selection	23
3.3.1 DLC Pre-selection	23
3.3.2 DLC final selection	24
4 Results and discussions	27
4.1 DLC 2.3	27
4.1.1 Load case description	27
4.1.2 Results and observations	27
4.1.3 Analysis	36
4.2 DLC 3.3	38
4.2.1 Load case description	38
4.2.2 Results and observations	38
4.2.3 Comparative study	46
4.2.4 Analysis	48
4.3 DLC 1.3	50
4.3.1 Load case description	50
4.3.2 Results and observations	50
4.3.3 Analysis	56

4.4	DLC 1.2	58
4.4.1	Load case description	58
4.4.2	Results and observations.	58
4.4.3	Analysis	62
5	Conclusions and recommendations	63
5.1	Conclusions.	63
5.1.1	Concluding remarks	64
5.2	Recommendations	64
	Bibliography	65
A	Appendix- A	67
A.1	DLC 2.3	67
A.2	DLC 3.3	68
A.3	DLC 1.3	70
A.4	DLC 1.2	72
A.5	Wake reduction	73
A.5.1	Wake Reduction effect	73

List of Figures

1.1	Levelized Cost of Electricity from different Energy sources[18]	1
1.2	An actuator disk and stream tube	3
1.3	Force diagram	4
1.4	Velocity diagram	4
1.5	Replacement of a wing filament with a horseshoe vortex[3]	6
1.6	Superimposition of the finite number of horseshoe vortices along the lifting line[3]	6
1.7	Aerodynamic load calculation procedure of the vortex theory model for unsteady flow[29]	8
2.1	Radial distribution of sectional forces for axial flow conditions [5]	15
2.2	Sectional force variation with rotor azimuth for yawed flow conditions for MEXICO test[5]	15
2.3	Sectional force variation with rotor azimuth for yawed flow conditions for NASA-Ames test[5]	16
2.4	Dynamic inflow condition[5]	16
3.1	Classification of the sources of unsteady loading[19]	20
3.2	IEC Design Load Cases-1[16]	21
3.3	Design Load Cases-continued[16]	21
3.4	Design Load Cases-continued[16]	22
3.5	Axially induced velocity	24
3.6	Axial induction factor	25
4.1	Wind speed profile	28
4.2	Axially induced velocity	28
4.3	Axial induction factor	29
4.4	Angle of attack	29
4.5	Normal aerodynamic force	30
4.6	Normal aerodynamic force statistics	30
4.7	Wind speed profile	31
4.8	Axially induced velocity	31
4.9	Axial induction factor	32
4.10	Angle of attack	32
4.11	Normal aerodynamic force	33
4.12	Normal aerodynamic force statistics	33
4.13	Wind speed profile	34
4.14	Axially induced velocity	34
4.15	Axial induction factor	35
4.16	Angle of attack	35
4.17	Normal aerodynamic force	36
4.18	Normal aerodynamic force statistics	36
4.19	Radial distribution of the Normal force in the case constant wind field	37
4.20	Wind velocity profile	39
4.21	Direction change angle	39
4.22	Axially induced velocity	40
4.23	Angle of attack	40
4.24	Lift coefficient	41
4.25	Normal force	41
4.26	Comparison of the standard deviation of the normal force at different radial locations	42
4.27	Product of the lift coefficient and the square of resultant wind velocity	42
4.28	Effect of lift coefficient and resultant wind velocity on the normal force	43
4.29	Decomposition of effective wind velocity term	43

4.30	Wind velocity profile	44
4.31	Direction change angle	44
4.32	Axially induced velocity	45
4.33	Angle of attack	45
4.34	Normal force	46
4.35	Maximum extreme normal force	46
4.36	Minimum extreme normal force	47
4.37	Average normal force	47
4.38	Standard deviation	48
4.39	Wind speed profile	51
4.40	Axially induced velocity	51
4.41	Axial induction factor	52
4.42	Angle of attack	52
4.43	Normal force	53
4.44	Radial distribution of the normal force at the time which marks the maximum normal force.	53
4.45	Wind speed profile	54
4.46	Axially induced velocity	54
4.47	Axial induction factor	55
4.48	Angle of attack	55
4.49	Normal force	56
4.50	Wind speed profile	59
4.51	Axially induced velocity	59
4.52	Axial induction factor	60
4.53	Angle of attack	60
4.54	Normal force	61
4.55	Radial distribution of the normal force at the time which marks the maximum normal force	61
4.56	Flapwise equivalent moments for the time period of 100 seconds to 300 seconds	62
A.1	Axially induced velocity	67
A.2	Angle of attack	68
A.3	Comparison of the axially induced velocity for various pitch angles.	68
A.4	Comparison of the angle of attack for various pitch angles	69
A.5	Comparison of the lift coefficient for various pitch angles	69
A.6	Comparison of the normal force for various pitch angles	70
A.7	Comparison of the ratio of the standard deviation of the normal force for various pitch angles	70
A.8	Axially induced velocity in the case of a flexible rotor	71
A.9	Axial induction factor in the case of a flexible rotor	71
A.10	Normal force in the case of a flexible rotor	72
A.11	Axially induced velocity in the case of a flexible rotor	72
A.12	Axial induction factor in the case of a flexible rotor	73
A.13	Normal force in the case of a flexible rotor	73
A.14	Effect of wake reduction technique on the normal force	74

List of Tables

2.1	Comparative analysis of the BEM and the AWSM based on the aerodynamic situation	17
2.2	AVATAR Wind turbine specifications	17
3.1	Abbreviations of the terms used in the above tables[16]	22
3.2	DLC pre-selection	23
3.3	DLC selection	25
4.1	Load case specifications	27
4.2	Load case specifications	38
4.3	DLC 1.3 load case specifications	50
4.4	Normal force statistics	53
4.5	Normal force statistics	56
4.6	DLC 1.2 load case specifications	58
4.7	Normal force statistics	61

Introduction

1.1. Overview

Wind energy is a clean, green and readily available renewable energy source. Wind turbines convert the kinetic energy in the wind into mechanical power. Further, a generator can convert this power into electricity. Windmills have a long history of several centuries. Traditionally, windmills were used to draw water, grind grains, etc. Over the years, windmills evolved into modern age wind turbines which are mainly used to produce electricity. Wind energy is one of the most important sources of renewable energy in the European Union (EU). As of December 2017, the total installed capacity of wind energy in the EU is 168.7 GW. WindEurope has estimated that the EU shall produce 17.4 GW of wind energy per year from 2018 to 2022 [21]. This would lead to 14-17% of the EU's electricity demand [21].

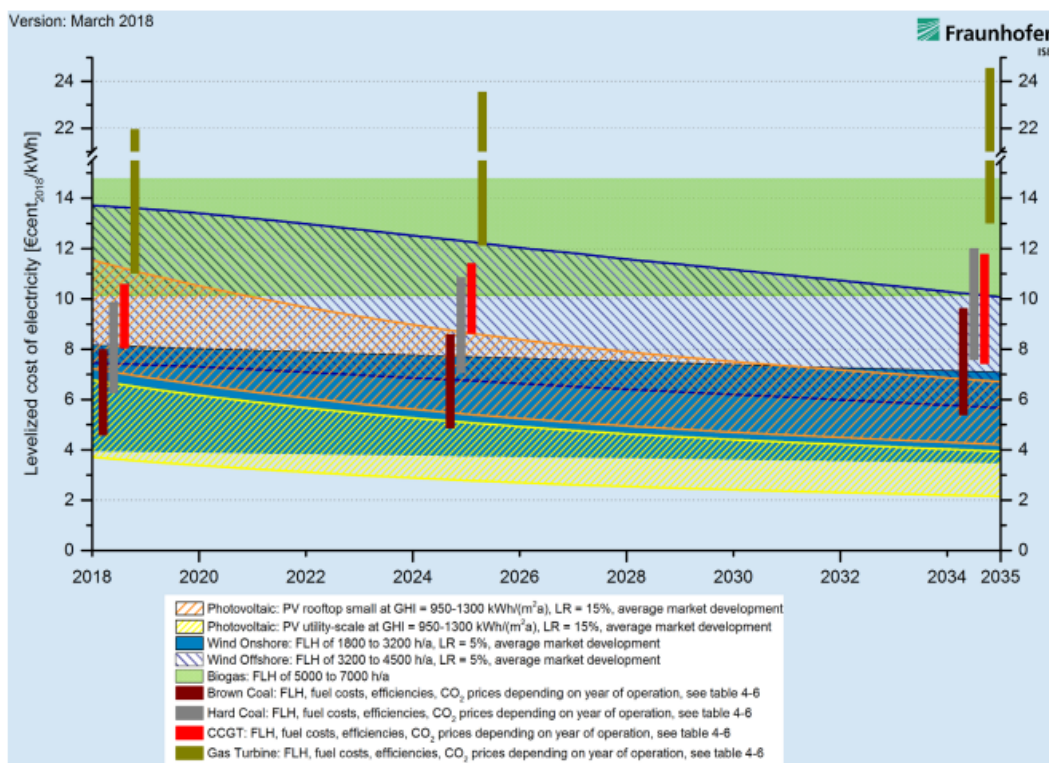


Figure 1.1: Levelized Cost of Electricity from different Energy sources[18]

The whole world is now striving towards clean, green and cheap energy. The wind energy is also clean and green energy but it is still a bit costly compared to others. As of 2018, according to Fraunhofer Institute the Levelized Cost of Electricity (LCOE) [18] for the Offshore wind energy projects was marked at Euro 0.12/KWh

and the institute has also projected the LCOE to be less than Euro 0.09/KWh by 2030. This LCOE cost of Euro 0.09/KWh can be possibly achieved by reducing manufacturing and material costs involved in the blade of a turbine. The higher material costs are possibly due to the over-designing of the blades. The reason behind the over-designing of the blades is mainly due to higher aerodynamic load prediction involved.

1.2. Background information

The Blade Element Momentum (BEM) method is the most popular method to calculate aerodynamic loads acting on a wind turbine. The BEM is used extensively by most of the wind turbine manufacturers. Although the most popular method, the BEM is not the most accurate method to carry out aerodynamic load calculations. The BEM model is mainly based on simple physics. The limitations of the BEM theory are the assumption of the radial independence of annuli and the lack of wake modeling [6]. The BEM model often fails to predict aerodynamic loads accurately in the case of complex inflow conditions, for example- yawed inflow, pitch asymmetry, turbulent inflow, etc. This inaccurate load calculation may probably predict higher loads, which may ultimately lead to the over-designing of the rotor blades.

Since the last few decades, the vortex wake method is researched extensively. The Vortex wake method is a physically more correct approach to model aerodynamic loads [6]. The research is mainly carried out to validate the results with the BEM and experimental results [5, 19]. A good agreement was observed for the results in axial flow for both of the approaches. The research proved that for complex inflow conditions, the Vortex wake method proved to be superior to the BEM. The Vortex wake method is not popular in the market due to the higher computational time involved in carrying out the load calculations [6].

1.3. Theory

The best way to start research is to understand the theories involved in the research. The research is based on aerodynamic load calculation models, which are- Blade Element Momentum (BEM) theory based model and the vortex wake theory based model. This section discusses both of the theories involved in this thesis report.

1.3.1. Blade Element Momentum (BEM) model

The wind turbine design and certification process involves numerous aerodynamic load calculation simulations. Historically, the BEM model has proved to be the most computationally efficient model to carry out those simulations. The BEM model is a couple of the momentum theory and the rotor element theory. In this section Blade Element Momentum (BEM) approach will be discussed. The discussion includes the assumptions, the theory of BEM, and the limitations involved in this approach.

Assumptions

The following are the assumptions involved in the application of BEM[22].

- No wake rotation
- In-compressible (in-viscid) flow
- Steady and axial flow
- The flow is uniform, homogeneous and non turbulent.
- Independent annular rings

The theory

The BEM theory is explained and discussed in most of the books and publications related to wind energy. In this section the theory behind the most popular approach will be discussed and is based on the Wind Energy handbook [9].

The Actuator Disk

An actuator disk is a device which helps to carry out analysis of the aerodynamic behavior of wind turbines by considering the energy extraction process. The stream-tube has a smaller and a larger cross-sectional area

upstream and downstream of the disc respectively. The stream-tube expands due to constant mass flow rate throughout the stream-tube. Therefore-

$$\rho A_{\infty} U_{\infty} = \rho A_d U_d = \rho A_w U_w \quad (1.1)$$

where,

$\rho = \text{density}$

$A = \text{cross-sectional area}$

$U = \text{flow velocity}$

The upstream conditions are represented by the symbol ' ∞ ', the conditions at the disc are represented by 'd' and the conditions downstream are represented by 'w'.

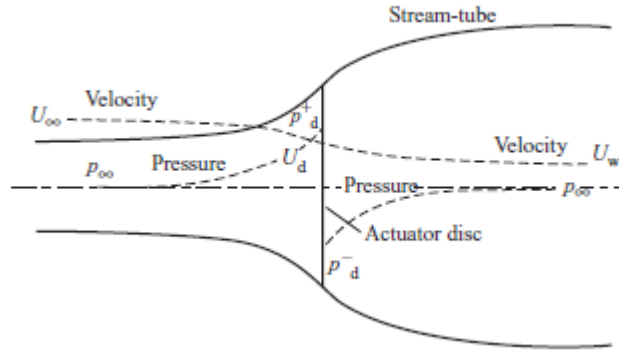


Figure 1.2: An actuator disk and stream tube

It is considered that a velocity variation induced by an actuator disk must be superimposed on the free stream velocity. The stream-wise component of this induced flow is represented by $-aU_{\infty}$, where a is called as axial flow induction factor.

$$U_d = U_{\infty}(1 - a) \quad (1.2)$$

Momentum Theory

The air that passes through the disc undergoes an overall change in velocity, $U_{\infty} - U_w$. The rate of change of momentum is given by-

$$\text{Rate of change of momentum} = (U_{\infty} - U_w)\rho A_d U_d \quad (1.3)$$

The pressure difference across the actuator disc leads to the change of momentum. Therefore,

$$(P_d^+ - P_d^-) = (U_{\infty} - U_w)\rho A_d U_{\infty}(1 - a) \quad (1.4)$$

The pressure difference ($P_d^+ - P_d^-$) can be obtained by applying Bernoulli's equation to the downstream and upstream sections of the stream-tube. After calculating the equations for upstream and downstream sections of the stream tube[9], therefore-

$$(P_D^+ - P_D^-) = \frac{1}{2}\rho(U_{\infty}^2 - U_w^2) \quad (1.5)$$

and

$$U_w = (1 - 2a)U_{\infty} \quad (1.6)$$

From the above equation, thus, $a < 0.5$.

From equation 1.4, the force (F) acting on the air is given by-

$$F = 2\rho A_d U_{\infty}^2 a(1 - a) \quad (1.7)$$

Hence, the power extracted from the air is given by-

$$\text{Power}(P) = FU_d = 2\rho A_d U_{\infty}^3 a(1 - a)^2 \quad (1.8)$$

The power coefficient (C_p) is given by

$$C_p = \frac{P}{\frac{1}{2}\rho U_\infty^3 A_d} \quad (1.9)$$

$$C_p = 4a(1-a)^2 \quad (1.10)$$

The thrust coefficient (C_T) is given by

$$C_T = \frac{P}{\frac{1}{2}\rho U_\infty^2 A_d} C_T = 4a(1-a) \quad (1.11)$$

Blade element theory

The aerodynamic forces acting on span-wise elements of radius r and length δr of the several blades of a wind turbine are accountable for the rate of change of momentum of the air passing through the annulus. The drop in pressure with the rotational velocity in the wake and the aerodynamic forces lead to the application of the force on the blade elements. Further, the aerodynamic forces acting on a blade element are calculated by the two-dimensional airfoil characteristics using an angle of attack which is derived from the incident resultant velocity in the cross-sectional plane of the element. The components of incident the resultant velocity include the wind speed, the induction factors and rotational speed of the rotor. Further, the coefficient of lift (C_l) and coefficient of drag (C_d) corresponding to the angle of attack is selected from the table of airfoil characteristics.

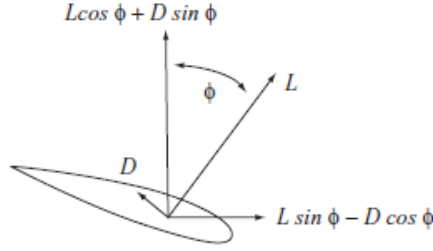


Figure 1.3: Force diagram

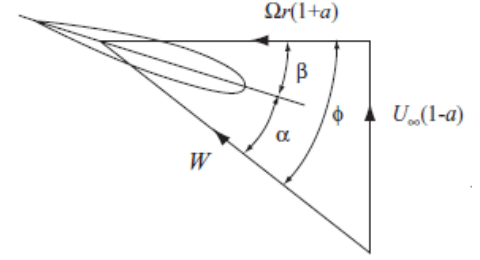


Figure 1.4: Velocity diagram

The figures 1.3 and 1.4 represent velocity and force diagram respectively for a wind turbine with N number of blades of tip radius (R) each with a chord length (c) and set pitch angle of β . According to figure 1.4, the resultant wind velocity (W) incident on the blade element is given by-

$$W = \sqrt{U_\infty^2(1-a)^2 + \Omega^2 r^2(1+a')^2} \quad (1.12)$$

Also from figure 1.4,

$$\sin \phi = \frac{U_\infty(1-a)}{W} \quad (1.13)$$

$$\cos \phi = \frac{\Omega r(1+a')}{W} \quad (1.14)$$

where ϕ = Inflow angle

Thus, the angle of attack can be given by-

$$\alpha = \phi - \beta \quad (1.15)$$

The lift force acting on the blade element is normal to the direction of W is given by-

$$\delta l = \frac{1}{2}\rho W^2 c C_l r \delta r \quad (1.16)$$

The drag force acting of the blade element is parallel to the direction of W and is given by-

$$\delta d = \frac{1}{2}\rho W^2 c C_d r \delta r \quad (1.17)$$

The blade element- momentum (BEM) theory

The BEM theory is based on the assumption that the force of a blade element is solely responsible for the change of momentum of the air which passes through the annulus swept by the element. Thus, it is assumed that there is no radial interaction between contiguous annuli and this assumption can only be satisfied if the axial flow induction factor does not vary radially.

The component of the aerodynamic force on N blade elements in the axial direction is

$$\delta L \cos \phi + \delta D \sin \phi = \frac{1}{2} \rho W^2 N c (C_L \cos \phi + C_d \sin \phi) \delta r \quad (1.18)$$

The flow induction factors are determined by solving the right-hand side of the following equations. The existing values of flow induction factors are iterated to determine new values of flow induction factor.

$$\frac{a}{1-a} = \frac{\sigma_r}{4 \sin^2 \phi} \left[C_x - \frac{\sigma_r}{4 \sin^2 \phi} C_y^2 \right] \quad (1.19)$$

$$\frac{a}{1+a'} = \frac{\sigma_r C_y}{4 \sin \phi \cos \phi} \quad (1.20)$$

Where,

$$\phi_r = \text{solidity of rotor} = \frac{Nc}{2\pi r} = \frac{Nc}{2\pi \mu R}$$

$$C_x = C_l \cos \phi + C_d \sin \phi$$

$$C_y = C_l \sin \phi - C_d \cos \phi$$

$$\mu = \frac{r}{R}$$

The full derivation of flow induction factor equations (1.19 and 1.20) can be found in the Wind Energy Handbook. The next step is to determine the coefficient of thrust (C_t) and the coefficient of power (C_p). Finally, power is calculated for a range of flow induction factors and power coefficients. A detailed derivation of equations and results is available in Wind energy handbook.

1.3.2. Vortex wake models

Although the most popular, the BEM model is not the most accurate aerodynamic load calculation model. Whereas, the CFD models are the most accurate aerodynamic load calculation models but they have a huge computational time. The vortex wake models provide a trade-off between the computational time and the accuracy. The vortex wake models are based on the vortex theory. The wake model is the key point for the vortex theory. The geometry of wake is simulated on the basis of models (rigid wake and free wake) developed by pioneer researchers. The wake region is divided into- near wake region, intermediate wake region and far wake region. The near wake region is the region concerned with the power extraction of the wind by a single turbine. Researchers have a varied opinion regarding the distance of this region, but can be assumed to be in the range of 1 to 5 rotor diameters downstream from the rotor. The far wake region is pertained to be farther than the distance of 14 rotor diameters downstream from the rotor. The region ranging from 5 to 15 rotor diameters is considered to be the intermediate wake region.

Since the last decade, these vortex models are tested by numerous researchers all around the globe. The results obtained from the vortex theory based models are in good agreement with the experimental results, which is the contrast in the case of traditional BEM theory. The comparative analysis of the vortex wake model with the BEM model and the experimental data can be found in these references [4–7, 28]. The common disadvantage of this approach is a comparatively higher computational time as compared to the BEM approach [28].

The lifting line theory

Ludwig Prandtl along with his colleagues developed a theory for predicting the aerodynamic properties of a finite wing. The theory was called as the Lifting line theory. According to the theory, a finite wing element of span b is replaced with a bound vortex. A vortex filament of strength Γ bound to a fixed location in a flow is called as a bound vortex. As per Helmholtz's theory, a vortex filament cannot end in the fluid. Therefore, it is assumed that the vortex filament continues as two free vortices trailing downstream from the wing tip to the infinity. This vortex is called as a Horseshoe vortex and it is a combination of the bound vortex and two free vortices.

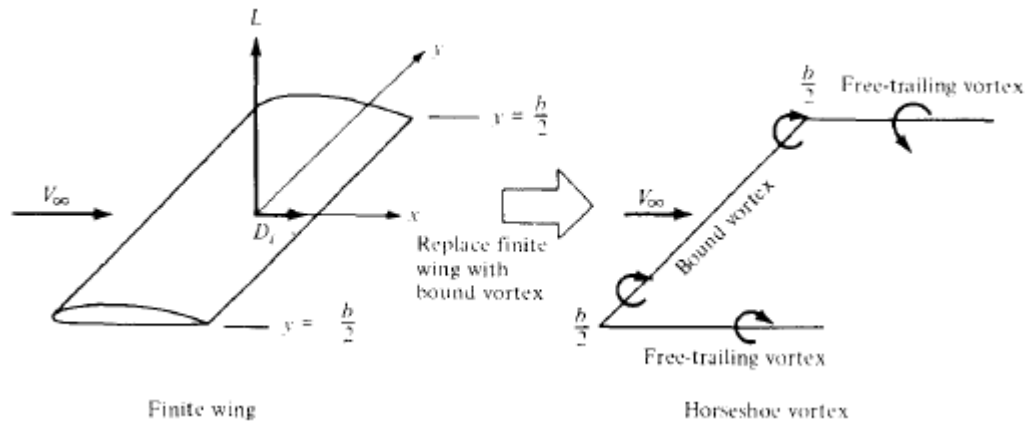


Figure 1.5: Replacement of a wing filament with a horseshoe vortex[3]

A single horseshoe vortex is superimposed into a large number of horseshoe vortices, each with a different length of the bound vortex, but with all the boundary vortices coincident along a single line, called a lifting line.

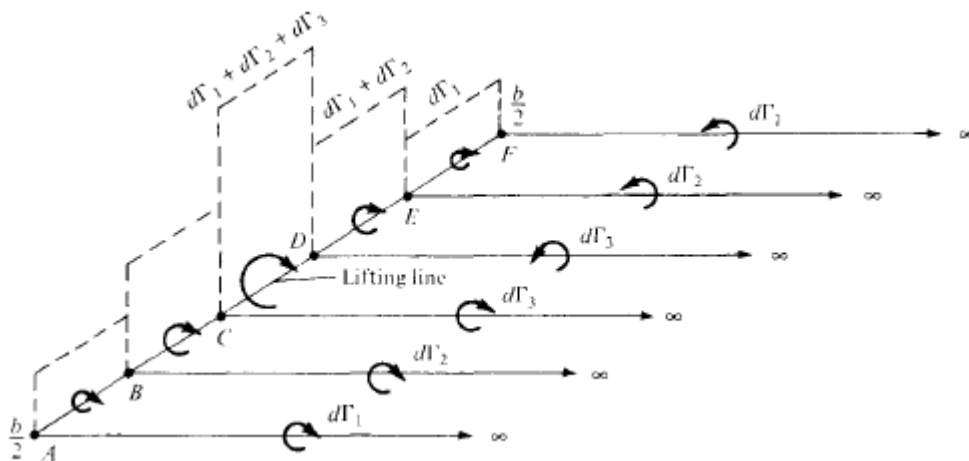


Figure 1.6: Superimposition of the finite number of horseshoe vortices along the lifting line[3]

Figure 1.6 is a schematic representation of the finite number of superimposed horseshoe vortices on a lifting line.

Assumptions involved in lifting line approach

Similar to every other engineering model, the lifting line model is also built on the basis of some assumptions. In this subsection assumptions regarding lifting line model are discussed[11]-

- The uniform stream flows parallel to the rotating axis of the turbine.
- Being a straight lifting surface, each blade is replaced by a lifting line, positioned at a quarter chord behind the leading edge.
- Any blade section is assumed to be working under 2D flow conditions. Thus, the induced radial velocity is neglected. Only the influence of the induced, rotational and axial velocities are taken into account.
- Viscous effects are taken into account only in the 2D properties.

Nonlinear lifting line method

The Prandtl's classical lifting line method as discussed in Fundamentals of Aerodynamics by Anderson[3] assumes linear variation of C_l and α_{eff} , where α_{eff} is the difference between the geometric angle of attack (α) and modified angle of attack due to effect of the downwash. Referring to Fundamentals of Aerodynamics by Anderson [3]; as the angle of attack approaches and exceeds stall angle, the lift curve becomes non-linear. The non-linear lifting line method includes the following iterative procedure which is explained in detail in the Fundamentals of Aerodynamics by Anderson.

Figure 1.7, represents a procedure for aerodynamic load calculation of the vortex theory for unsteady flow. The procedure begins with an initial approximation of the induced velocity using the BEM. The angle of attack and bound circulation is then calculated for this approximate velocity. Finally, the wake strength, induced velocity, load distribution and performance is then calculated. An iterative process is undertaken and the process is repeated until it satisfies the convergence test of bound circulation[29].

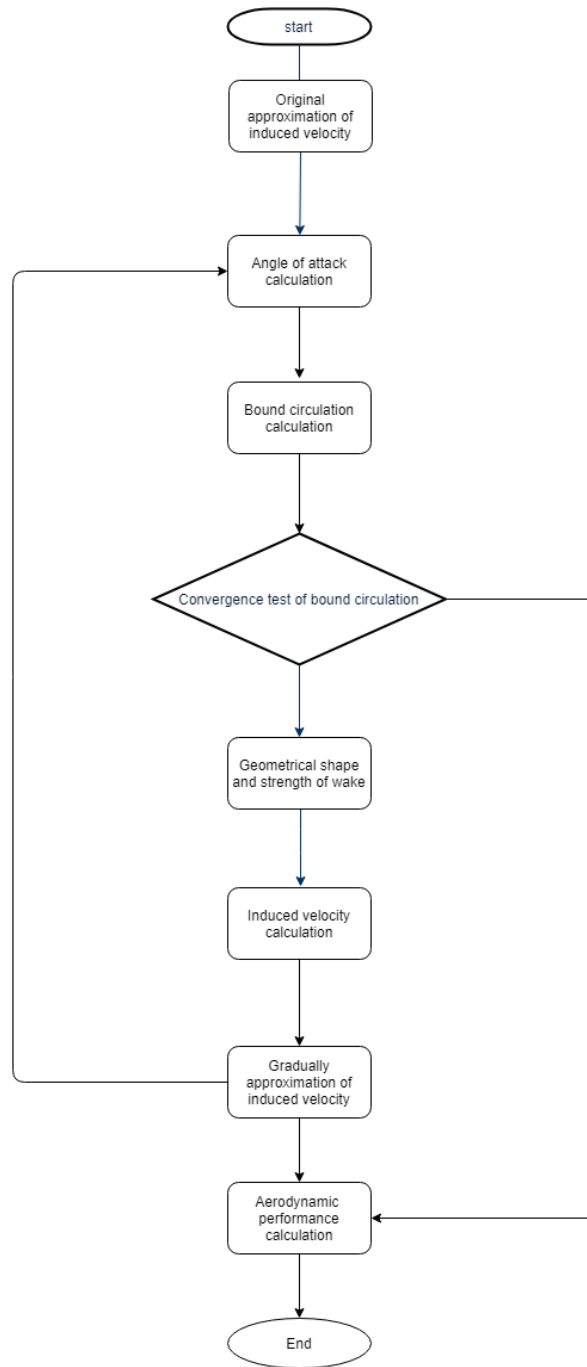


Figure 1.7: Aerodynamic load calculation procedure of the vortex theory model for unsteady flow[29]

Free and Prescribed wake models

There are two methods to aerodynamic load calculations based on the vortex wake theory, namely- the free wake vortex method and the prescribed wake vortex method.

Free wake vortex method

The free wake vortex method does not require a theoretical specification of the position of the vortex elements. Under the influence of the local flow velocity field, the vortex elements are allowed to distort freely. Biot-Savart law is used to calculate the induced velocities over vortex elements. This method can be applied to a wide range of operating conditions and hence have lower limitations. The resultant velocity comprises of the free stream velocity, the induced velocity from the vortex filaments and any other external velocities. The computational time associated with this method is very large as compared to the BEM method[13]. Free vor-

the wake method can be classified into the *Relaxation method* and the *Time-marching method*. The steady-state wake structure is assumed to be periodic at the rotor frequency in the case of the relaxation method. The governing equations are modified to include a pseudo time term-

$$\frac{\partial r}{\partial \tau} + \frac{\partial r}{\partial \psi} + \frac{\partial r}{\partial \zeta} = \frac{V(r)}{\Omega} \quad (1.21)$$

The above equation solved in the pseudo-time domain (τ) until a steady-state is reached. The wake solution is relaxed until the vortex element positions remain unchanged. The limitation of this method is the inability to capture the transient wake aerodynamics[13].

The time marching method can capture the transient wake aerodynamics. Hence, this method is suitable for the simulations of a wind turbine under unsteady flow conditions and can be used to calculate transient loads on a wind turbine.

Prescribed wake vortex method

The Prescribed wake vortex method is another vortex wake method to calculate aerodynamic loads. This method requires a theoretical specification of the vortex elements. The prescribed model is derived from the free vortex wake model. The aim of this model is to reduce the computational time and only lose a minimum accuracy involved in the free vortex wake model. The research involved in this method mainly aims to find a proper combination of blade and wake model influencing the aerodynamic loads and making the model time efficient[2]. This model is based on Prandtl's lifting line theory as discussed in section 1.3.2.

1.4. Research questions and objectives

1.4.1. Research questions

Based on the literature survey in the previous section, the important questions which will be researched in this thesis include-

1. What is the added value of using the Vortex wake model for IEC load calculations?
2. How can we make IEC load calculations more accurate with acceptable computational time?

1.4.2. Research objectives

The objective of this research project is two-fold:

1. Comparative analysis and evaluation of the results obtained from the momentum equations based model and the vortex wake model for the IEC design load cases.
2. To recommend a practice for more accurate and fast results.

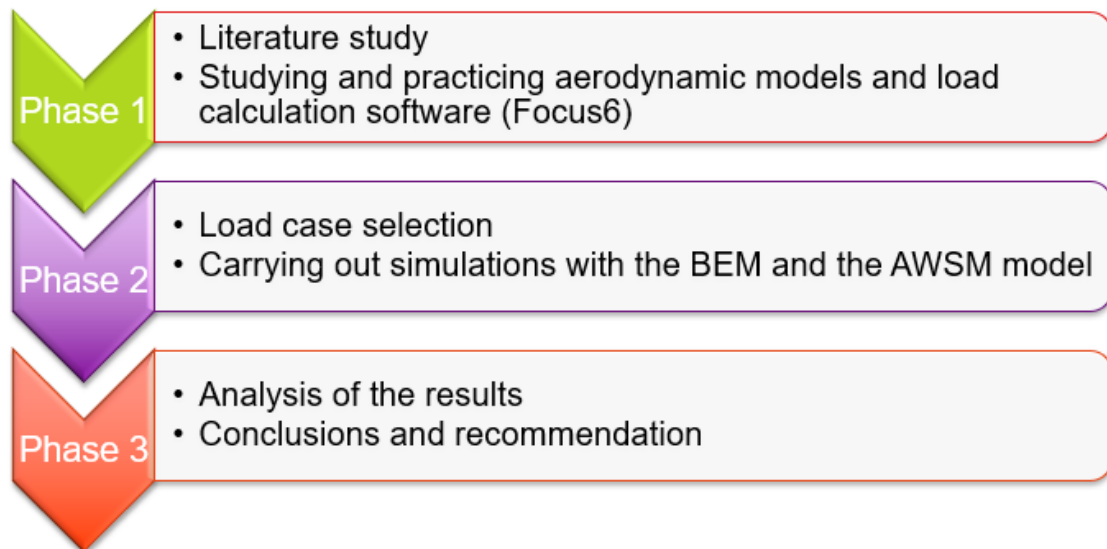
1.5. Research methodology

The approach that will be followed to address the research questions and objectives discussed in section 1.4 will be discussed in the current section. The foundation will be the existing work discussed in chapter 1.3. The research framework provides a schematic overview of how the project objective is to be achieved with the current background knowledge according to the logical project phases mentioned below.

In the first phase of the project the literature was studied and the theories involved (for example- Blade element and momentum theory, lifting line theory, etc.) were understood. In the next phase, Focus6 software and ECN Aeromodule was learned and practiced. This was done by running the shear load cases to recreate results from previous work. Along with practicing the above mentioned software, a study of the IEC design load manual was done.

In the second phase, several load cases were to be selected for further analysis. The selected load cases were simulated with the BEM and the vortex wake model in the Focus6 environment. Later on, the load case simplification will be done by reducing complexities (for example- Yaw misalignment, control mechanism, etc.). This will play an important role in understanding the root cause of the difference and physics involved.

Finally, in the last phase of the project, based on previously done analysis and observations a practice will be recommended for more accurate results.



1.6. Report outline

The thesis report begins with a short introduction about the current aerodynamic load calculation modules, namely- Blade Element Momentum (BEM) model and the vortex wake model. Both of the modules have their theories, advantages and disadvantages which are discussed in this report extensively.

Chapter 2 elaborates the modules, software and the test wind turbine involved in this project. Additionally, an overview of a comparative study of the results obtained from both of the modules with the experimental results for certain conditions is provided.

Chapter 3 discusses the IEC Design load cases considered in this project. Furthermore, the procedure involved in the load case selection is discussed.

Chapter 4 analyzes the DLC 2.3 (section 4.1), DLC 3.3 (section 4.2), DLC 1.3 (section 4.3) and DLC 1.2 (section 4.4) from the IEC standard. The analysis includes results and observations involved in the above mentioned load case.

Chapter 5 provides the reader with the key outcomes of the thesis project and discusses the scope for future development in the BEM model.

2

Aerodynamic models and the test turbine

The research aims to compare the results obtained from the aerodynamic load calculation models developed by ECN. The chapter discusses those models, namely the ECN AERO-BEM and ECN AERO-AWSM, in section 2.1.2. In section 2.1.1, the features of Focus6 software are discussed. Further in section 2.2.2, the test turbine employed in this project is presented.

2.1. Aerodynamic load calculation models

In this section, several aerodynamic models that are used in the thesis project will be discussed.

2.1.1. FOCUS6

FOCUS6 is the integrated modular tool to design wind turbines and wind turbine components like rotor blades. The tool is being used by wind energy OEMs, research centres and universities for nearly two decades. FOCUS6 integrates onshore and offshore wind turbine design with blade and support structure design. Following are the packages included in FOCUS6 software-

- FOCUS Core
- Rotor pre-design, Aero-elasticity 1
- Turbine design, Aero-elasticity 2
- Noise emission
- Structural blade design
- Bladed 4 Interface
- FEM for Blade Design
- Offshore
- FEM Mesh Export for Blade Design
- Extreme Extrapolation
- Queue Manager
- Blade testing
- Small Wind turbines
- Tidal

Phatas

Phatas is a BEM based computer program developed by WMC. The main goal of this program is to perform aerodynamic load calculations for Horizontal Axis Wind Turbines (HAWT). It is developed for time-domain calculation of the dynamic behavior and corresponding loads on a HAWT. The load calculations are based on the BEM theory as discussed in section 1.3.1. The detailed theory regarding inputs and outputs for this program can be found in the Phatas user manual[20]. The Focus6 software is supported by the Phatas program for carrying out aerodynamic load calculations.

2.1.2. ECN Aeromodule

ECN Aeromodule[7] features momentum equations based method similar to the implementation in Phatas and a free vortex wake code in form of Aerodynamic Windturbine Simulation Module (AWSM). The package uses the blade position and wind velocity as an input to run the model and the forces and moments are obtained as an output by the user. In regards to the thesis project, ECN Aeromodule shall be coupled to the FOCUS6 software so that the structural dynamics of a wind turbine can be solved. Further, in this section, the features of this package are discussed briefly.

ECN Aeromodule- BEM

ECN Aeromodule- BEM is momentum equations based model similar to the Phatas program discussed in the previous section 2.1.1. The background theory involved can be found in section 1.3.1 and the information regarding the inputs and outputs for this module can be found in section 2.1.2. As discussed previously, the BEM based solvers are not accurate for certain load cases and often require additional engineering models to overcome the flaws involved. Several such additional models are developed by ECN and are included in the ECN Aeromodule.

ECN- Yaw model-

The ECN Yaw model is based on the theory discussed in [26] The blade will be retreating in the upper-half plane and advancing in the lower-half plane, in case of a positive yawed flow. This leads to effective inflow velocity of-

$$W = \sqrt{(U_\infty^2 (\cos \phi_y - u_i)^2) + ((\omega r)^2 + (U \sin \phi_y \cos \phi_{r,b})^2)} \quad (2.1)$$

And inflow angle (ϕ) is given by-

$$\tan \phi = \frac{U_\infty \cos \phi_y - u_i}{\omega r + U_\infty \sin \phi_y \cos \phi_{r,b}} \quad (2.2)$$

where,

ϕ_y = Yaw angle

$\phi_{r,b}$ = Azimuth angle

A disk averaged induction is calculated according to Glauert's equation-

$$F_{ax} = \rho S |\vec{U}_\infty + \vec{u}_i| 2\vec{u}_{i,0} \quad (2.3)$$

where,

F_{ax} = Axial force

$u_{i,0}$ = disc averaged induced velocity

But, an additional dynamic inflow term discussed in 2.4 is added to equation 2.3, that is, the equation is now applied to an annular ring level. Thus, $u_{i,0}$ is no longer a disc averaged induced velocity value. The induced velocity distribution can be given by-

$$u_i = u_{i,0} (1 - f_{2,ecn} \frac{r}{R} \tan \frac{\chi}{2} \sin \phi_{r,b}) \quad (2.4)$$

where,

χ = skew angle

$f_{2,ecn} \frac{r}{R} = \frac{15\pi r}{64R}$

ECN- Dynamic inflow model-

Snel and Schepers[26] from ECN have also outlined a dynamic inflow model, based on integral relations of a stream tube model [22]. In this model, an additional time dependent term is added to the axial induction and momentum theory relation, that is-

$$\tau \frac{da}{dt} + 4a(1 - a) = C_t \quad (2.5)$$

where, τ is the time constant and C_t is the thrust coefficient.

The time constant increases along the diameter of the blade. In case of an equilibrium situation, the time constant goes to zero and the above equation goes to 1.11.

Engineering extensions for the BEM approach

As we know, the BEM theory is valid for stable and steady conditions. To overcome the limitations of the BEM based models during unstable and unsteady inflow conditions several engineering models are developed [14]. These models are discussed below-

- **Tip and root loss correction** To account the finite number of blades, empirical Prandtl's correction is calculated. Root and tip loss factors are multiplied, which results in a total Prandtl's correction factor. This factor relates to the annulus averaged axial and tangential induction to the local induction at each element.
- **Oblique inflow correction** The rotor is yawed in the direction of the incoming wind, this results in a condition that is different from that in case of an axial flow. To counter this unfavorable condition, a model developed by Schepers [23] is implemented. This function is determined as a function of yaw angle, azimuth angle and radial location. This skew function relates local induction to axial induction.
- **Dynamic inflow model** This model adds up another term to the axial momentum equation to account for the inertia of flow stream that interacts with the rotor in case of pitch action, rotational speed variation or wind speed variation [25].
- **Turbulent wake state model** The wake transforms into a turbulent state but BEM theory predicts flow reversal in the wake. To account for this effect the momentum equation is replaced by a turbulent wake state equation.
- **Dynamic stall model** The local state at each airfoil section does not respond instantaneously to changing conditions like- turbulence, blade deformation or tower effects. Dynamic stall models are developed to overcome these limitations.

Aerodynamic Windturbine Simulation Module (AWSM)

This is a time-accurate aerodynamics module, based on non-linear vortex wake theory in which shape and strength of the wake will develop in time. In this approach the aerodynamic lift, drag and pitching moment characteristics of the blade cross-sections are assumed to be known and are corrected for effects of blade rotation. This module provides a more accurate analysis of the aerodynamic loads for the situations where local aerodynamic characteristics are time dependent and dynamic wake effects are significant. The detailed features and summary of this module can be found in its manual [12]. It is very important to define several input parameters correctly, such that the model can be used without any errors. The extensive definition of parameters and the usage of the model can be found in ECN Aeromodule manual [4]. Few important parameters mentioned in the manual are discussed below-

Time Step-

The numerical stability and accurate results can be obtained by defining a time step corresponding to the angular step less than 10° , but for aeroelastic calculations it is recommended to have a much smaller time step than the one mentioned earlier. Additionally, it is observed that the AWSM model often fails in case of a very small time step.

Streamwise wake points (SWP)-

This input parameter corresponds to the number of wake points in the specified time interval. It is recommended to have a value corresponding to a convected wake distance of 3 rotor diameters.

$$SWP = \frac{nD}{U_\infty(1-a)} \quad (2.6)$$

where,

n = number of rotors

Free stream wake points (FWP)

AWSM model works in case of both a free or a fixed wake. Compared to a fixed wake model, a free wake model provides more accurate results but the computational time is very high. Thus, in order to have a good compromise between accuracy and the computation time, it is recommended to have a free stream wake

points corresponding to the convected rotor distance of 2 diameters. The number of FWP can be calculated by the equation 2.6.

Ramp time and Ramp factor-

Often the starting vortex creates numerical stability problems for AWSM. In order to overcome these issues, an increasing value starting with a low wind speed can be stipulated. In order to achieve normal working conditions a ramp-up time corresponding to 90° of rotor revolution and a ramp factor of 0.3 is recommended.

Wake reduction-

AWSM model is based on non-linear vortex wake theory 1.3.2 and therefore leads to very high computational time. In order to have a lower computational time a wake points skipping routine called the Wake reduction is available in AWSM. In the case of smaller time steps, a very high number of wake points are required to cover the wake length. To reduce the necessary number of wake points a wake reduction routine can be applied. This routine skips a few streamwise wake points and thus, adjusts the number of SWP's and FWP's such that the computation time can be curtailed. It is recommended to apply the routine after wake length corresponding to convected wake distance of 0.5 rotor diameter. This wake length is represented by a keyword WAKEREDUCTIONSTART and can be calculated by equation 2.6. Now, let us assume, WAKEREDUCTIONSTART= 300 and WAKEREDUCTIONSkip= 4, the adjusted number of streamwise wake points (SWP_{adj}) can be given by-

$$SWP_{adj} = 300 + \frac{SWP - 300}{4 + 1} \quad (2.7)$$

Similarly, the adjusted number of freestream wake points can be calculated by replacing SWP by FWP in equation 2.7.

2.1.3. Comparison of the BEM and vortex wake approach on the basis of different parameters and results

Over the decades, the BEM theory and the vortex wake theory are researched and the results are compared. It is found that the results obtained from the models based on the vortex wake theory are in good agreement with experimental results. Yet, these models are not that popular due to a large computational time involved. In this section several results for different inflow conditions and situations obtained from the BEM model and the vortex wake model will be compared.

Axial flow condition

Sectional forces are calculated for several axial flow operating conditions, varying tunnel speed and pitch angle. For both NASA-Ames [24] and MEXICO test [27], the BEM and the AWSM results are good in agreement with each other [5]. In a special test case, in figure 2.1 ($U= 10\text{m/s}$, $\text{pitch}= 3^\circ$), a standing vortex at the inboard position was observed. The resulting span wise discontinuity is more accurately accounted and also tip and root effects are more accurately implemented with AWSM compared to Prandtl's correction factor in the BEM model [5].

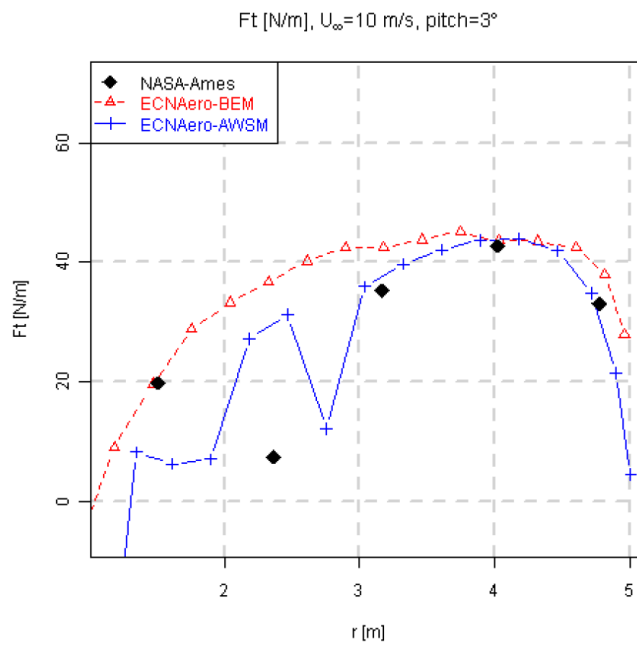


Figure 2.1: Radial distribution of sectional forces for axial flow conditions [5]

Yawed flow condition

For yawed flow condition sectional forces are displayed for a fixed position as a function of azimuth angle. AWSM results are in better agreement with the measurements than the BEM. In figures (2.2 and 2.3) below, we can see that the AWSM predictions are in good agreement with the test results[5].

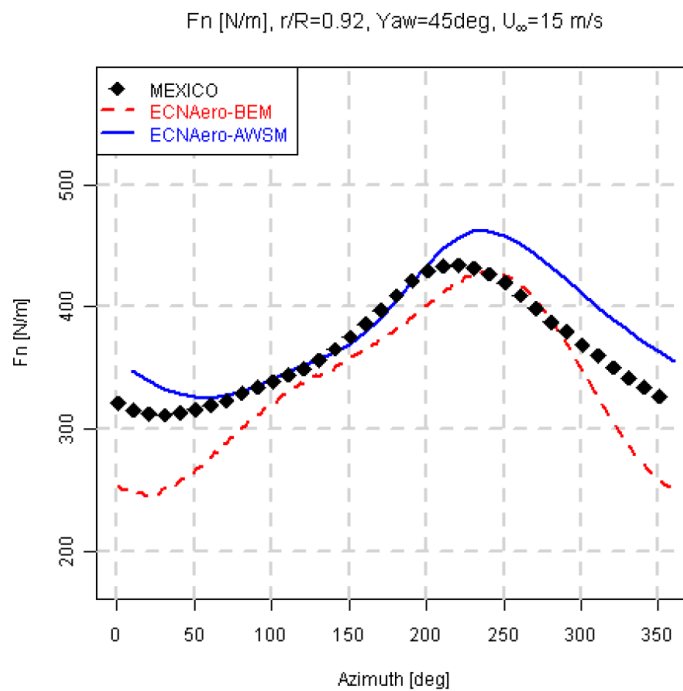


Figure 2.2: Sectional force variation with rotor azimuth for yawed flow conditions for MEXICO test[5]

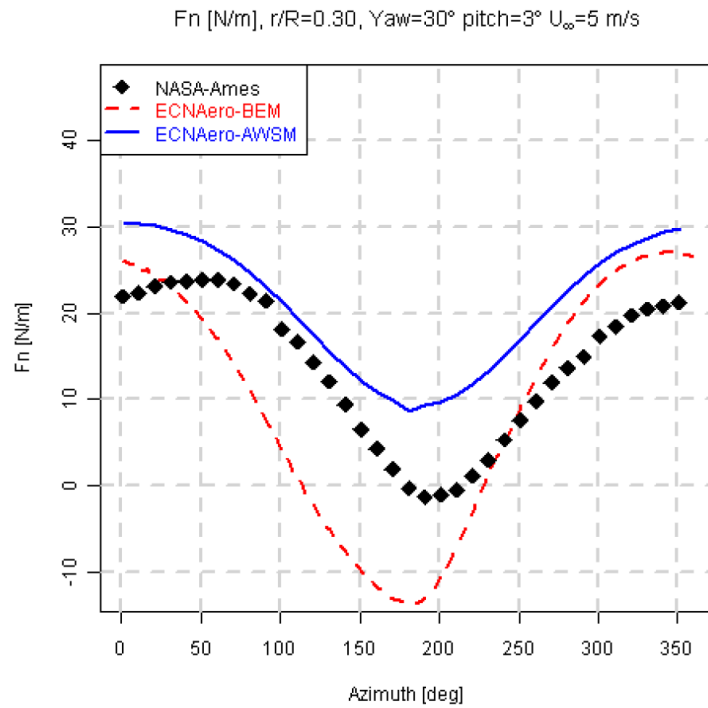


Figure 2.3: Sectional force variation with rotor azimuth for yawed flow conditions for NASA-Ames test[5]

Dynamic inflow

The NASA-Ames experiment included a pitch step test case to take a dynamic inflow condition into account. An overshoot was predicted by the BEM model which can be seen in the figure 2.4. More correct representation of physics can be seen by the AWSM model [5].

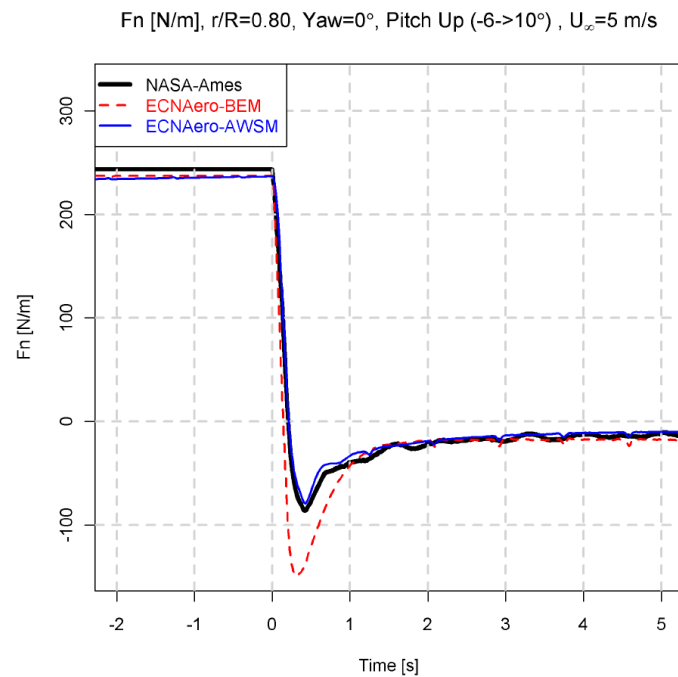


Figure 2.4: Dynamic inflow condition[5]

Table 2.1: Comparative analysis of the BEM and the AWSM based on the aerodynamic situation

Comparative analysis		
Situation	BEM	AWSM
Axial induction	Intrinsic	Intrinsic
Tangential induction	Intrinsic	Intrinsic
Radial induction	Not available	Intrinsic
Yawed inflow	Engineering model	Intrinsic
Turbulent wake state	Engineering model	Intrinsic
Dynamic inflow	Engineering model	Intrinsic
Dynamic stall	Engineering model	Engineering model

The table 2.1, provides an overview of all the features and additional engineering models required in the case of the BEM and the AWSM model for various aerodynamic situations.

2.2. Test Wind turbine

In this section the properties and specifications of the test wind turbine to be considered in this thesis project will be discussed.

2.2.1. AVATAR Project

AVATAR was the project commenced by the European Energy Research Alliance (EERA) and was part of the FP7 program of the European Union. The project consortium composed of 14 partners, which included several educational institutions, research organizations and companies[1]. The project was led and coordinated by the Energy research Centre of the Netherlands. The main goal of the project was to develop and validate advanced aerodynamic models for the next generation large scale wind turbines[1].

2.2.2. The AVATAR Wind turbine

As part of the AVATAR project, a 10 MW wind turbine was developed. This turbine would be further considered for this thesis project. Below are the specifications of the wind turbine.

Table 2.2: AVATAR Wind turbine specifications

AVATAR Wind Turbine		
General Specifications		
Specification	Value	Unit
Wind regime	IEC Class 1A	-
Rotor orientation	Clockwise rotation Up-wind	-
Cut in wind speed	4	m/s
Cut out wind speed	25	m/s
Rated wind speed	10.75	m/s
Rated power	10	MW
Rotor diameter	205.8	m
Hub diameter	5.6	m
Hub height	132.7	m
Min. rotor speed	6	rpm
Max. rotor speed	9.5	rpm
Max. Generator speed	480	rpm
Gear ratio	50	-
Max. tip speed	103.9	rpm
Rotor blade Specifications		
Rotor radius	102.88	m
Blade length	100.08	m
Blade root	2.8	m

3

IEC Design Load Cases

Wind energy standards, for example- IEC 61400, etc. are used for designing wind turbines. In these standards, many Design Load Cases (DLC's) are analyzed. DLC's are a combination of the design situations of a wind turbine with wind conditions (gusts) and other external factors(e.g. grid failures and lightening). This chapter discusses the sources of unsteady flow and the various DLC's analyzed in this thesis project.

3.1. Sources of unsteady loading

The BEM theory is valid for steady flow conditions. Practically, a wind turbine is often subjected to unsteady flow conditions. The sources of unsteady flow which lead to dynamic inflow conditions will be discussed in this section.

1. **Turbulence** It refers to fluctuations in wind speed on a relatively fast time-scale, typically less than about 10 minutes. The turbulence flow towards a wind turbine is modeled on the basis of similarity theory in combination with computational fluid dynamics methods (CFD)[8]. A gust is an extreme form of turbulence. The description and adverse effects of such extreme gust is provided by Jung[17]. The significance of turbulence is also considered in the design and validation of a wind turbine as mentioned in IEC design load standards[10].
2. **Turbine wake** A wind turbine is also subjected to higher turbulence levels than the atmospheric turbulence level caused due to the wake of another turbine.
3. **Tower shadow** A wind turbine blades indeed see a lower wind speed when it crosses the tower. This unsteady cyclic loading adds up to the total fatigue loads. Such an effect is observed due to the weakening of wind speed in front of the tower.
4. **Wind shear** Wind speed increases as we go higher from the sea level. Thus, the tip of the rotor blade faces higher wind speed than the speed when it is at 180°azimuth location. This, periodic load variation leads to cyclic loading.
5. **Turbine operation** The wind turbine is also subjected to unsteady loading due to its own operation. The stoppages and restarts often lead to unexpected loading on the blades and drive train of the turbine. Along with, starts and stops, there are many other operations for example- pitching of the blades, yawing of the nacelle, etc. which lead to unsteady loading on the wind turbine. An exclusive module is provided in IEC design load cases for such type of loading.

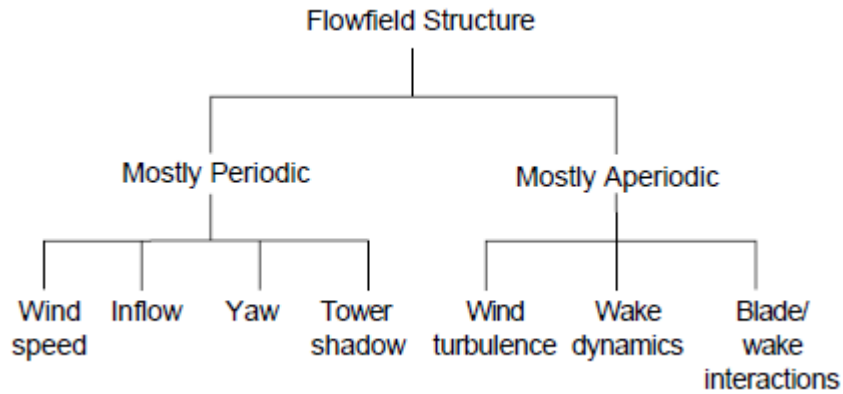


Figure 3.1: Classification of the sources of unsteady loading[19]

Figure 3.1 summarizes the various sources of aerodynamic loads subjected to a wind turbine. The effect of aerodynamic loads is that the wind turbine operates in adverse and unsteady working conditions.

3.2. IEC Design Load Case overview

For this thesis project IEC 61400-3 and DNVGL-ST-0437[10] wind energy standard shall be considered. Since 2005, the IEC 61400-1 standard was adopted by the international wind community[16]. The main objectives of this standard include[10]-

- Provide an internationally accepted level of safety by defining minimum requirements for the determination of loads of wind turbines,
- Serve as a design basis for designers, suppliers, purchasers and authorities.
- Specify requirements for wind turbines and wind farms subject to DNV GL certification.

The standard applies to all types of wind turbines. However, it is most effective for two or three bladed turbines with active pitch and yaw mechanisms. The standard contains the following features[10]-

- Definition and theory regarding external conditions.
- Determination of site specific design conditions.
- Calculation and evaluation of loads.
- Model validation by measurements of loads and power curve.

Design Situation	DLC	Wind Condition	Marine Condition				Other Conditions:	Type of Analysis		Partial safety factor
			Waves	Wind and wave directionality	Sea Currents	Water Level		Onshore	Offshore	
1) Power Production:	1.1	NTM $V_{in} < V_{hub} < V_{out}$	NSS $H_s = E[H_s V_{hub}]$	COD, UNI	NCM	MSL	For extrapolation of extreme loads (offshore – only RNA)	U	U	N (1.25)
	1.2	NTM $V_{in} < V_{hub} < V_{out}$	NSS Joint prob. distribution of H_s, T_p, V_{hub}	MIS, MUL	No Currents	NWLR or \geq MSL		F/U	F/U	F/N
	1.3	ETM $V_{in} < V_{hub} < V_{out}$	NSS $H_s = E[H_s V_{hub}]$	COD, UNI	NCM	MSL		U	U	N
	1.4	ECD $V_{hub} = V_r - 2 \text{ m/s}, V_r, V_r + 2 \text{ m/s}$	NSS $H_s = E[H_s V_{hub}]$	MIS, wind direction change	NCM	MSL		U	U	N
	1.5	EWS $V_{in} < V_{hub} < V_{out}$	NSS $H_s = E[H_s V_{hub}]$	COD, UNI	NCM	MSL		U	U	N
	1.6	NTM $V_{in} < V_{hub} < V_{out}$	SSS $H_s = H_{s,SSS}$	COD, UNI	NCM	NWLR		-	U	N
	1.7	NTM $V_{in} < V_{hub} < V_{out}$	NSS Joint prob. distribution of H_s, T_p, V_{hub}	MIS, MUL	No Currents	NWLR or \geq MSL	Ice formation	F/U	F/U	F/N
2) Power Production + occurrence of fault:	2.1	NTM $V_{in} < V_{hub} < V_{out}$	NSS $H_s = E[H_s V_{hub}]$	COD, UNI	NCM	MSL	Normal control system fault or primary layer control function fault	U	U	N
	2.2	NTM $V_{in} < V_{hub} < V_{out}$	NSS $H_s = E[H_s V_{hub}]$	COD, UNI	NCM	MSL	Abnormal control system fault or secondary layer protection function fault	U	U	A
	2.3	EOG $V_{hub} = V_r \pm 2 \text{ m/s}$ and V_{out}	NSS $H_s = E[H_s V_{hub}]$	COD, UNI	NCM	MSL	External or internal electrical fault including loss of electrical network	U	U	A
	2.3 alternatively	NTM $V_{in} < V_{hub} < V_{out}$	NSS $H_s = E[H_s V_{hub}]$	COD, UNI	NCM	MSL	External or internal electrical fault including loss of electrical network	U	U	N
	2.4	NTM $V_{in} < V_{hub} < V_{out}$	NSS $H_s = E[H_s V_{hub}]$	COD, UNI	No currents	NWLR or \geq MSL	Normal control system fault or loss of electrical network or primary layer control function fault	F/U	F/U	F/N
	2.5	NWP $V_{in} < V_{hub} < V_{out}$	NSS $H_s = E[H_s V_{hub}]$	COD, UNI	NCM	MSL	Fault ride through	U	U	N (1.20)

Figure 3.2: IEC Design Load Cases-1 [16]

Design Situation	DLC	Wind Condition	Marine Condition				Other Conditions:	Type of Analysis		Partial safety factor
			Waves	Wind and wave directionality	Sea Currents	Water Level		Onshore	Offshore	
3) Start up	3.1	NWP $V_{in} < V_{hub} < V_{out}$	NSS $H_s = E[H_s V_{hub}]$	COD, UNI	No currents	NWLR or \geq MSL		F/U	F/U	F/N
	3.2	EOG $V_{hub} = V_{in}, V_r \pm 2 \text{ m/s},$ and V_{out} or ETM $V_{in} < V_{hub} < V_{out}$	NSS $H_s = E[H_s V_{hub}]$	COD, UNI	NCM	MSL	The timing of the gust and the start-up event chosen for minimum 4 distinct points	U	U	N
	3.3	EDC $V_{hub} = V_{in}, V_r \pm 2 \text{ m/s}$ and V_{out}	NSS $H_s = E[H_s V_{hub}]$	MIS, wind direction change	NCM	MSL		U	U	N
4) Normal shutdown	4.1	NWP $V_{in} < V_{hub} < V_{out}$	NSS $H_s = E[H_s V_{hub}]$	COD, UNI	No currents	NWLR or \geq MSL		F/U	F/U	F/N
	4.2	EOG $V_{hub} = V_r \pm 2 \text{ m/s}$ and V_{out} or ETM $V_{in} < V_{hub} < V_{out}$	NSS $H_s = E[H_s V_{hub}]$	COD, UNI	NCM	MSL	The timing of the gust and the shutdown event chosen for minimum 6 distinct points	U	U	N
5) Emergency stop	5.1	NTM $V_{hub} = V_r \pm 2 \text{ m/s}$ and V_{out}	NSS $H_s = E[H_s V_{hub}]$	COD, UNI	NCM	MSL	Azimuth position at the time of the emergency stop shall be randomly selected	U	U	N
6) Parked (standing still or idling)	6.1	EWM $V_{hub} = V_{ref}$	ESS $H_s = H_{s,50}$	MIS, MUL	ECM $U = U_{50}$	EWLR	Yaw misalignment of ± 8 deg Possible yaw slippage	U	U	N
	6.2	EWM $V_{hub} = V_{ref}$	ESS $H_s = H_{s,50}$	MIS, MUL	ECM $U = U_{50}$	EWLR	Loss of electrical network Yaw misalignment of $\pm 180^\circ$	U	U	A
	6.3	EWM $V_{hub} = V_1$	ESS $H_s = H_{s,1}$	MIS, MUL	ECM $U = U_1$	NWLR	Extreme yaw misalignment Yaw misalignment of ± 20 deg	U	U	N
	6.4	NTM $V_{hub} < V_{in}$ and $V_{out} < V_{hub} < 0,7 V_{ref}$	NSS Joint prob. distribution of H_s, T_p, V_{hub}	COD, MUL	No currents	NWLR or \geq MSL	Investigation of natural frequencies during idling	F/U	F/U	F/N
	6.5	EWM $V_{hub} = V_1$	ESS $H_s = H_{s,1}$	MIS, MUL	ECM $U = U_1$	NWLR	Ice formation on structure	-	U	N

Figure 3.3: Design Load Cases-continued [16]

Design Situation	DLC	Wind Condition	Marine Condition				Other Conditions:	Type of Analysis		Partial safety factor
			Waves	Wind and wave directionality	Sea Currents	Water Level		Onshore	Offshore	
7) Parked and fault conditions:	7.1	EWM $V_{hub} = V_1$	ESS $H_s = H_{s,1}$	MIS, MUL	ECM $U = U_1$	NWLR	Fault that produces deviations from the normal turbine behaviour while parked; including loss of electrical network	U	U	A
	7.2	NTM $V_{hub} < V_{out}$	NSS Joint prob. distribution of H_s, T_{Dr}, V_{hub}	COD, MUL	No currents	NWLR or \geq MSL		-	F/U	F/N
8) Transport, installation, maintenance and repair	8.1	NTM $V_{hub} = V_T$ to be stated by the manufacturer	NSS $H_s = H_{sT}$ to be stated by the manufacturer	COD, MUL	No currents	NWLR	Design conditions shall be stated by the manufacturer	U	U	N
	8.2	EWM $V_{hub} = V_1$	ESS $H_s = H_{s,1}$	COD, MUL	No currents	NWLR	Transport, installation, maintenance and repair	U	U	A
	8.3	EWM $V_{hub} = V_1$	ESS $H_s = H_{s,1}$	COD, UNI	ECM $U = U_1$	NWLR	Vortex-induced vibrations due to wind, waves or currents	F/U	F/U	F/N
	8.4	NTM $V_{hub} < 0,7V_{ref}$	NSS Joint prob. distribution of H_s, T_{Dr}, V_{hub}	COD, MUL	No currents	NWLR or \geq MSL	No grid during installation period	-	F/U	F/N
	8.5	NTM $V_{hub} = V_T$	ESS $H_s = H_{sT}$	COD, MUL	ECM $U = U_1$	NWLR	Service vessel impact and helicopter loads – normal event	-	U	N
	8.6	NTM $V_{hub} = V_T$	ESS $H_s = H_{sT}$	COD, MUL	ECM $U = U_1$	NWLR	Supply vessel impact – abnormal event	-	U	A

Figure 3.4: Design Load Cases-continued[16]

The tables above represent Design Load Cases (DLC's) to be considered and simulated as part of this thesis assignment. The DLC's are designed to take into account all of the conditions and situations faced by a wind turbine in the course of its lifetime.

Table 3.1: Abbreviations of the terms used in the above tables[16]

A	Abnormal
COD	Co-directional
ECD	Extreme Coherent gust with direction change
ECM	Extreme Current Model
EDC	Extreme Direction Change
EOG	Extreme Operating Gust
ESS	Extreme Sea State
ETM	Extreme Turbulence Model
EWLR	Extreme Water Level Range
EWM	Extreme Wind speed Model
EWS	Extreme Wind Shear
F	Fatigue loads
MIS	Misaligned
MSL	Mean Sea Level
MUL	Multi-directional
N	Normal loads
NCM	Normal Current Model
NSS	Normal Sea State
NTM	Normal Turbulence Model
NWLR	Normal Water Level Range
NWP	Normal Wind Profile model
SSS	Severe Sea State
U	Ultimate loads
UNI	Uni-directional

3.3. DLC selection

In section 2.1.3, the comparison between the BEM model and the AWSM model is briefly discussed for various load situations. Based on the comparison in section 2.1.3, the BEM model is often expected to fail in several complex situations, such as- yawed inflow condition, turbulent inflow condition, etc. These failures probably occur due to violation of assumptions involved in the BEM model. Contrast to the BEM model, the AWSM model may provide improved results in such complex situations.

As wind energy technology advances, its continued safety, reliability and performance must be assured. Thus, it becomes highly important to have a comparative study for the results obtained from simulating IEC DLC's with the BEM and the AWSM model.

3.3.1. DLC Pre-selection

The complete certification process for IEC 61400-1 involves 1880 load situations, unfortunately, due to higher simulation time involved in the AWSM model is not feasible to simulate all of the load situations mentioned in the certification standard. Thus, a few load situations were selected on the basis of the complexity involved.

Table 3.2: DLC pre-selection

Design load case	Load situation	Remarks
DLC 1.2	NTM, misalignment of wind	Violates steady and uniform inflow assumptions in the BEM
DLC 1.3	Extreme turbulence due to the environment and the wake	Violates steady and uniform inflow assumptions in the BEM
DLC 2.3	Extreme coherent gust	The gust violates flow homogeneity
DLC 3.3	Extreme direction change(Wind) at start up	Violates axial inflow assumption in the BEM
DLC 4.2	Extreme operating gust at shut down	The gust violates flow homogeneity
DLC 6	Extreme wind condition	Violates steady and uniform inflow assumptions

DLC 1.2- It is a normal production case and is one of the most important fatigue load case involved in certification process. The simulations are carried out for the wind speeds ranging from a cut in wind speed to a cut out wind speed [10]. This load case is a significant fatigue load case.

DLC 1.3- It is a normal production case and represents the requirements for the ultimate loading due to extreme turbulence conditions. These conditions include environmental turbulence and turbulence due to the turbine wake [10]. The simulations are carried out for the wind speeds ranging from a cut-in wind speed to a cut-out wind speed [10]. This load case is selected to analyze possible inaccuracies in load results due to the turbulent inflow conditions in the case of the BEM model.

DLC 2.3- It is a normal production load case with a coherent operating gust. The inflow conditions include a coherent operating gust for the duration of 10.5 s [10]. The simulations are carried out for the wind speeds of $V_{rated} \pm 2$ and cut-out wind speed [10]. This load case is selected to analyze possible inaccuracies in load results due to an extreme operating gust in the case of the BEM model.

DLC 3.3- It is a start up load case with an extreme direction change at a certain time during the course of the start up process. The turbine is subjected to an oblique (yawed) inflow condition due to the direction change involved[10]. The simulations are carried out for the wind speeds of cut-in wind speed, $V_{rated} \pm 2$ and cut-out wind speed [10]. This loads case aims to analyze the probable failure in the BEM model due to yawed inflow conditions.

DLC 4.2- This load case represents the load situation at the shut down of the turbine. The situation includes an extreme operating gust at the time of shut down [10]. The simulations are carried out for the wind speeds of $V_{rated} \pm 2$ and cut-out wind speed [10]. This load case is selected to analyze possible inaccuracies

in load results due to an extreme operating gust in the case of the BEM model at cut-out wind velocities.

DLC 6- In this load situation an extreme wind speed model is considered. This load case involves a parked rotor and is subjected to extreme wind speed (storm) [10]. The simulation is carried out for the 50 years maximum wind speed and may depend upon the location [10]. This load case is selected to analyze the BEM results with the vortex model results for the turbulent inflow conditions at extremely high wind speed.

3.3.2. DLC final selection

The load cases discussed in section 3.3 were simulated using the ECN Aeromodule in the Focus6 environment. The simulations were done with both of the aerodynamic load calculation models. On the basis of results a few load cases were selected. The reasons and the idea behind the load case selection shall be discussed further in this section.

DLC 4.2

DLC 4.2 is the load case, which represents the situation at the shut down of the turbine. During this turbine approaches the vane angle and the blades are expected to be loaded very lightly. This load case shall not be treated further due to very low loading and the load case situation is quite similar to the *DLC 2.3*.

DLC 6

DLC 6 is the load case, which represents the situation during which the turbine is subjected to an extreme wind speed (for example- storm). The rotor is at the parked position.

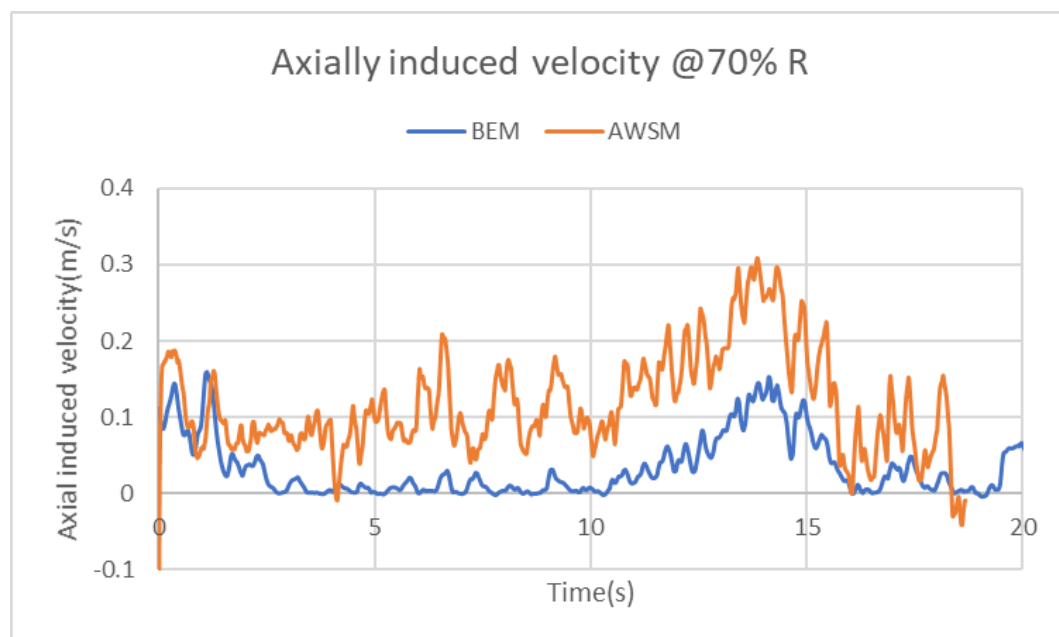


Figure 3.5: Axially induced velocity

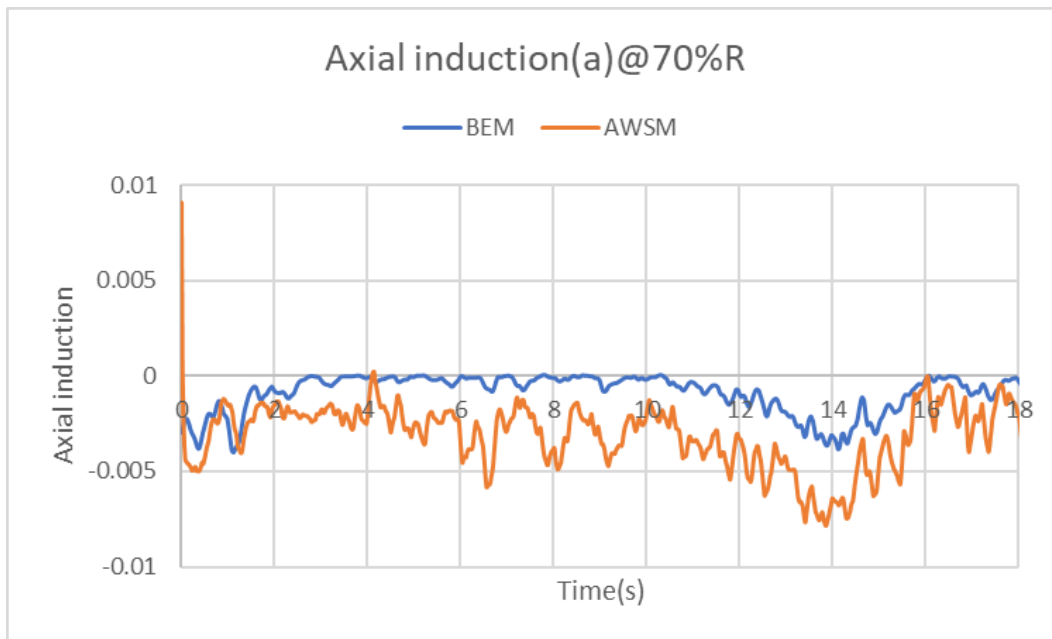


Figure 3.6: Axial induction factor

The figures 3.5 and 3.6, represent a time series for axially induced velocity and axial induction respectively. The axial induction appears to be negative due to very high wind velocity of **40 m/s** and a high pitch angle of 90° . A negative magnitude of induction leads to a lower magnitude of the aerodynamic force coefficients and the thrust coefficient. Therefore, DLC 6 shall not be further treated in the thesis project.

Table 3.3: DLC selection

Design load case	Load situation
DLC 1.2	NTM, misalignment of wind
DLC 1.3	Extreme turbulence due to the environment and the wake
DLC 2.3	Extreme coherent gust
DLC 3.3	Extreme direction change(wind flow) at start up

The above table lists the load cases to be further studied, analyzed and discussed in this thesis project.

4

Results and discussions

In this chapter, the results for the selected design load cases mentioned in section 3.3.2 are discussed. The IEC design load cases that have been reviewed are DLC 2.3 (section 4.1), DLC 3.3 (section 4.2), DLC 1.3 (section 4.3), and DLC 1.2 (section 4.4). The discussion involves comparative analysis of the results obtained from the BEM and the AWSM simulations. The results discussed in this chapter are implied to the AVATAR wind turbine model and may vary in the case of other wind turbine models.

4.1. DLC 2.3

In this section, the results and analysis regarding the IEC DLC 2.3 shall be presented.

4.1.1. Load case description

As discussed in section 3.3, DLC 2.3 is a normal production load case. Additionally, the wind turbine is subjected to an extreme operating gust for a defined duration. The load case is designed for the whole range of wind speeds starting from cut-in wind speed to cut-out wind speed. For each of the wind speeds, the gust duration and amplitude are maintained constant. As part of the thesis report, a few load case situations are selected and shall be treated for the comparative analysis of the results obtained by simulating the load case with two aerodynamic load calculation models discussed in the previous sections. The simulations were carried out with the AWSM model and the BEM model (with and without the ECN dynamic inflow model) in the Focus6 environment. The simulations were performed without pitch control. The load case specifications involved are as follows-

Table 4.1: Load case specifications

General specifications		
Specification	Value	Unit
Gust duration	10.5	seconds
Gust amplitude	6.6781	-
Starting yaw angle	0	degree
Rotor speed	7	rpm

4.1.2. Results and observations

In this section, the results obtained by simulating the load case with two aerodynamic load calculation models discussed in the previous sections are discussed. The section is divided into few subsections which shall aim to discuss several load case situations as described in the IEC design load case standard.

DLC 23816

DLC 23816 is a load case situation included in the DLC 2.3 for cut out wind speed. Below are the load case specifications exclusive for this situation-

- Wind speed- 25 m/s

- Pitch angle- 14.81°

As discussed in section 2.1.2, the AWSM model requires several settings for its error free usage. Below are the settings involved in carrying out the AWSM simulations-

- Time step- 0.1 seconds, equivalent to 5.7° azimuth change
- Stream-wise wake points- 246 ~ 3 rotors diameter (based on equation 2.6)
- Free stream-wise wake points- 164 ~ 2 rotors diameter (based on equation 2.6)

Wind speed profile

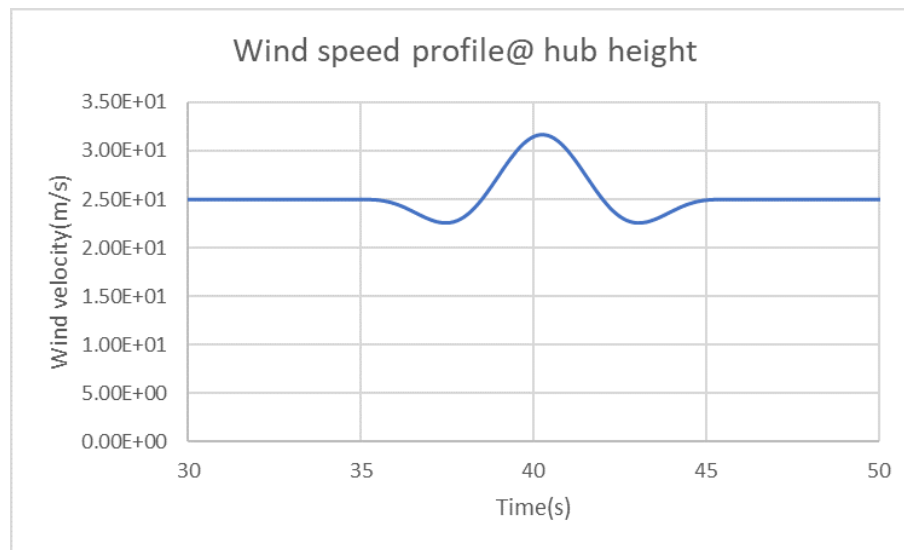


Figure 4.1: Wind speed profile

Figure 4.1 represents a wind profile with extreme operating gust subjected to the wind turbine.

Induced velocity

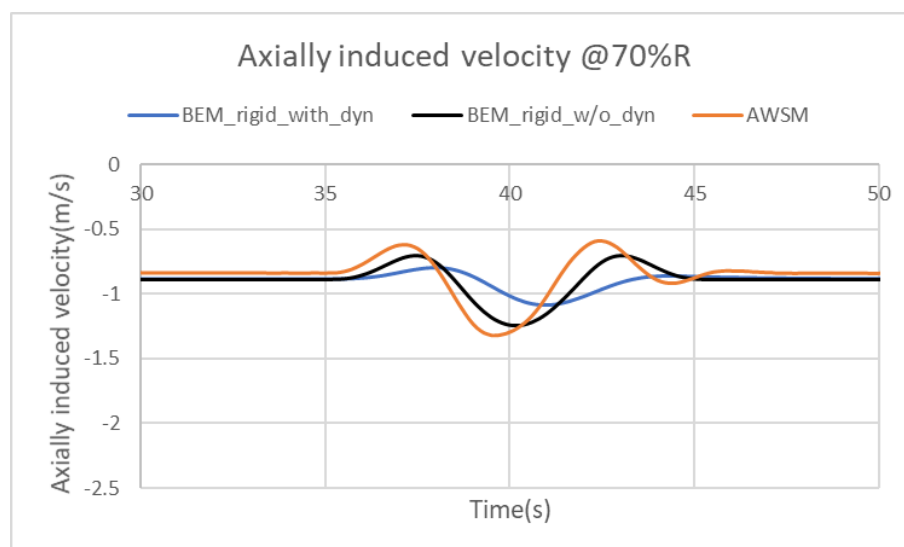


Figure 4.2: Axially induced velocity

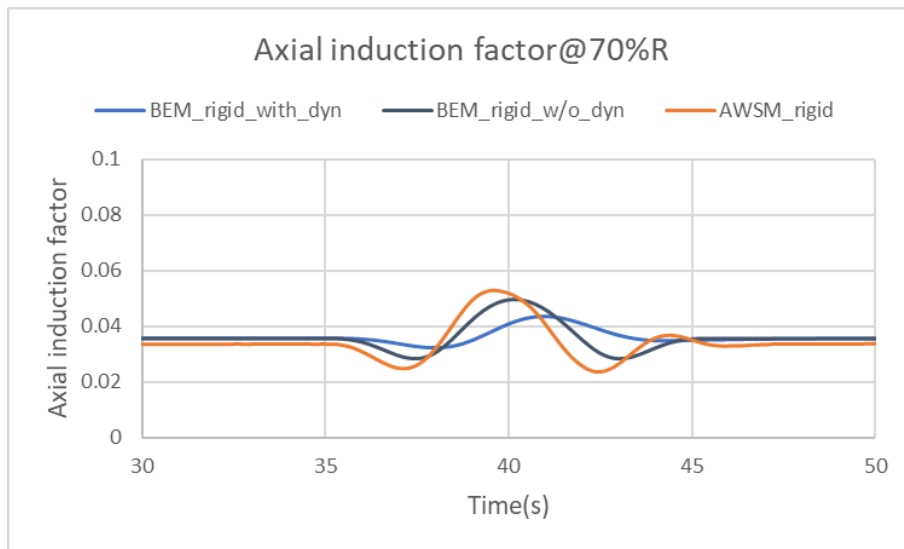


Figure 4.3: Axial induction factor

Figures 4.2 and 4.3, represent axially induced velocity and axial induction factor respectively. The axial induction factors represent a reduction in wind speed due to the rotor. In the case of the BEM without a dynamic inflow model, the induction factor appears to be maximum ($a_{max} = 0.027$). In the case of the AWSM and the BEM with a dynamic inflow model, the values of the induction factors are almost equal. In the subsequent section, the effect of the induction factor on the angle of attack shall be discussed.

Angle of attack

The angle of attack is an angle between the chord of an airfoil and the resultant wind direction.

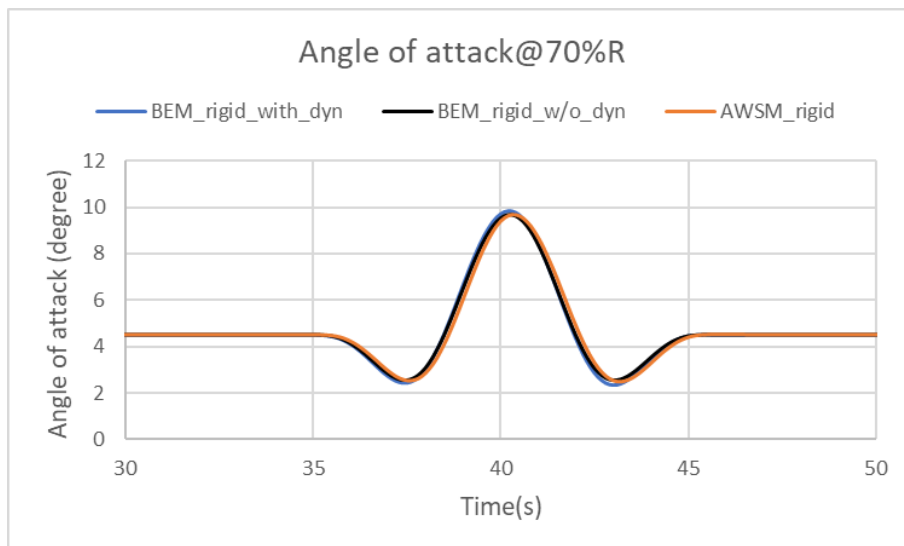


Figure 4.4: Angle of attack

Figure 4.4, represents the time series of the angle of attack. Contrast to the huge variation in the prediction of axial induced velocities, the angle of attack prediction is similar in the case of all of the aerodynamic load calculation models. The similarity in the angle of attacks leads to similar lift and drag coefficients. Reader can refer to appendix A.1 for clarifications. In the following section, the aerodynamic force prediction shall be discussed.

Normal aerodynamic force

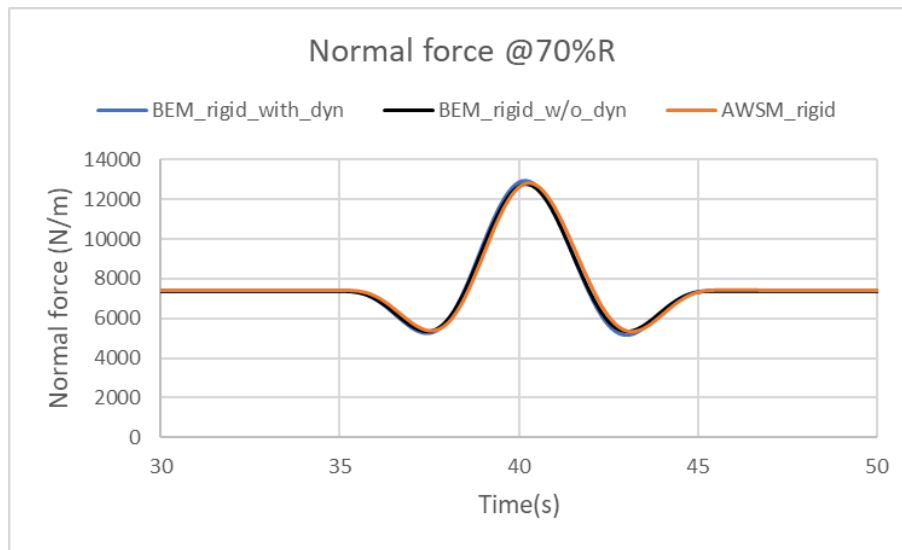


Figure 4.5: Normal aerodynamic force

In figure 4.5, the time series of the normal aerodynamic force is represented. As expected the force prediction is indeed similar for all of the aerodynamic load calculation models. As discussed in chapter 1.3, the normal force is a function of the lift coefficient and the square of resultant wind velocity. Irrespective of the significant variations in induced velocities for all of the models, the normal force prediction appears to be with a negligible variation for all of the models. The comparison of the normal force prediction can be observed in the table below.

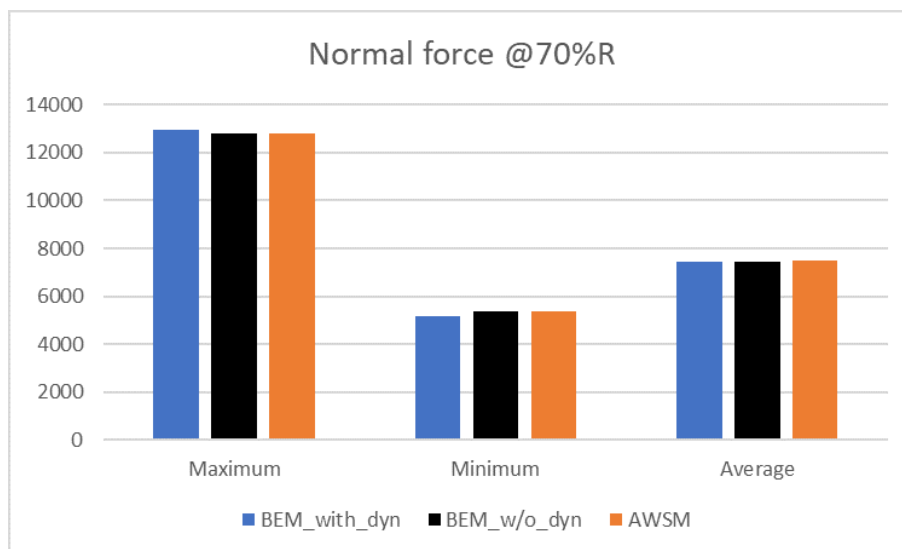


Figure 4.6: Normal aerodynamic force statistics

In figure 4.6, it is clearly visible that the higher and lower extremes and the average aerodynamic forces predicted by the aerodynamic load calculation models have a negligible variation. **The BEM model with dynamic inflow model and without dynamic inflow model predicts a 1.2% and 0.5% higher force compared to the force predicted by the vortex wake model respectively.**

DLC 23400

DLC 23400 is a load case situation included in the DLC 2.3 for the rated wind speed. Below are the load specifications exclusive for this situation.

- Wind speed- 11.40 m/s
- Pitch angle- 0°

As discussed in section 2.1.2, the AWSM model requires several settings for its usage without any errors. Below are the settings involved in carrying out the AWSM simulations-

- Time step- 0.1 seconds, equivalent to 4.2°azimuth change
- Stream-wise wake points- 539 ~ 3 rotors diameter(based on equation 2.6)
- Free stream-wise wake points- 359 ~ 2 rotors diameter (based on equation 2.6)

Wind speed profile

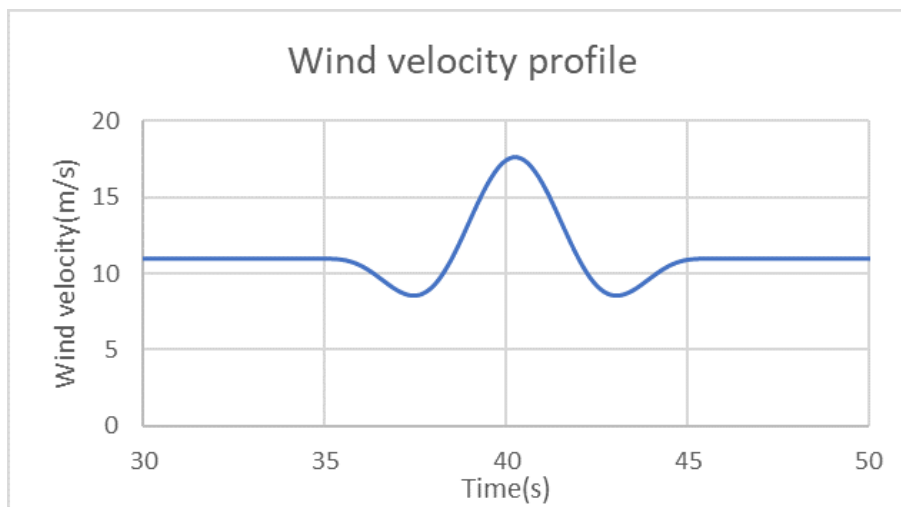


Figure 4.7: Wind speed profile

Figure 4.7, represents wind profile at hub height with extreme operating gust subjected to the wind turbine.

Induced velocity

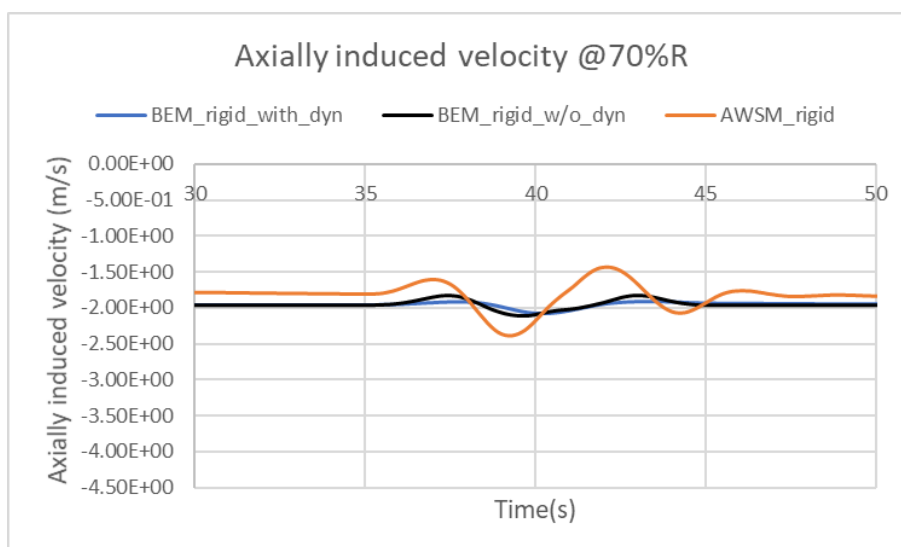


Figure 4.8: Axially induced velocity

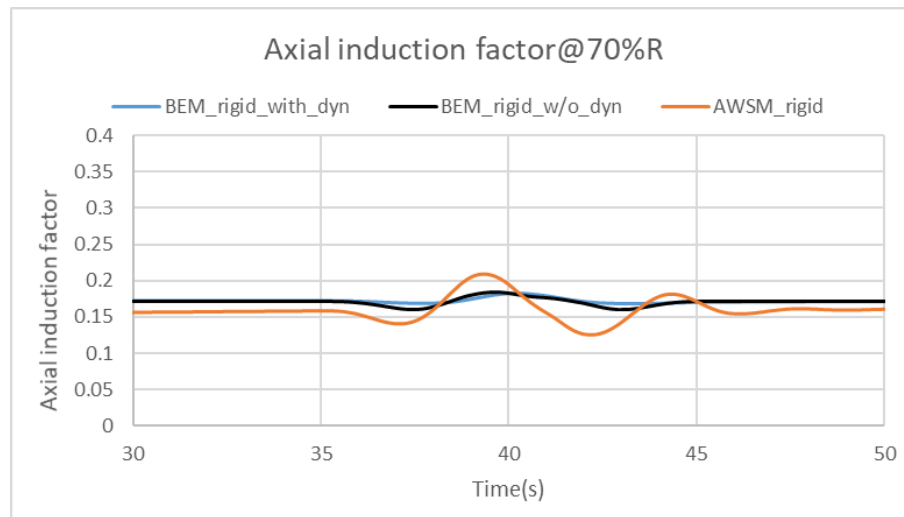


Figure 4.9: Axial induction factor

The figures 4.8 and 4.9 represent axially induced velocity and axial induction factor respectively. The axial induction factors represent a reduction in wind speed due to the rotor. The induced velocity prediction is quite similar in the case of BEM models but varies significantly in the case of the AWSM model. Similar trend can be observed in the case of the axial induction factor. In the subsequent section, the effect of induction factor on the angle of attack shall be discussed.

Angle of attack

The angle of attack is an angle between the chord of an airfoil and the resultant wind direction.

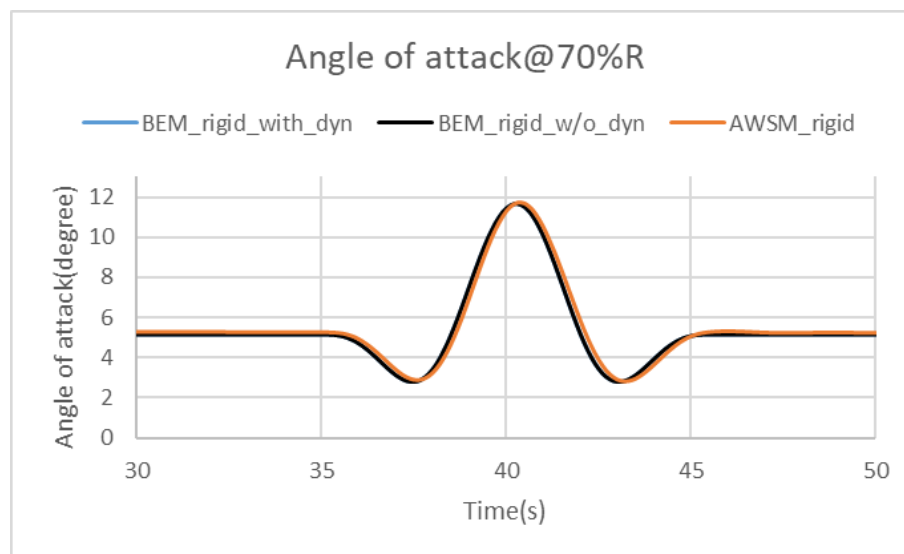


Figure 4.10: Angle of attack

Figure 4.10, represents the time series of the angle of attack. In contrast to section 4.1.2, the effect of the variation in the induction factor is percolated into the predictions of the angle of attack prediction. The angle of attack predicted by the BEM model is higher than that predicted by the AWSM model. The variation in the angle of attacks leads to variations in the lift and drag coefficients. In the following section, the aerodynamic force prediction shall be discussed.

Normal aerodynamic force

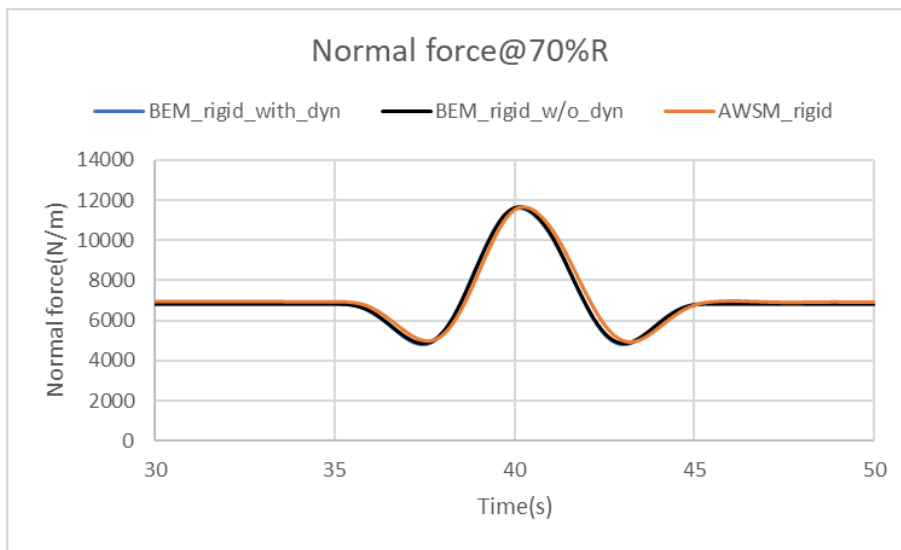


Figure 4.11: Normal aerodynamic force

In figure 4.11, the time series of the normal aerodynamic force is represented. As expected, the force predicted by the BEM models tends to be higher than that predicted by the AWSM model. As discussed in chapter 1.3, the normal force is a function of the lift and drag coefficients and the square of resultant wind velocity. The significant variations in induced velocities and the angle of attacks for all of the models are sipped into the normal force prediction. The comparison of the normal force prediction can be observed in the table below.

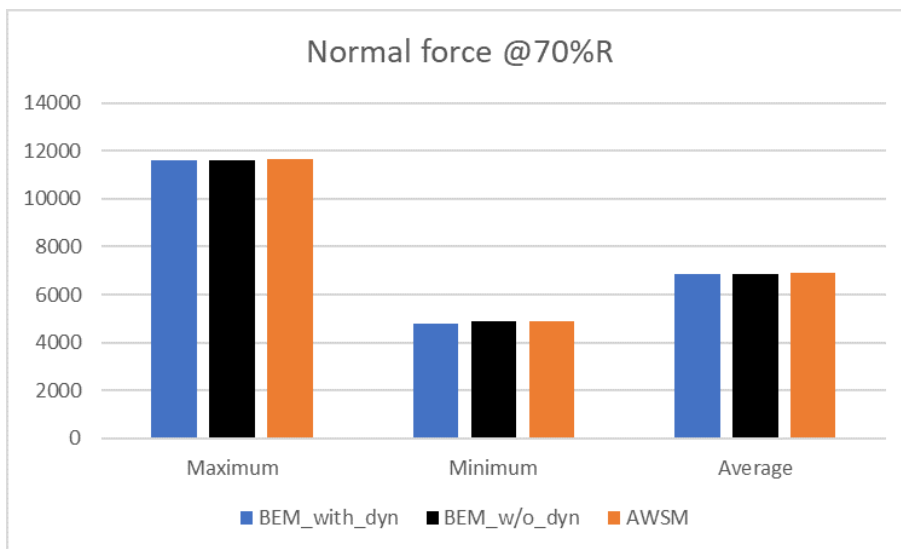


Figure 4.12: Normal aerodynamic force statistics

In figure 4.12, it is clearly visible that the higher extreme aerodynamic forces predicted by the aerodynamic load calculation models show a significant variation. **The BEM model with dynamic inflow model and without predicts 0.6% higher force compared to the force predicted by the vortex wake model.**

DLC 23200

DLC 23400 is a load case situation included in the DLC 2.3 for the rated wind speed. Below are the load specifications exclusive for this situation.

- Wind speed- 10.75 m/s

- Pitch angle- 0°

As discussed in section 2.1.2, the AWSM model requires several settings for its usage without any errors. Below are the settings involved in carrying out the AWSM simulations-

- Time step- 0.1 seconds, equivalent to 4.2° azimuth change
- Stream-wise wake points- 559 ~ 3 rotors diameter (based on equation 2.6)
- Free stream-wise wake points- 359 ~ 2 rotors diameter (based on equation 2.6)

Wind speed profile

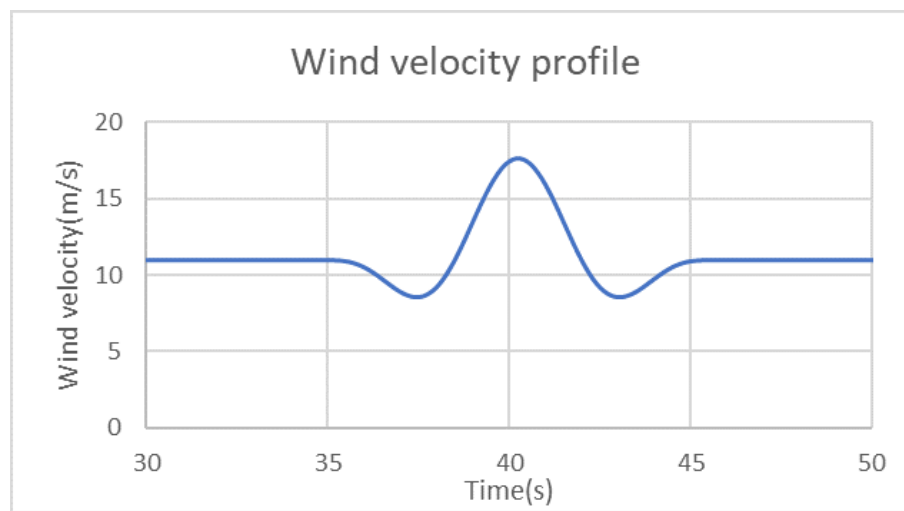


Figure 4.13: Wind speed profile

Figure 4.13, represents wind profile at hub height with extreme operating gust subjected on the wind turbine.

Induced velocity

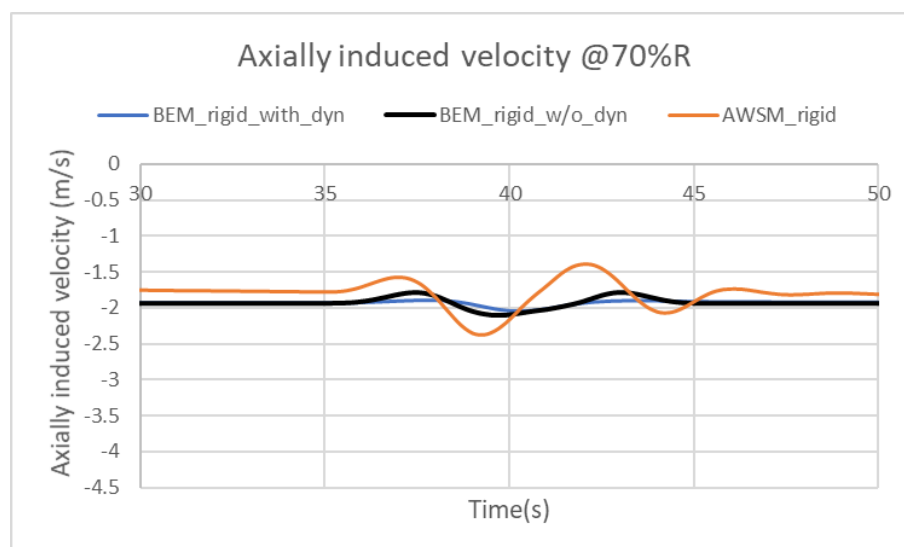


Figure 4.14: Axially induced velocity

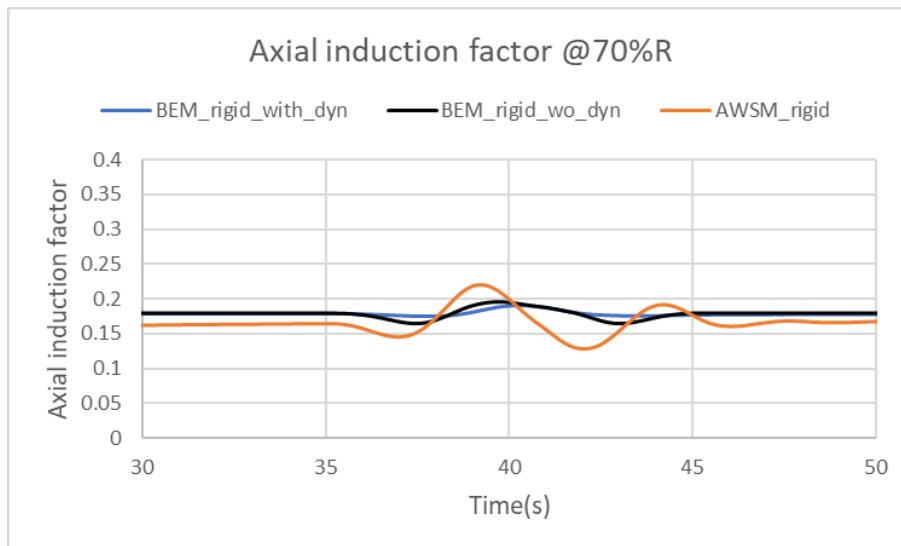


Figure 4.15: Axial induction factor

The figures 4.14 and 4.15 represent axially induced velocity and axial induction factor respectively. The axial induction factors represent a reduction in wind speed due to the rotor. The induced velocity prediction is quite similar in the case of BEM models but varies significantly in the case of the AWSM model. A similar trend can be observed in the case of the axial induction factor. In the subsequent section, the effect of the induction factor on the angle of attack shall be discussed.

Angle of attack

The angle of attack is an angle between the chord of an airfoil and the resultant wind direction.

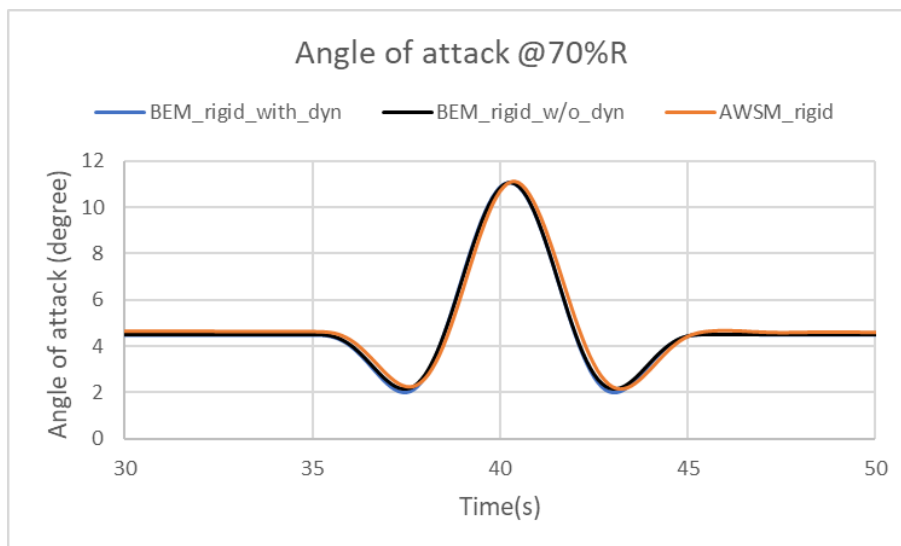


Figure 4.16: Angle of attack

Figure 4.16, represents the time series of the angle of attack. In contrast to the section 4.1.2, the effect of the variation in the induction factor is percolated into the predictions of the angle of attack prediction. The angle of attack predicted by the BEM model is higher than that predicted by the AWSM model. The variation in the angle of attacks leads to variations in the lift and drag coefficients. In the following section, the aerodynamic force prediction shall be discussed.

Normal aerodynamic force

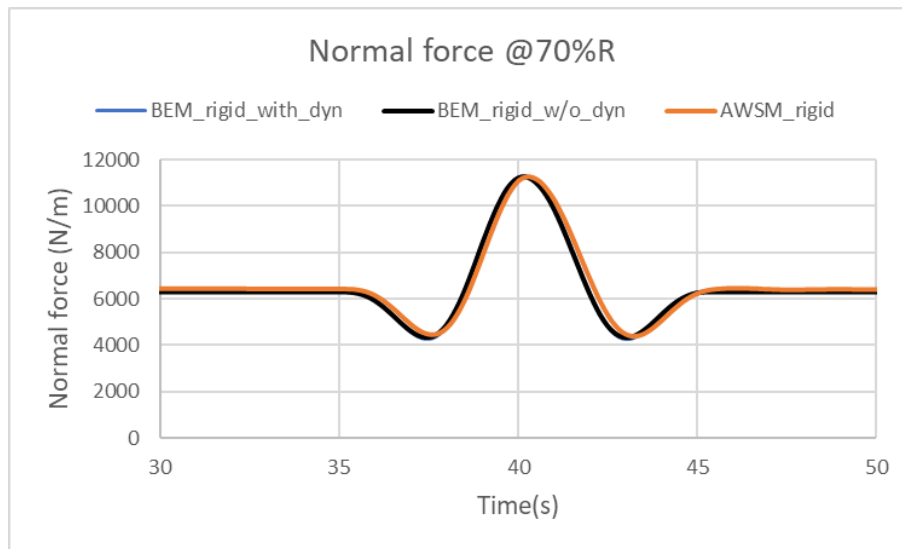


Figure 4.17: Normal aerodynamic force

In figure 4.17, the time series of the normal aerodynamic force is represented. As expected, the force predicted by the BEM models tends to be higher than that predicted by the AWSM model. As discussed in chapter 1.3, the normal force is a function of the lift and drag coefficients and the square of resultant wind velocity. The significant variations in induced velocities and the angle of attacks for all of the models are siped into the normal force prediction. The comparison of the normal force prediction can be observed in the table below.

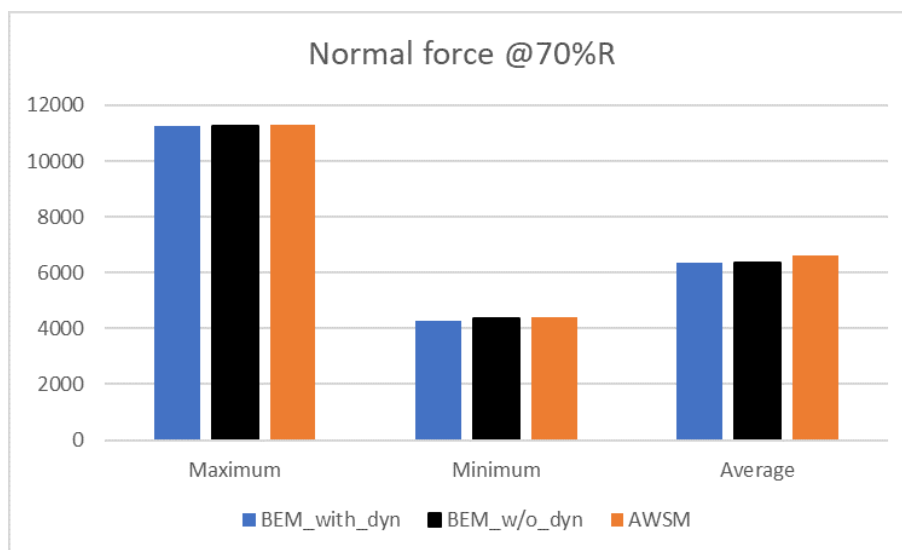


Figure 4.18: Normal aerodynamic force statistics

In figure 4.18, it is clearly visible that the higher extreme aerodynamic forces predicted by the aerodynamic load calculation models show a significant variation. **The BEM model with dynamic inflow model and without dynamic model predicts 1.0% and 0.9% higher force compared to the force predicted by the vortex wake model respectively.**

4.1.3. Analysis

- The design load case aims to discover the effect of an extreme operating gust on a wind turbine for a range of wind velocities.

- In section 4.1.2, the effect of the variations in axially induced velocities is negligible on the normal force predictions in the case of all of the aerodynamic load calculation models involved. This occurs due to very low induction which leads to a negligible effect on the resultant wind speed. Thus, this ultimately leads to a very small variation in the load prediction for all of the models.
- Similar the DLC 23816 (4.1.2), the effect of variation in axially induced velocities becomes important in the case of DLC 23400 (4.1.2) and DLC 23200(4.1.2). The normal force predicted is 0.6% and 1.0% higher in the case of DLC 23400 and DLC 23200 respectively.
- This load case was treated as a baseline load case to understand the working of both of the models. Additionally, it was understood that the effect of the calculation of the induced velocity shall play an important role in the analysis of other load cases.
- For example- the addition of 2 liters of the water into a tank with 10 litre water shall have a significant effect on the volume of water than that by adding 2 litres of water to a tank with 100 liters of water. This analogy shall explain the effect of induced velocities discussed in this chapter more clearly.
- Additionally, it was observed that in the case of constant wind field the force calculated by both of the models displayed variation. This variation is illustrated in the figure 4.19. The variation was essentially due to different procedure involved in the calculation of the induced velocities by both of the models. The reader can refer to the [4] for the validation.

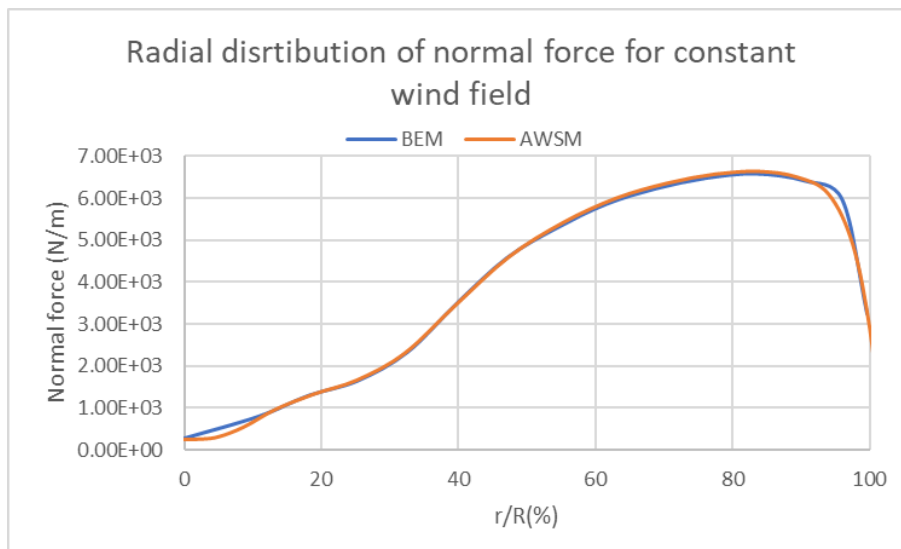


Figure 4.19: Radial distribution of the Normal force in the case constant wind field

4.2. DLC 3.3

This section discusses the results and analysis regarding the DLC 3.3 from the IEC 61400-3 standard.

4.2.1. Load case description

The DLC 3.3 is a start-up load case with an extreme direction change at a certain time during the start-up process. The extreme direction change leads to an oblique inflow condition. The load case takes into account start-up speed ranging from the cut-in wind velocity to cut-out wind velocity. The wind direction change is implemented by allowing the wind flow from the 'V' direction which is parallel to the plane of the rotor. The average wind velocity is maintained constant by decreasing the wind velocity from the 'U' direction. The angle of direction change is constant for the whole range of wind velocities. The simulations were carried out with the AWSM model and the BEM model with the ECN Yaw model in the Focus6 environment. The simulations are done without any pitch control. The load case specification involved are as follows

Table 4.2: Load case specifications

General specifications		
Specification	Value	Unit
Direction change angle	31.7432	degree
Starting yaw angle	0	degree
Pitch angle	0	degree
Wind velocity	10.75	m/s
Rotor speed	7.95	rpm

4.2.2. Results and observations

The section discusses the results and the observations obtained by simulating the load case with different aerodynamic load calculation models. To understand the effect of the direction change on the load predictions, the angle of the direction change was varied. Further, in this section the effect of direction change shall be discussed in brief.

Case A

In this case, the angle of direction change is considered to be equal to the angle suggested in the IEC 61400-3 standard.

As discussed in section 2.1.2, the AWSM model requires several settings for its usage without any errors. Below are the settings involved in carrying out the AWSM simulations-

- Time step- 0.1 seconds, equivalent to 4.77°azimuth change
- Stream-wise wake points- 572 ~ 3 rotors diameter (based on equation 2.6)
- Free stream-wise wake points- 381 ~ 2 rotors diameter (based on equation 2.6)

Wind speed profile

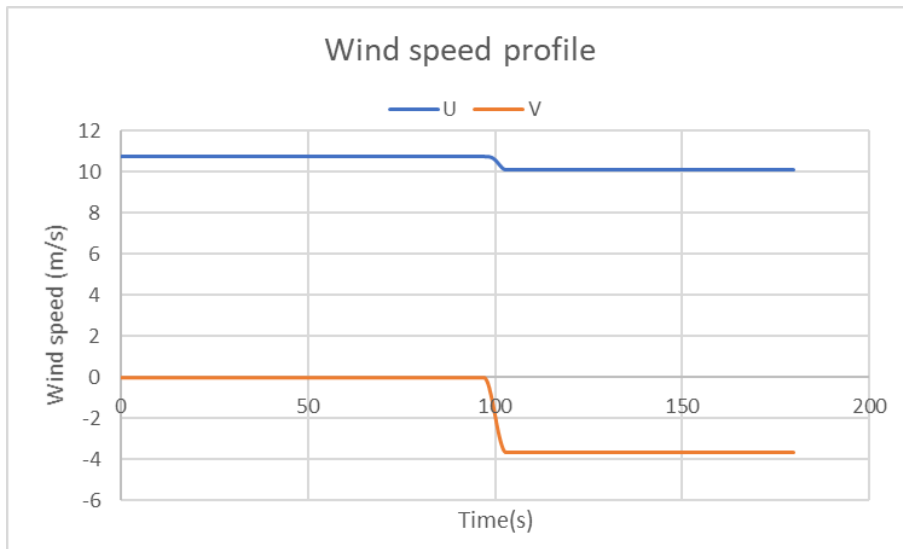


Figure 4.20: Wind velocity profile

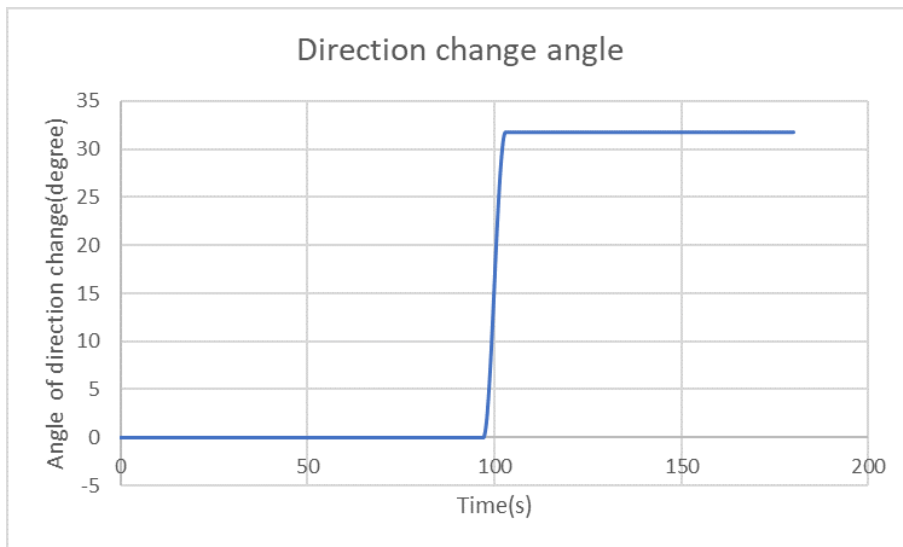


Figure 4.21: Direction change angle

Figures 4.20 and 4.21, represent wind velocity profile at the hub height and variation in the wind direction respectively. The wind direction change starts at 97 seconds and it remains constant further during the simulation.

Axial Induction

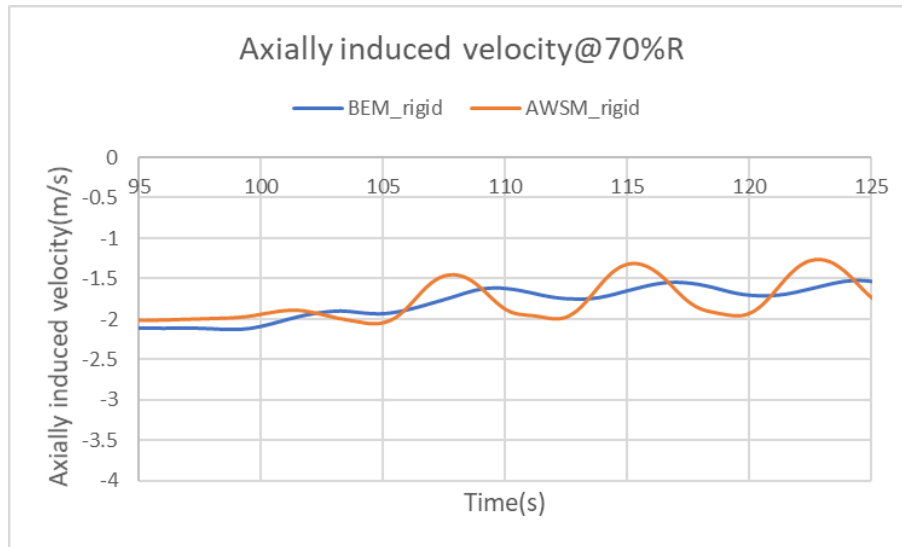


Figure 4.22: Axially induced velocity

The figure 4.22, represents a time series of axially induced velocity. The magnitude of axially induced velocity decreases with the beginning of the direction change. The main reason for the significant variation in the axially induced velocity is the methodology incorporated by the models. The AWSM model includes the vortex strength due to vortices developed along the lifting line. Whereas the BEM model does not take into consideration the effect of induced vorticity and thus a flat graph can be seen for the BEM model in figure 4.22.

The angle of attack

The angle of attack is a function of the resultant wind velocity (W) and the chord. Whereas, the vortex theory also takes into the account effect of induced velocity. The lift coefficient is given by $C_l = 2\pi\alpha$ in case of steady aerodynamics. In the case of unsteady aerodynamics the lift coefficient loses its linearity and thus, the relation between lift coefficient and the angle of attack becomes parabolic.

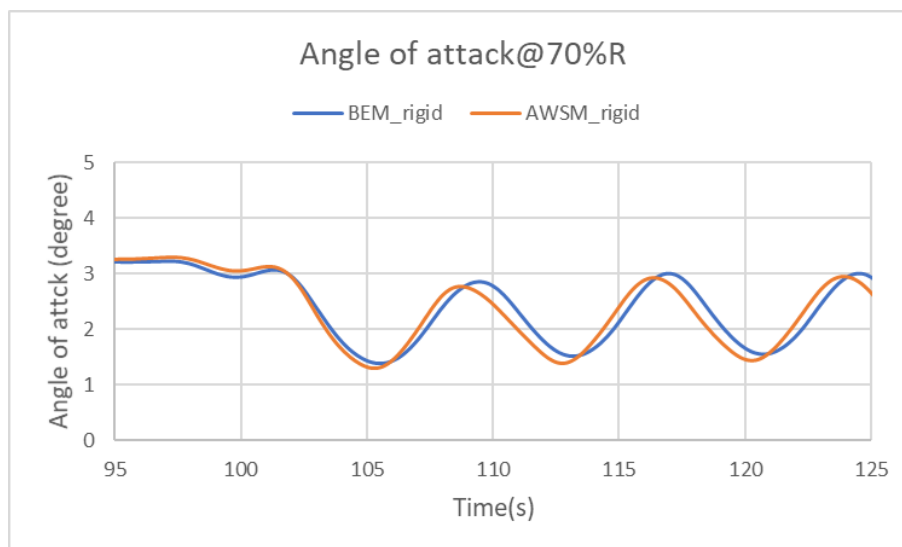


Figure 4.23: Angle of attack

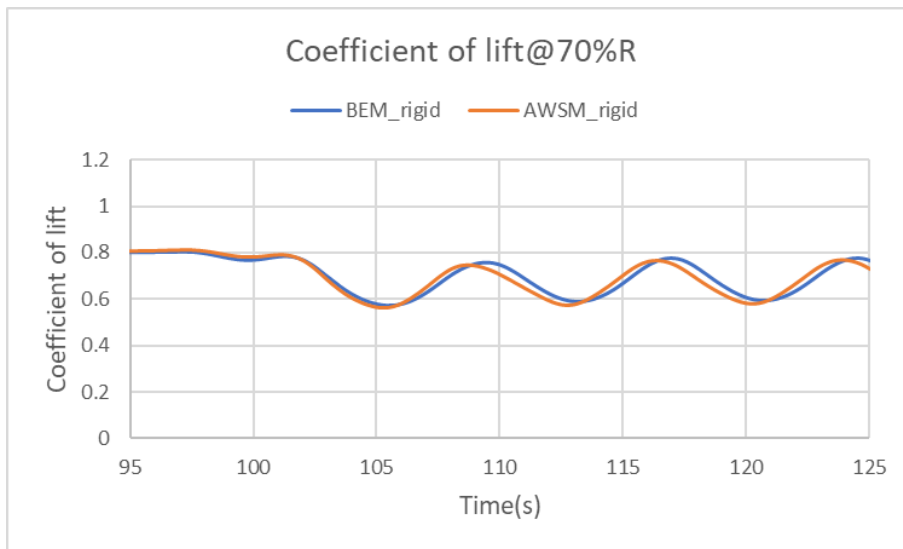


Figure 4.24: Lift coefficient

The figures 4.23 and 4.24, represent the time series of the angle of attack and lift coefficient respectively. Both of the terms (C_l and α) show variations in trends. The terms predicted by the AWSM model appear to have slightly larger amplitude as compared to the BEM model. In the consequent sections, the effect of an axially induced velocity and the lift coefficients on the normal force will be discussed.

Normal Aerodynamic force

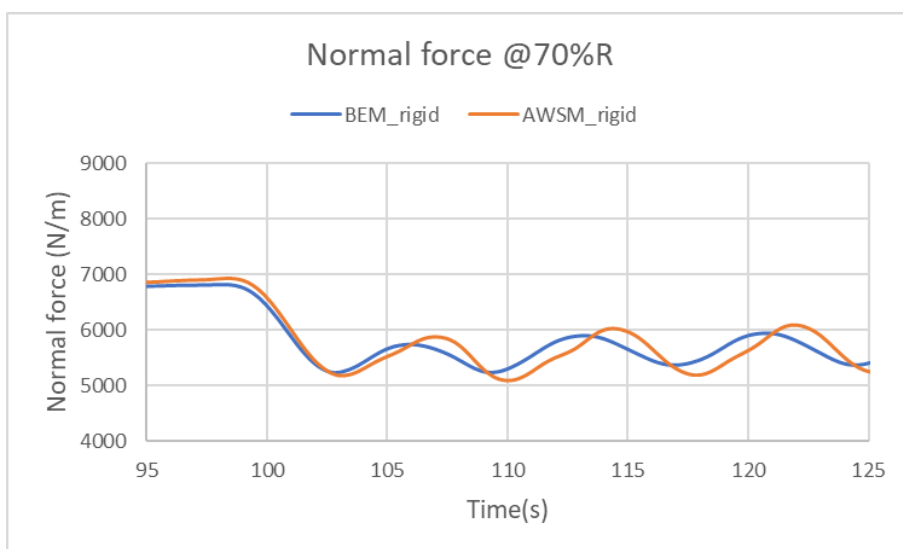


Figure 4.25: Normal force

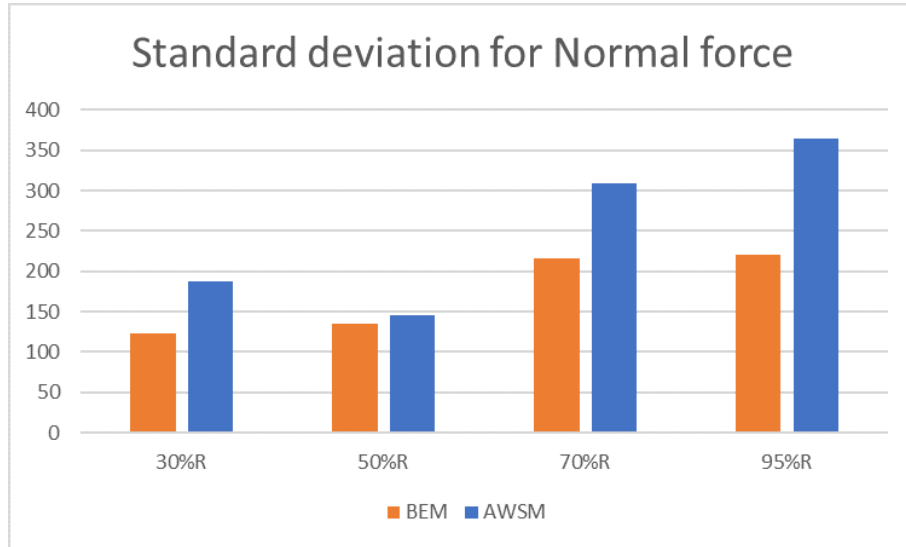


Figure 4.26: Comparison of the standard deviation of the normal force at different radial locations

The figures 4.25, represents the time series of the normal aerodynamic force the lift force. In contrast to the trend of the angle of attack and lift coefficient in figure 4.23, the amplitude of the normal force. Additionally, in figure 4.26 it can be also observed that the standard deviation of the normal force is higher at most of the radial locations. However, the magnitude of the differences increases with radius. As we discussed in chapter 1.3, the lift force is the function of the lift coefficient and square of the resultant wind velocity (W). The resultant wind velocity in case of a yawed flow is given by-

$$W = \sqrt{(U \cos \phi_y - u')^2 + (\omega r + U \sin \phi_y \cos \phi_{azim})^2} \quad (4.1)$$

Where-

ϕ_y = Oblique angle

ϕ_{azim} = Azimuth angle

The formulation of the above equation 4.1 can be found in [26].

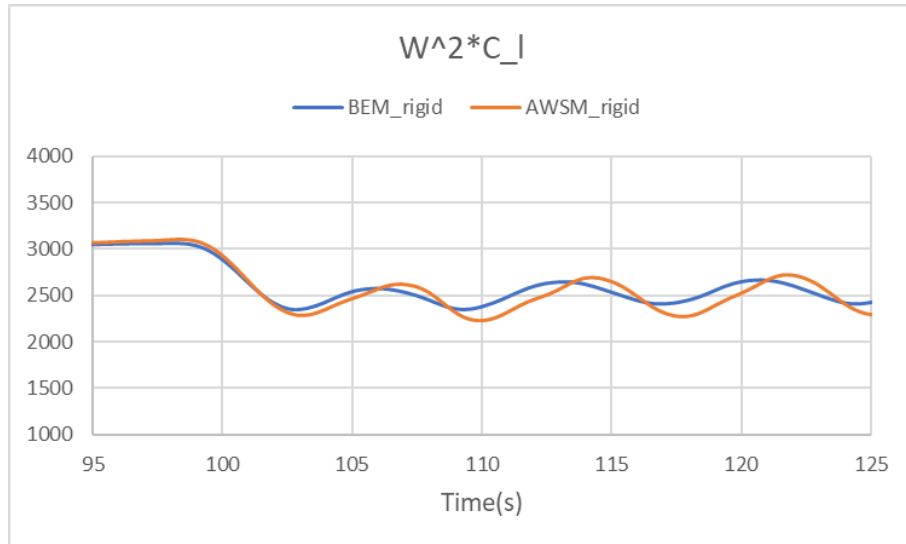


Figure 4.27: Product of the lift coefficient and the square of resultant wind velocity

Figure 4.27, represents the product of lift coefficient and square of the resultant wind velocity for both of the load calculation models. From the figure it can be incurred that the the product of the lift coefficient and square of the resultant wind velocity is in a good agreement with the normal force.

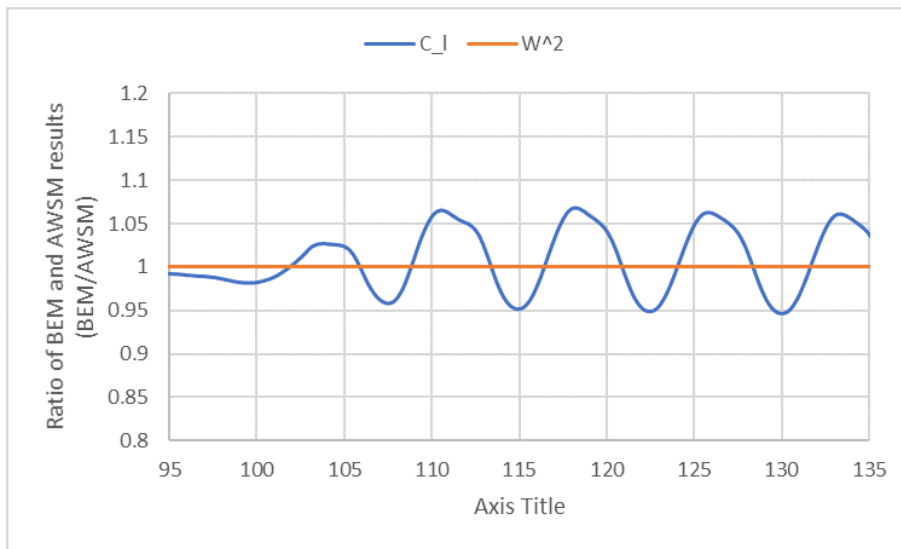


Figure 4.28: Effect of lift coefficient and resultant wind velocity on the normal force

Figure 4.28, represents the time series of the ratio of the BEM and the AWSM models for the lift coefficient and the square of resultant wind velocity. As we know, the lift force is the function of the product of the lift coefficient and square of resultant wind velocity. From figure 4.28, it is clear that the lift coefficient plays a significant role than that played by the effective wind velocity in the lift force calculations by the two models. From figures 4.22, 4.24 and 4.28 it can be observed that the induced velocity in the axial direction is the root cause for the variation in the calculation of the lift force. Furthermore, this effect of the induced velocity can be also observed in the normal force. It may be noted that the standard deviation after direction of the function ($C_l * W^2$) predicted by the AWSM model **24.8%** is higher than that by the BEM model. Additionally, the standard deviation after direction change of the normal force predicted by the AWSM model is **29%** higher than that predicted by the BEM model. The two ratios mentioned above are in good alignment with each other.

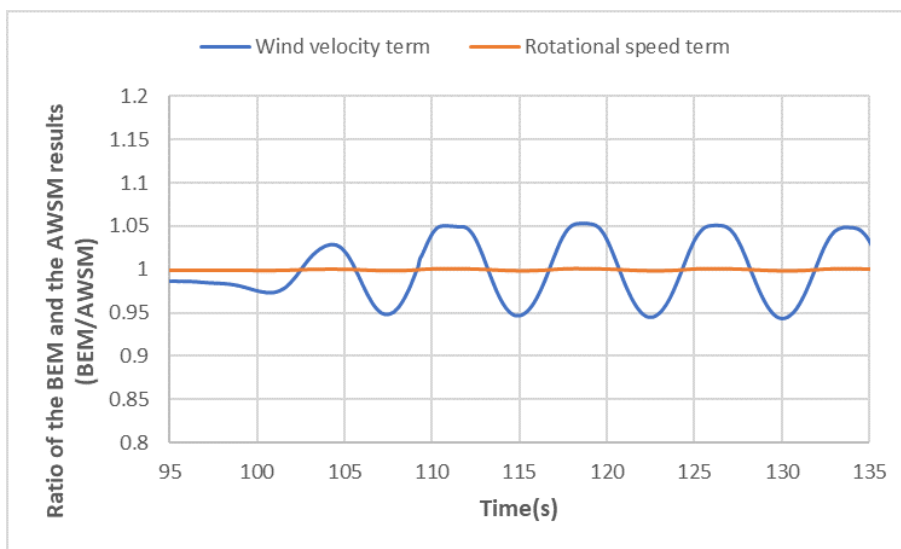


Figure 4.29: Decomposition of effective wind velocity term

As we know that the rotational speed term in equation 4.1 is constant for both of the load calculation models. Therefore, the wind velocity term in equation 4.1 accounts for the variation in the effective wind velocity. This is well illustrated in figure 4.29.

Case B

In case B, the angle of direction change is considered to be equal to 40° . As discussed in section 2.1.2, the AWSM model requires several settings for its usage without any errors. Below are the settings involved in carrying out the AWSM simulations-

- Time step- 0.1 seconds, equivalent to 4.77° azimuth change
- Stream-wise wake points- 572 ~ 3 rotors diameter (based on equation 2.6)
- Free stream-wise wake points- 381 ~ 2 rotors diameter (based on equation 2.6)

Wind speed profile

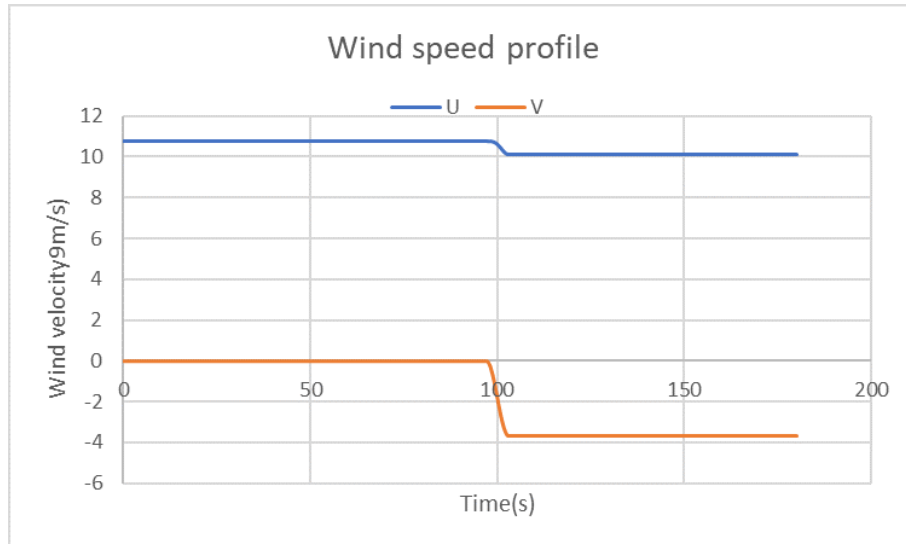


Figure 4.30: Wind velocity profile

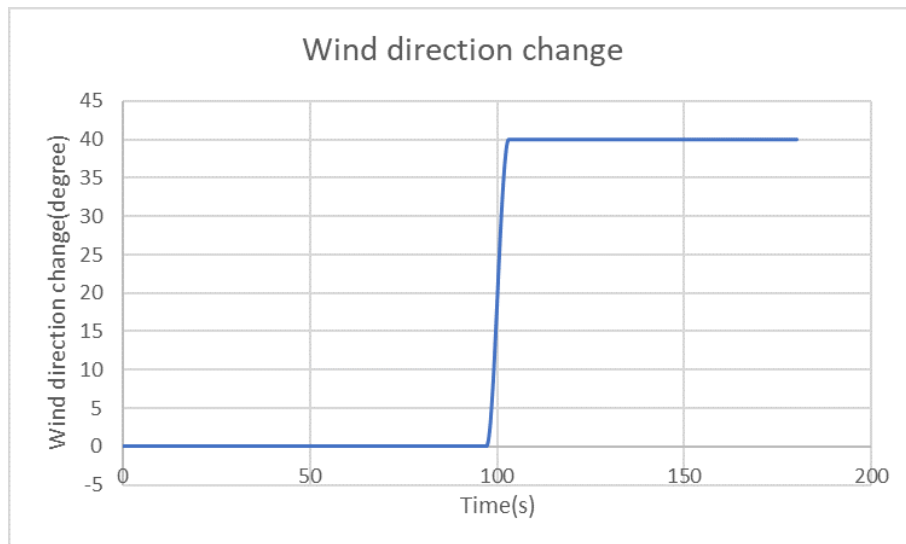


Figure 4.31: Direction change angle

Figures 4.30 and 4.31, represent the wind velocity profile at the hub height and variation in the wind direction respectively. The wind direction change starts at 97 seconds and it remains constant further during the simulation.

Axial Induction

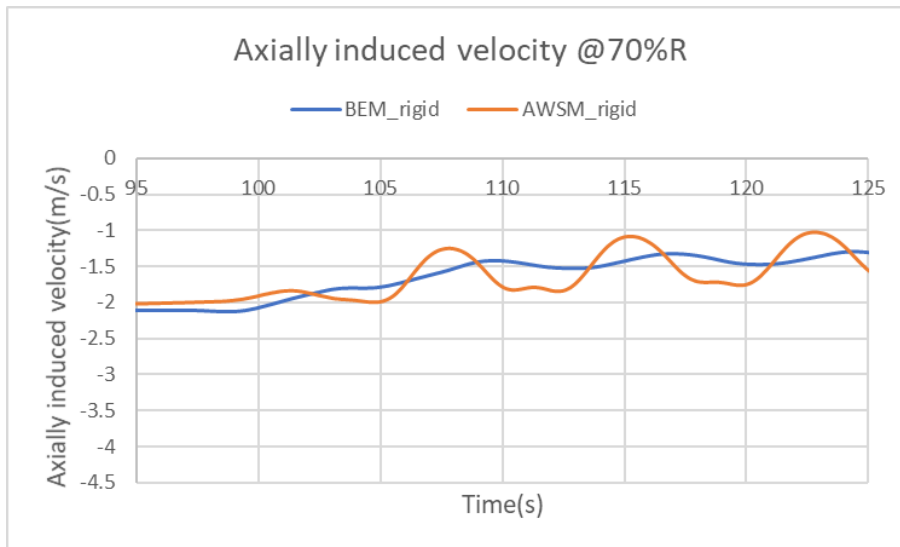


Figure 4.32: Axially induced velocity

Figure 4.32, represents axially induced velocity. Compared to the case A and B, wind speed reduction after the wind direction change is a higher in the case C. This occurs due to a higher angular change in the wind direction. Essentially, this could lead to small variations in the results of force prediction for both of the models used. This shall be discussed in the following sections.

Angle of attack

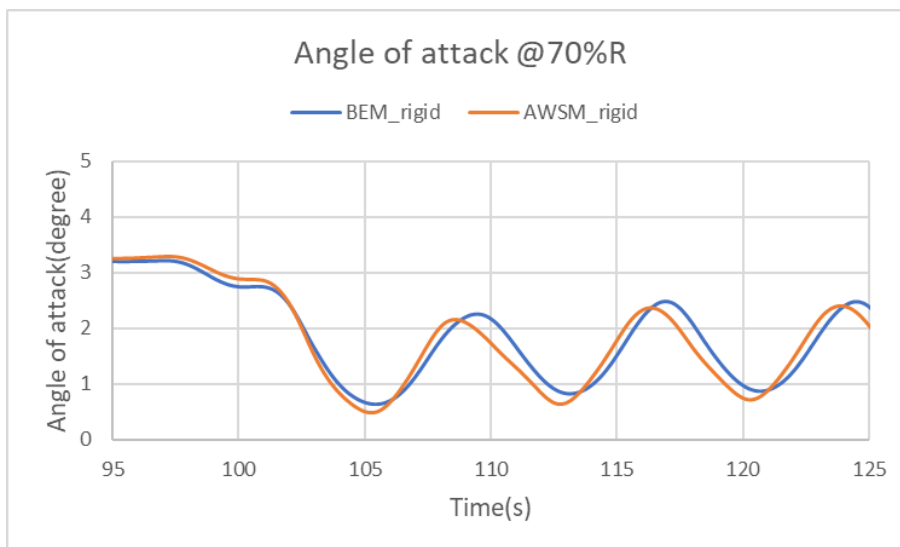


Figure 4.33: Angle of attack

Figure 4.33, represents the time series of the angle of attack. The angle of attack predicted by the BEM model is slightly higher than that predicted by the vortex wake model. At times, in the case of the AWSM model, a negative angle of attack can also be observed. This happens due to comparatively low resultant wind velocity subjected to the turbine. This may indeed lead to a similar trend for lift and drag coefficients.

Normal Aerodynamic force

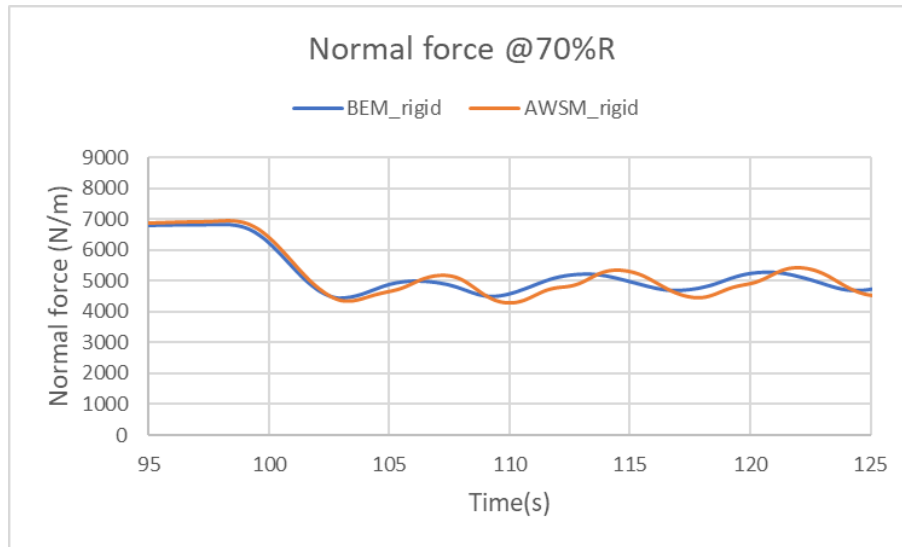


Figure 4.34: Normal force

Figure 4.34, represents the time series of normal aerodynamic force. Similar to case A in section 4.2.2, the normal force prediction by the AWSM model is quite higher than that predicted by the BEM model. The reason for such a variation is discussed extensively in the case A. The reader can refer to it for further clarification. In the consequent section, a comparative study of the cases included in this chapter shall be discussed.

4.2.3. Comparative study

In this section, a comparative study of the cases discussed in the previous sections shall be discussed. The study involves a comparison of extreme load results obtained from the BEM and the AWSM model simulations. The study focuses on the yaw misaligned region.

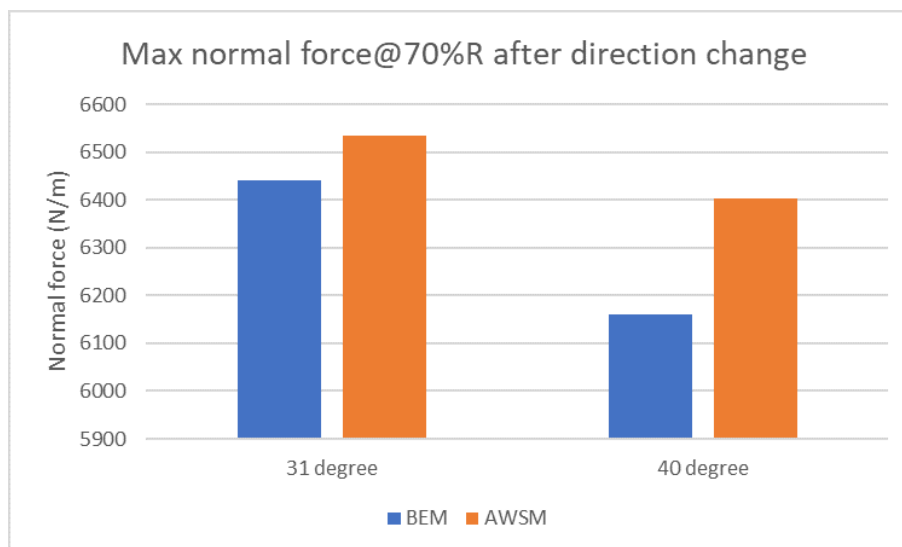


Figure 4.35: Maximum extreme normal force

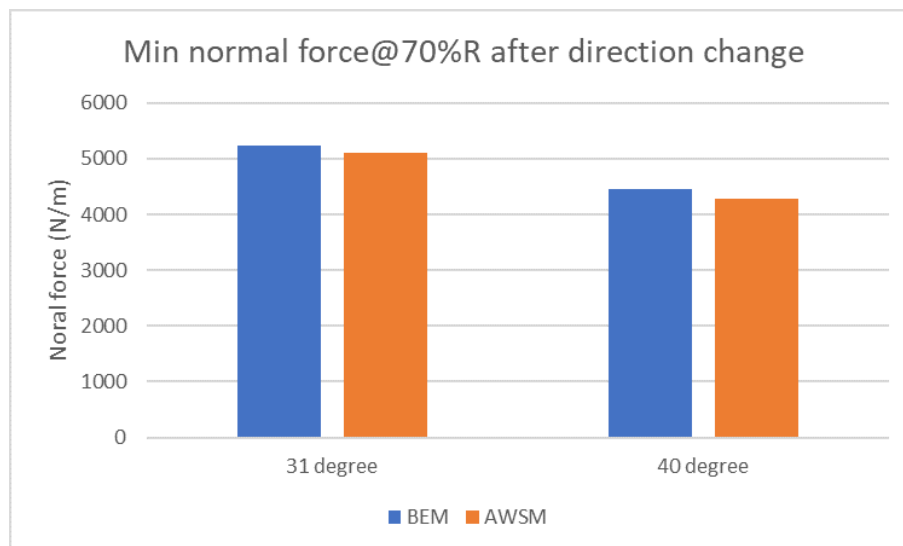


Figure 4.36: Minimum extreme normal force

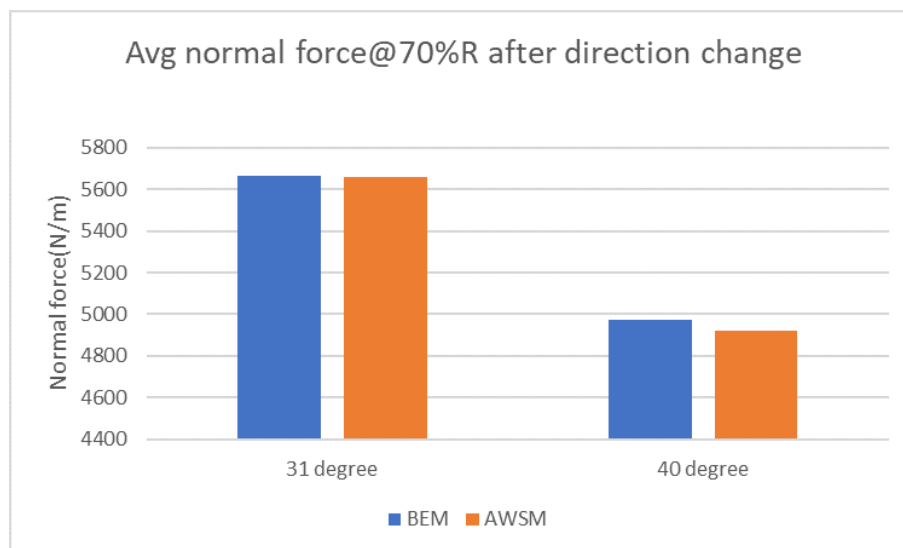


Figure 4.37: Average normal force

Figures 4.35, 4.36, 4.37 and 4.38, represent a comparison of extreme load test results for different direction change angles with the BEM and the AWSM simulations.

In figure 4.35, the maximum normal force predicted by the AWSM model is higher than that predicted by the BEM model. This is true for all of the direction change angles. However, the difference between the extremes obtained from both of the models does not remain constant. The maximum extreme normal force predicted by the AWSM model is 1.6% and 3.8% higher than the BEM model for direction change angle of 31° and 40° respectively.

In figure 4.36, the minimum normal force predicted by the AWSM model is lower than that predicted by the BEM model. This is true for all of the direction change angles. However, the difference between the extremes obtained from both of the models does not remain constant. The minimum extreme normal force predicted by the AWSM model is 2.8% and 3.8% lower than the BEM model for direction change angle of 31° and 40° respectively.

In figure 4.37, the average normal force predicted by the AWSM model is almost equal to that predicted by the BEM model. This is true for all of the direction change angles. Unlike the maximum and minimum extreme loads, the difference between the average normal force is also constant. The average normal force

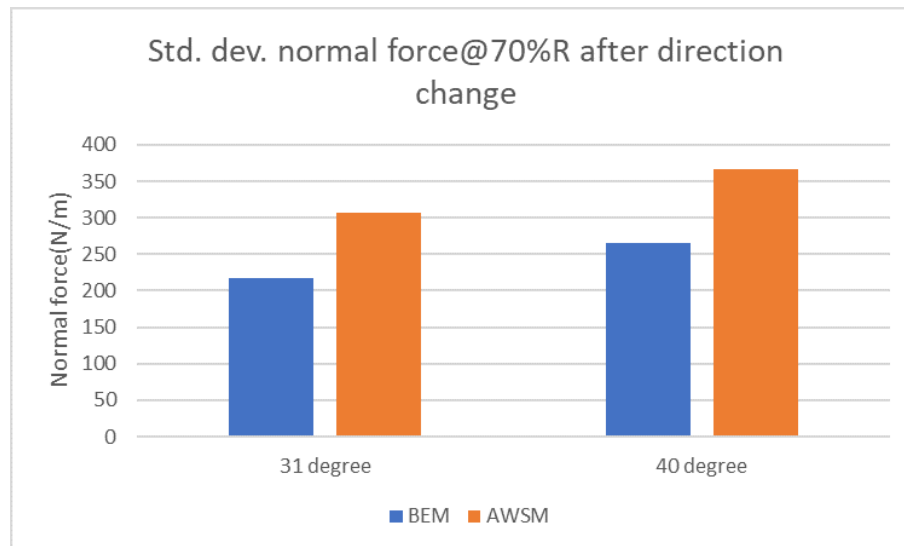


Figure 4.38: Standard deviation

predicted by the AWSM model is 0.1% and 0.9% higher than the BEM model for direction change angle of 31° and 40° respectively.

In figure 4.38, the standard deviation of the normal force predicted by the AWSM model is extremely higher than that predicted by the BEM model. This is true for all of the direction change angles. Furthermore, the difference between the standard deviation obtained from both of the models remains constant. The standard deviation of the normal force predicted by the AWSM model is 29.9% and 27.2% higher than the BEM model for direction change angle of 31° and 40° respectively.

The huge difference between the standard deviation may lead to higher fatigue loads. Often, it is discussed that the BEM model over predicts the fatigue loads, but this appears to be a contrast for this blade location and the load situation.

4.2.4. Analysis

- The load case situation violates the assumption of an axial inflow condition involved in the BEM model. The violation of the assumptions led to significantly different results than those obtained from the AWSM model in figure 4.38. The analyses in this section is based on the AVATAR wind turbine model and may vary in the case different wind turbine models.
- It is often discussed that the BEM model predicts a higher fatigue load than that predicted by the vortex wake model. However, in the case of yawed flow, the amplitude of loads predicted by the BEM model is smaller than that predicted by the vortex wake model. This observation can be validated in the manual of the ECN-Aeromodule[4].
- The main reason for a higher fatigue loading in the case of the AWSM model can be derived from the variation in the prediction of the lift coefficient in the case of the AWSM model and the BEM model. Furthermore, it can be concluded that differences in the prediction of the axial induced velocities by both of the models have led to the variations in the lift coefficients and subsequently to the variation in the force calculations in the case of the yawed inflow conditions.
- In the case of the axial inflow condition, the trends of axial induction are similar and flat in the case of both of the BEM and the AWSM model. This flatness in the amplitude starts transforming into a sinusoidal wave as the angle of yaw misalignment increases.
- This trend can also be further observed in the case of normal force prediction. In figure 4.38, the difference between standard deviation of the normal forces remains almost constant for each of the yaw misalignment angle in the case of both of the models. However, the magnitude of the standard deviation keeps on increasing with the angle of yaw.

-
- The effect of the pitch angle was also found to be significant. With addition of the pitch angle to the blade, the variation in the axial induction decreases and subsequently the variation in the normal force by both of the models.
 - An experimental validation can be performed to validate this load case because the results seem to be quite critical for wind turbine design.

4.3. DLC 1.3

In this section, the results and analysis of the DLC 1.3 as mention in section 3.3.2 shall be discussed extensively.

4.3.1. Load case description

As discussed in the previous section 3.3, the DLC 1.3 is a normal power production load case. The load case situation involves a turbulent inflow condition. The load case situation is designed for the range of wind velocities from 7 m/s to cut-out wind velocity. Additionally, a positive and a negative yaw angle can be applied to add up complexities in the load situation. The reference turbulence intensity is maintained constant for the whole range of wind velocities, whereas the standard deviation of the wind velocity field subjected to the rotor is given by the following equation [16]-

$$\sigma_1 = c I_{ref} (0.072 (\frac{V_{avg}}{c} + c) (\frac{V_{hub}}{c} - 4) + 10) \quad (4.2)$$

where, $c = 2 \text{ m/s}$

In equation 4.2, represents the standard deviation of the wind velocity field. The standard deviation depends on the wind velocity at hub height and the reference turbulence intensity. The simulations were carried out with the AWSM model and the BEM model with the ECN dynamic inflow model in the Focus6 environment. In the subsequent sections, two load case situations (with and without yaw misalignment) shall be discussed. The load case specification involved are as follows-

Table 4.3: DLC 1.3 load case specifications

General Specifications		
Specification	Value	Unit
Wind regime	IEC Class 1A	-
Turbulence model	ETM	-
Reference turbulence intensity	0.16	-
Wind velocity	10.75	m/s
Rotor speed	7.95	rpm
Simulation time	300	seconds

The simulation time was reduced from 600 seconds (as given in the IEC standards) to 300 seconds. The reduction in the simulation time was done in order to speed up the AWSM model simulations.

4.3.2. Results and observations

In this section, the results obtained by simulating the load case with two aerodynamic load calculation models discussed in the previous sections are discussed. The section is divided into few subsections which shall aim to discuss several load case situations as described in the IEC design load case standard.

DLC 13119

DLC 13119 is a load situation designated for the rated wind velocity. The wind flow is considered to be axial, that is, without yaw misalignment. As discussed in section 2.1.2, the AWSM model requires several settings for its error-free application. Below are the settings involved in carrying out the AWSM simulations-

- Time increment- 0.1 seconds (equivalent to 4.21° azimuth change)
- Stream-wise wake points- 572 ~ 3 rotors diameter (based on equation 2.6)
- Free stream-wise wake points- 381 ~ 2 rotors diameter (based on equation 2.6)

Wind velocity profile

Figure 4.45 represents the wind speed profile with turbulence subjected to the wind turbine.

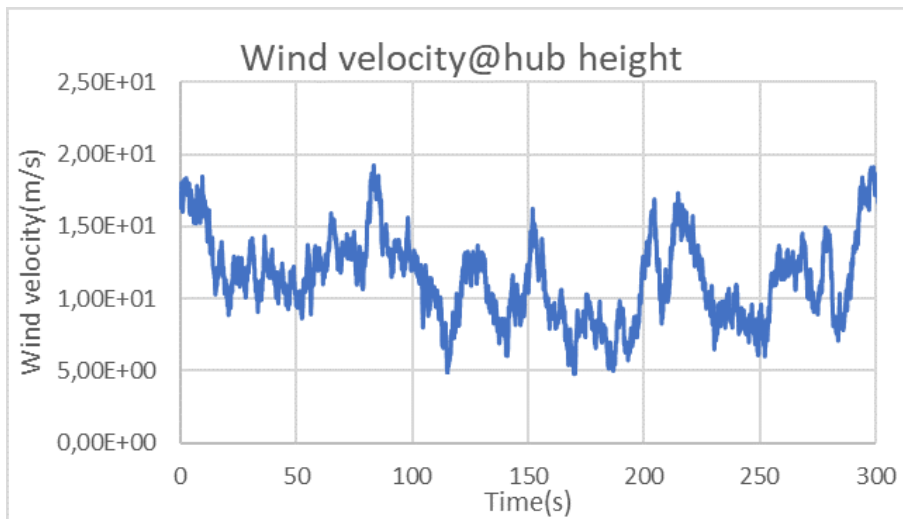


Figure 4.39: Wind speed profile

Induced velocity

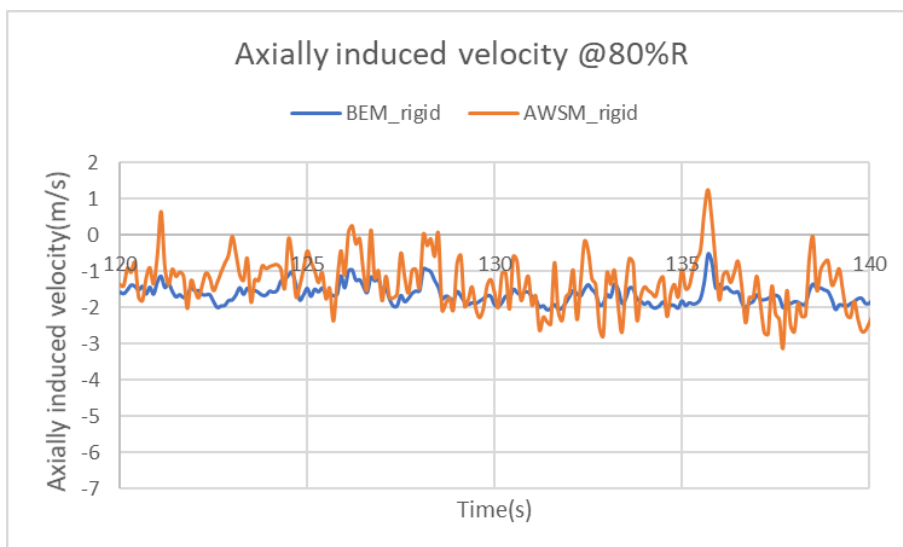


Figure 4.40: Axially induced velocity

Figures 4.40 and 4.41, represent axially induced velocity and axial induction factor respectively. The axial induction factor represents a reduction in wind speed due to the rotor. The vortex wake model treats the blade more locally for varying inflow wind velocities. Whereas, the BEM model balances the induced velocity field along the stream-tube. This leads to the differences in the angle of attack and the normal force prediction in the case of the BEM model and the AWSM model.

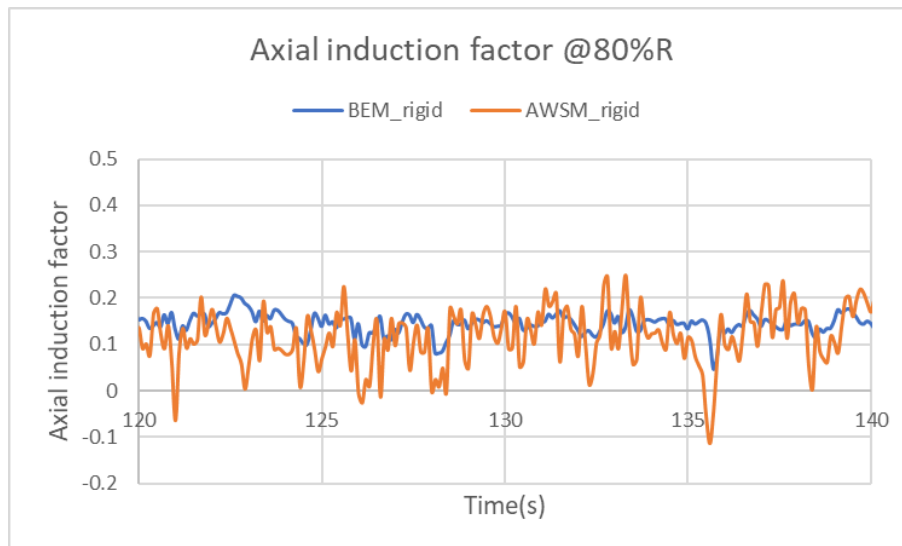


Figure 4.41: Axial induction factor

Angle of attack

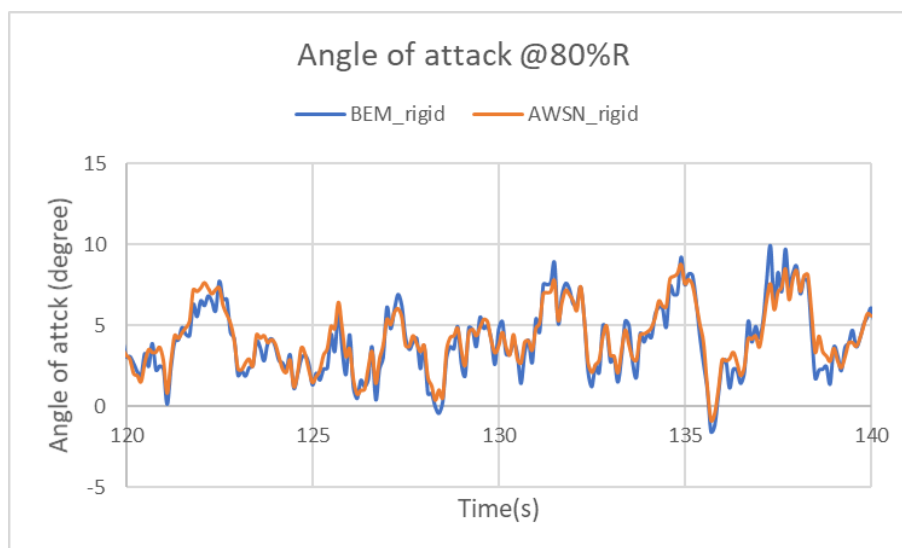


Figure 4.42: Angle of attack

Figure 4.42 represents, the time series of the angle of attack. The results obtained from both the models vary significantly. The differences in the calculation of the axially induced velocities in the case of the BEM and the AWSM simulations have led to such variations in the results. In the subsequent section, a comparative analysis of the normal force shall be discussed.

Normal force

Figure 4.43 represents a time series of the normal force for both the models used. The variation in the calculation of the axial induction and the angle of attack have led to a variation in the normal force prediction by both of the models. The normal force predicted by the BEM model is 7.3% higher than that predicted by the AWSM model. As represented in figure 4.44, the signal location of 80%R is selected because at this radial location the normal force was marked to be maximum.

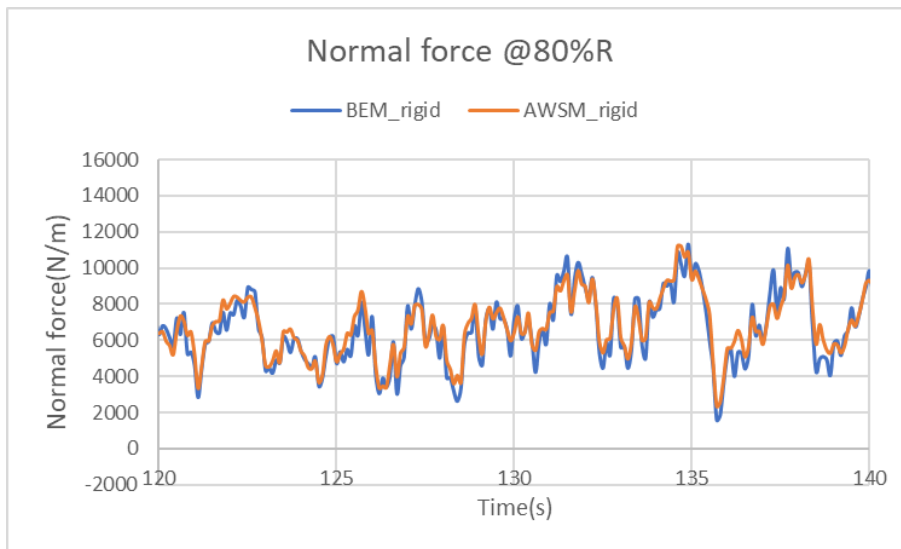


Figure 4.43: Normal force

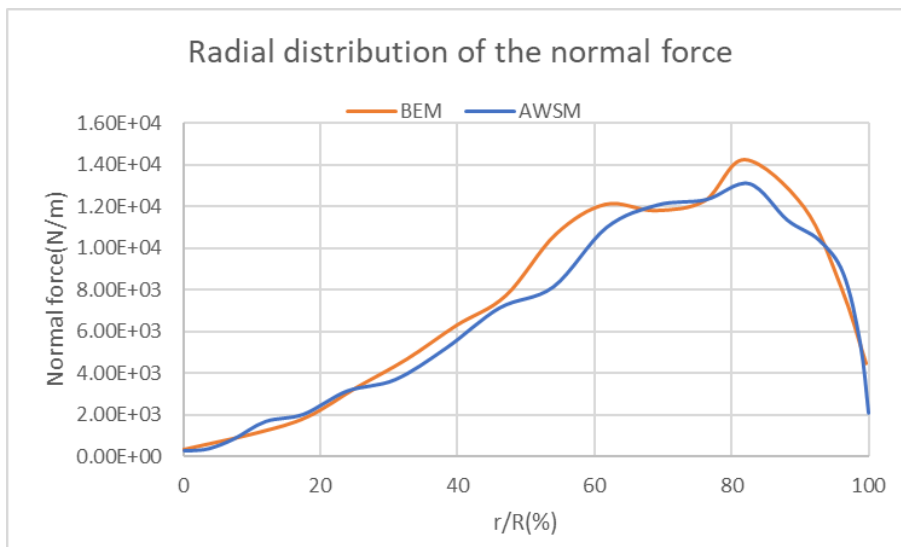


Figure 4.44: Radial distribution of the normal force at the time which marks the maximum normal force.

Table 4.4: Normal force statistics

Normal force(N/m) @80%R			
	BEM	AWSM	Difference
Maximum	14792.82	14079.85	4.8%
Minimum	-475.95	-547.62	-
Average	6818.32	6788.21	0.4%
Std. Dev.	2496.33	2353.51	5.7%

In the above table, the extreme normal force is tabulated. As in table 4.4, the standard deviation of the normal force predicted by the BEM model is around 5.7% higher than that predicted by the AWSM. The reason behind this higher load prediction was mentioned previously. The difference in the extreme loads and the normal force amplitude lead to the difference in the standard deviation for the normal force. Thus, the larger standard deviation in the case of the BEM model may reflect into higher fatigue load.

DLC 13116

DLC 13119 is a load situation designated for the rated wind velocity. The wind flow is considered to be yawed, that is, with a yaw misalignment of $+8^\circ$. As discussed in section 2.1.2, the AWSM model requires several settings for its error-free application. Below are the settings involved in carrying out the AWSM simulations-

- Time increment- 0.1 seconds (equivalent to 4.21° azimuth change)
- Stream-wise wake points- 572 \sim 3 rotors diameter (based on equation 2.6)
- Free stream-wise wake points- 381 \sim 2 rotors diameter (based on equation 2.6)

Wind velocity profile

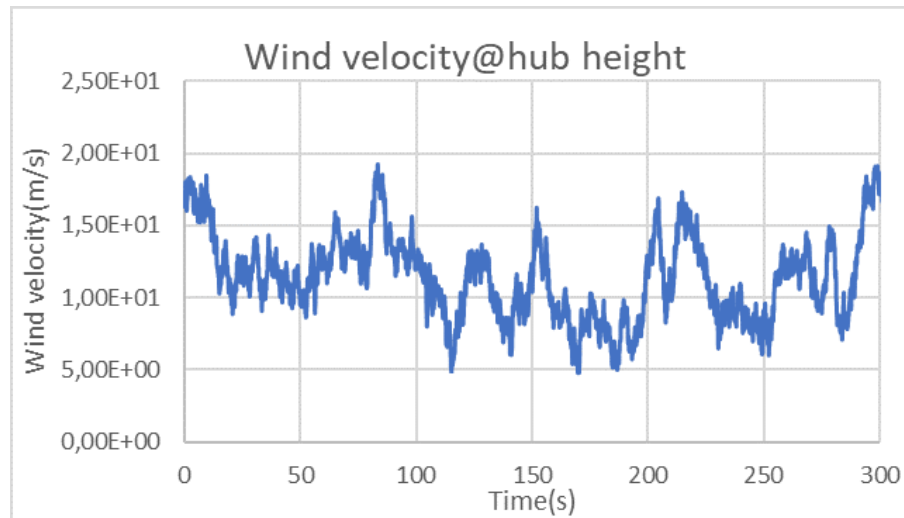


Figure 4.45: Wind speed profile

Figure 4.45 represents the wind profile with turbulence subjected to the wind turbine.

Induced velocity

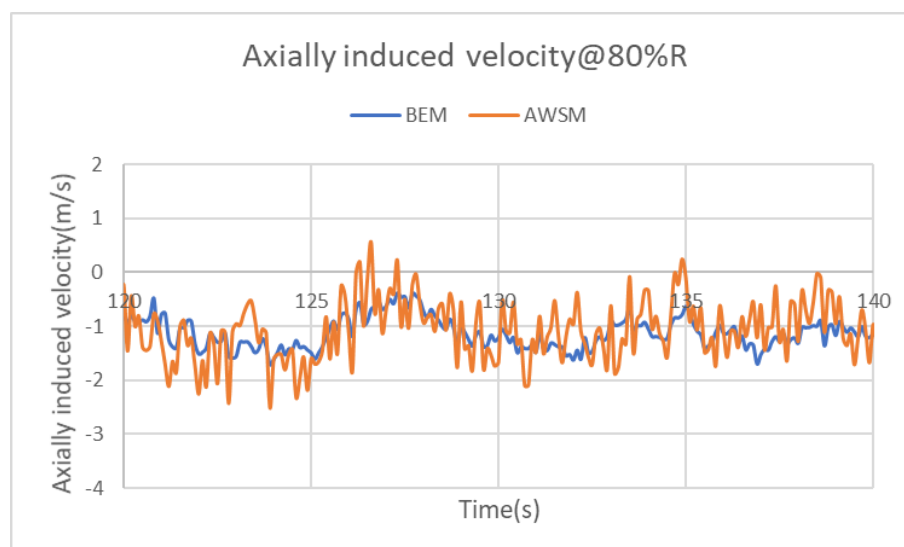


Figure 4.46: Axially induced velocity

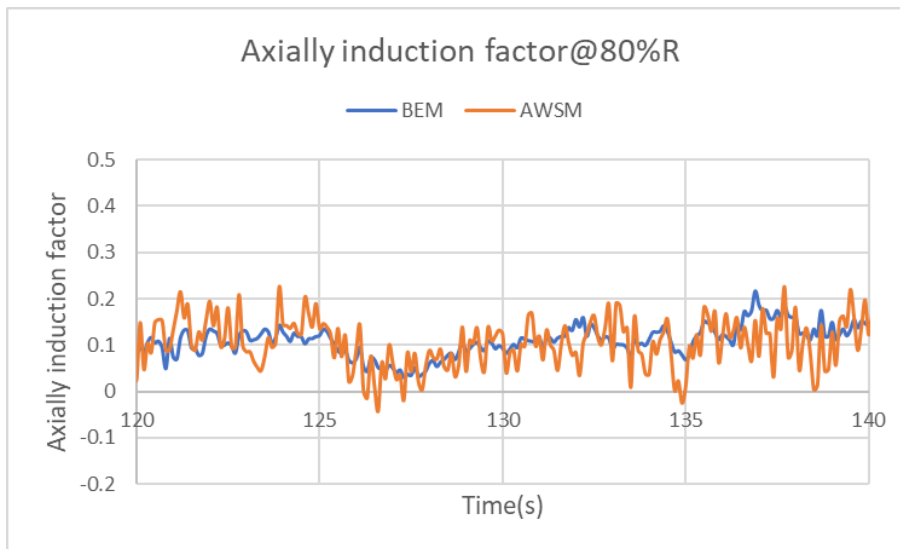


Figure 4.47: Axial induction factor

Angle of attack

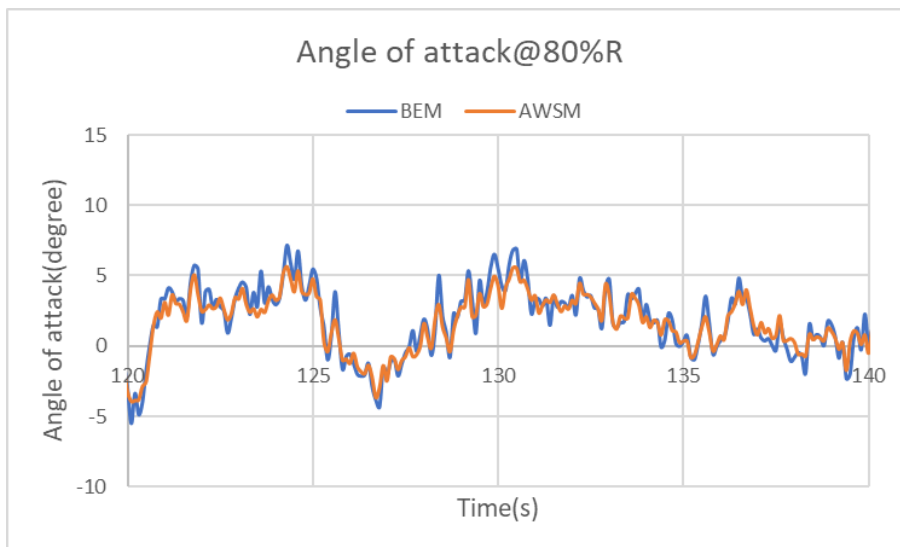


Figure 4.48: Angle of attack

Figure 4.48 represents, the time series of the angle of attack. The results obtained from both of the models vary significantly. The difference in the calculation of the axially induced velocities by both of the models has led to such variation in the results. In the subsequent section, a comparative analysis of the normal force shall be discussed.

Normal force

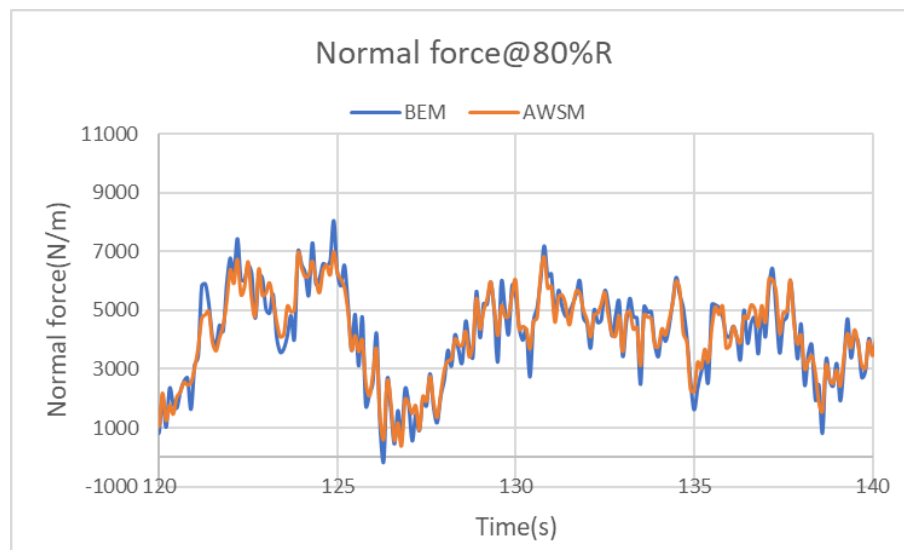


Figure 4.49: Normal force

Figure 4.49 represents a time series of the normal force for both of the models used. The variations in calculation of the axial induction and the angle of attack have led difference in the normal force prediction by both of the models. The normal force predicted by the BEM model is 6.9% higher than that predicted by the AWSM model.

Table 4.5: Normal force statistics

Normal force(N/m) @80%R			
	BEM	AWSM	Difference
Maximum	14130.65	13149.95	6.9%
Minimum	-409.13	108.5	-
Average	5581.65	5578.36	0.058%
Std. Dev.	2257.64	2095.21	7.2%

In the above table, the extreme normal force is tabulated. As in table 4.4, the maximum normal force predicted by the BEM model is 6.9% higher than that predicted by the AWSM. The reason behind this higher load prediction is mentioned previously. The difference in the extreme loads and the normal force amplitude lead to the difference in the standard deviation for the normal force. Thus, the larger standard deviation in the case of the BEM model may reflect into higher fatigue load.

4.3.3. Analysis

- In this load case situation, the turbulent wind inflow field leads to a violation of the assumptions of the steady and uniform wind inflow involved in the BEM model. This violation of the assumption led to variations in the results obtained by both of the models.
- The fatigue loads appear to be higher in the case of the BEM model for both of the inflow situations. The fatigue loading is higher for the BEM model due to the violation of the assumption of steady and uniform inflow conditions.
- The higher prediction of the fatigue loads by the BEM model may lead to the over-designing of the rotor. This may probably make the design safer but would increase the material cost involved. Eventually, increasing the capital investment and the LCOE for wind energy.
- Additionally, it can be observed that the turbine with rigid structure predicts higher magnitude of loads for both of the aerodynamic load calculation models. However, the difference between the standard

deviation of the normal force predicted by both of the models decreases in the case of rigid rotor. The results in the case of a flexible rotor can be found in the appendix.

- This load case situation may not be appropriate for the analysis of the yawed inflow conditions because of the very small yaw misalignment angle. Thus, very scarce variation is noted for the condition of the yawed and turbulent inflow.

4.4. DLC 1.2

In this section, the results and conclusions of the DLC 1.2 mentioned in section 3.3.2 shall be discussed extensively.

4.4.1. Load case description

As discussed in the previous section 3.3, the DLC 1.2 is a normal power production load case. The load case situation involves a turbulent inflow condition. The load case situation is designed for the range of wind velocities from cut-in wind velocity to cut-out wind velocity. Additionally, a positive and a negative yaw angle can be applied to add up complexities in the load situation. DLC 1.2 is the most significant fatigue load case described in the IEC 61400-3 standard. The reference turbulence intensity is maintained constant for the whole range of wind velocities, whereas the standard deviation of the wind velocity field subjected to the rotor is given by the following equation [16]-

$$\sigma_1 = I_{ref}(0.075V_{hub} + b) \quad (4.3)$$

where, $b = 5.6$ m/s

In equation 4.3, represents the standard deviation of the wind velocity field. The standard deviation depends on the wind velocity at hub height and the reference turbulence intensity. The simulations were carried out with the AWSM model and the BEM model with the ECN dynamic inflow model in the Focus6 environment. In the subsequent sections, two load case situations (with and without yaw misalignment) shall be discussed. The load case specification involved are as follows-

Table 4.6: DLC 1.2 load case specifications

General Specifications		
Specification	Value	Unit
Wind regime	IEC Class 1A	-
Turbulence model	NTM	-
Reference turbulence intensity	0.16	-
Wind velocity	10.75	m/s
Rotor speed	7.95	rpm
Simulation time	300	seconds

The simulation time was reduced from 600 seconds (as given in IEC standards) to 300 seconds. The reduction in the simulation time was done in order to speed up the AWSM model simulations.

4.4.2. Results and observations

In this section, the results obtained by simulating the load case with two aerodynamic load calculation models discussed in the previous sections are discussed. In section 4.3, it was concluded that the load situation with a turbulent wind inflow and small yaw angle does not reproduce significantly different results than that produced in the case of axial turbulent inflow conditions. Therefore, the section focuses on the comparative analysis of the fatigue load results with an axial wind inflow condition.

DLC 12112

DLC 12112 is a load situation designated for the rated wind velocity. The wind flow is considered to be axial, that is, without yaw misalignment. As discussed in section 2.1.2, the AWSM model requires several settings for its error-free application. Below are the settings involved in carrying out the AWSM simulations-

- Time increment- 0.1 seconds (equivalent to 4.21° azimuth change)
- Stream-wise wake points- 572 ~ 3 rotors diameter (based on equation 2.6)
- Free stream-wise wake points- 381 ~ 2 rotors diameter (based on equation 2.6)

Wind velocity profile

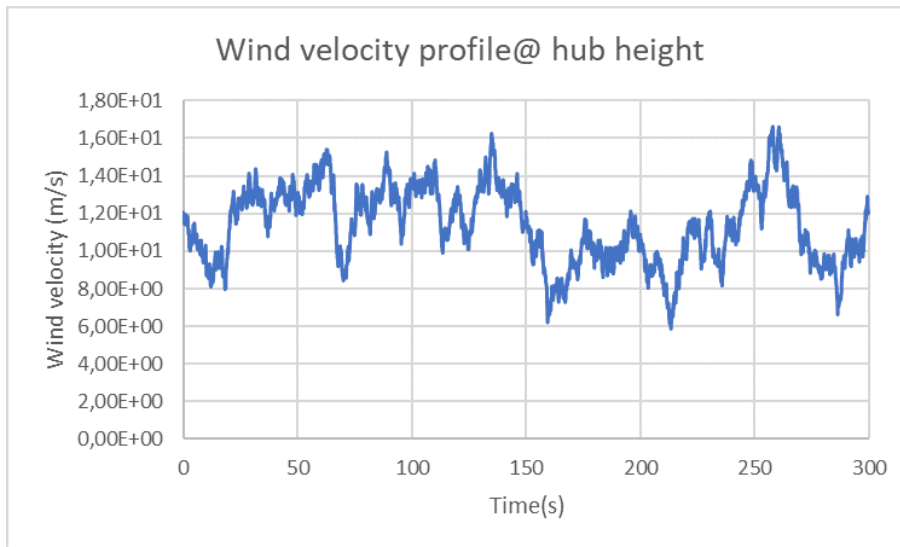


Figure 4.50: Wind speed profile

Figure 4.50 represents the wind speed profile with turbulence subjected to the wind turbine.

Induced velocity

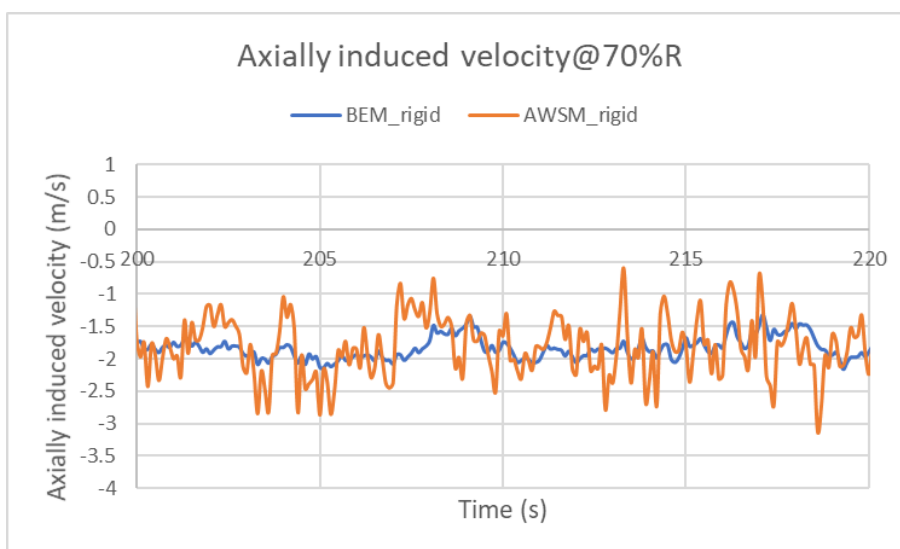


Figure 4.51: Axially induced velocity

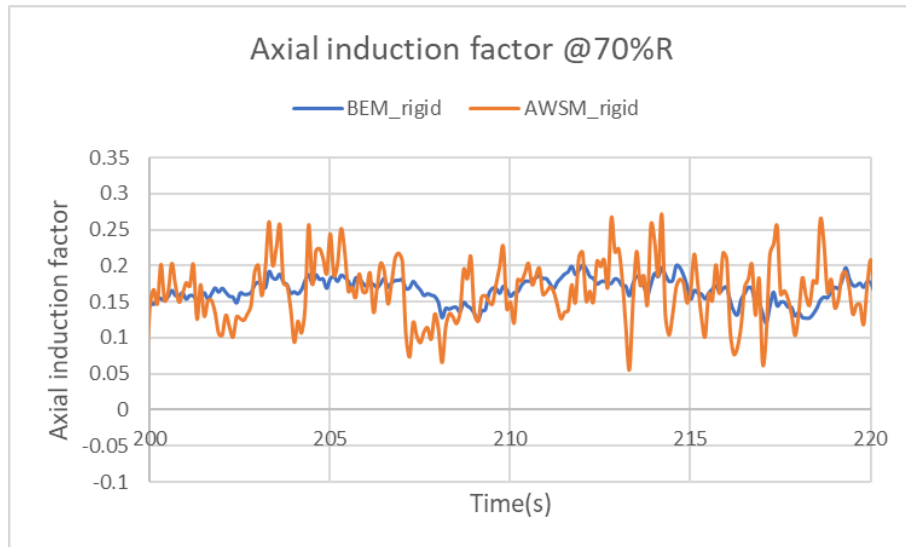


Figure 4.52: Axial induction factor

Figures 4.51 and 4.52, represent axially induced velocity and axial induction factor respectively. The vortex wake model treats the blade more locally for varying inflow wind velocities. Whereas, the BEM model balances the induced velocity field within the annulus. This leads to difference in the angle of attack and the normal force prediction.

Angle of attack

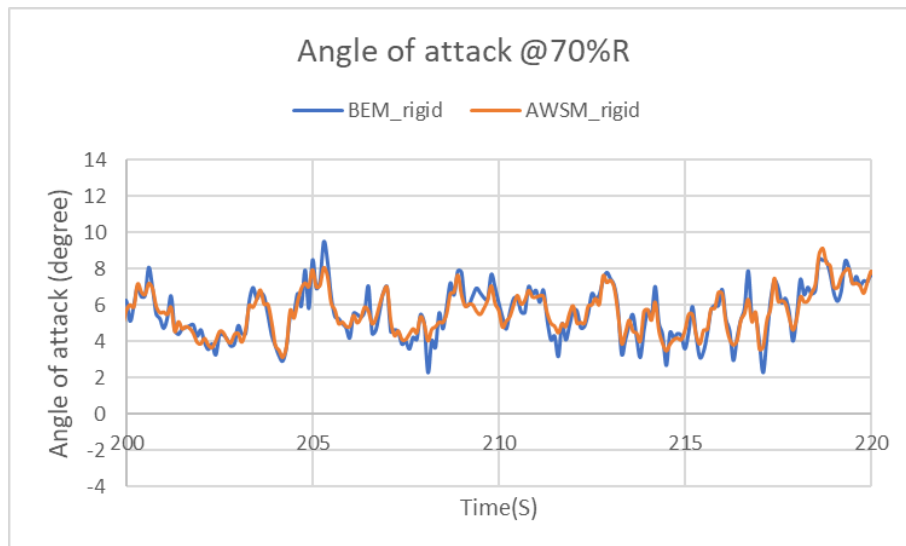


Figure 4.53: Angle of attack

Figure 4.53 represents, the time series of the angle of attack. The results obtained from both of the models vary significantly. The variation in the calculation of the axially induced velocities has led to such variation in the results. In the subsequent section, a comparative analysis of the normal force shall be discussed.

Normal force

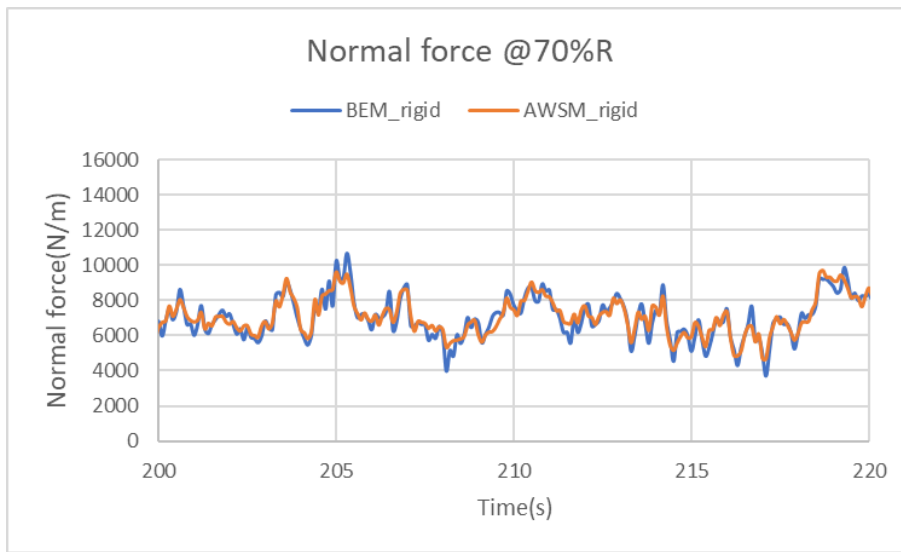


Figure 4.54: Normal force

Figure 4.54 represents a time series of the normal force for both the models used. The differences in the calculation of the axial induction and the angle of attack have led to a variation of the normal force prediction by both of the model. As represented in figure 4.55, the signal location of 70%R is selected because at this radial location the normal force was found to be maximum. Additionally, the radial distribution is plotted at the time where the normal force is found to be maximum.

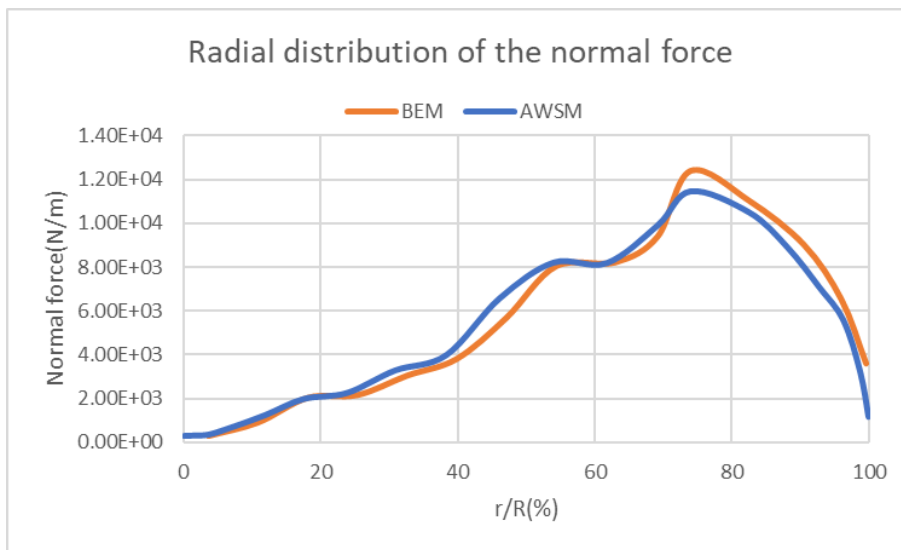


Figure 4.55: Radial distribution of the normal force at the time which marks the maximum normal force

Table 4.7: Normal force statistics

Normal force(N/m) @70%R			
	BEM	AWSM	Difference
Maximum	13367.26	11606.92	13.1%
Minimum	1060.45	1069.42	-
Average	6555.10	6506.97	0.6%
Std. Dev.	1737.11	1622.05	6.6%

In the above table, the extreme normal force is tabulated. As in table 4.7, the standard deviation of the Normal force predicted by the BEM model is around 6.6% higher than that predicted by the AWSM. The reason behind this higher load prediction is mentioned previously. The difference in the extreme loads and the normal force amplitude lead to the differences in the standard deviation for the normal force. Thus, the bigger standard deviation in the case of the BEM model may reflect into higher fatigue load.

4.4.3. Analysis

- In this load case situation, the turbulent wind inflow field leads to a violation of the assumption of the steady wind inflow involved in the BEM model. This violation of the assumption led to variations in the results obtained by both of the models.
- The fatigue loading due to the flapwise moment is significant near the blade root. This is illustrated in figure 4.56.
- The higher fatigue load prediction by the BEM model results from the difference in the calculation of the induced velocity, followed by a variation in the angle of attack and aerodynamic force prediction.
- Vortex models were shown to yield the lowest fatigue loads due to better (more local) tracking of induced velocity variations with inflow variations together with intrinsic modeling of the effect of shed vorticity variation with time.
- Additionally, it can be observed that the turbine with rigid structure predicts higher magnitude of loads for both of the aerodynamic load calculation models. However, the difference between the standard deviation of the normal force predicted by both of the models decreases in the case of rigid rotor. The results in the case of a flexible rotor can be found in the appendix

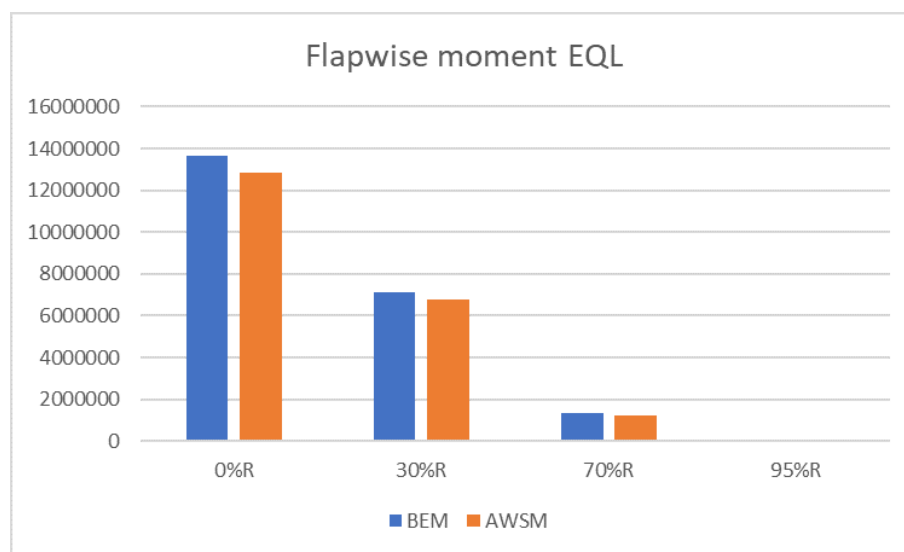


Figure 4.56: Flapwise equivalent moments for the time period of 100 seconds to 300 seconds

Figure 4.56, represents flapwise damage equivalent loads. The equivalent loads were marked for the slope (m) of 9. The equivalent loads were calculated by the rainflow counting method. In this method, the spectrum of the loads is decomposed into a number of bins of sizes corresponding to the load. The reader can refer to [15] for the detailed procedure of the equivalent load calculation.

5

Conclusions and recommendations

To reiterate the research objectives of this project, the aim was to perform a comparative analysis of the results obtained from the BEM and the vortex wake model calculations for the IEC design load cases. Such that, on the basis of analysis a more accurate practice with acceptable computational time could be recommended. The chapter discusses the key findings of the research and recommendations for more accurate results. The conclusions discussed in this chapter are implied to the AVATAR wind turbine model and may vary in the case of other wind turbine models.

5.1. Conclusions

- The aero-elastic calculations have been performed using the BEM model and the AWSM model in the Focus6 environment. The load situations are based on the IEC 61400-1 standard. Primarily, the load situations mentioned in the standard appear to be less complex than the load situations described in the literature studied for this project. A lesser complexity in the load situations made the selection process of the load cases more difficult.
- The literature [26] claims that the extreme operating gust (EOG) causes minimal differences in the results obtained by the BEM and the vortex wake model. The DLC 2.3, in section 4.1 aims to test the wind turbine with an EOG. The simulations were performed for the rated wind speed and a cut-out wind speed with both of the aerodynamic simulation models.
- Irrespective of the significant differences in the axial induction in the case of cut-out wind speed condition, the normal force variation is minimal for both of the aerodynamic simulation models. The significantly low axial induction shows no effect on the normal force. Similarly, the variation in the normal force was found to be minimal in the case of a rated and a sub-rated wind velocity conditions in the case of the BEM and the AWSM simulations.
- However, the variation in the extreme normal force recorded in the case of the BEM and the AWSM model simulations is much smaller than that recorded for the turbulent and the yawed inflow conditions. Thus, the analysis discussed in section 4.1 reaffirms the claim stated in the literature mentioned above.
- DLC 3.3 in section 4.2, is an appropriate load situation to analyze the effect of the yawed inflow condition. The main conclusion for this load case is the prediction of a higher extreme and fatigue loads by the AWSM model.
- Further research proved that the variation in the prediction of lift coefficients led to the variation in the load calculations in the case of the BEM model and the AWSM model. A standard deviation of the normal force predicted by the BEM model was around 59% lower to the AWSM model. It was also found that this difference in the extreme force and a standard deviation predicted by both of the models increases with the increase in the yaw angle. Thus, due to a lower extreme load and standard deviation it is safe to claim that for this load situation the BEM model predicts lower fatigue loads than those predicted by the AWSM model. Moreover, a similar trend is observed over the length of the blade.

- Additionally, the addition of the pitch angle to blade led to reduction in the magnitude and the variation of the the normal force by both of the models and certainly it occurred due to reduction in the axial induced factor.
- DLC 1.3 and DLC 1.2 in sections 4.3 and 4.4 respectively, aim to assess the effect of the turbulent inflow condition on the wind turbine. The DLC 1.3 focuses on the extreme turbulence condition, while the DLC 1.2 focuses on the normal atmospheric turbulence. Both of the load situations reproduced similar result trends and hence shall be discussed together.
- The fatigue load prediction in the case of BEM simulations was significantly higher than that in the case of AWSM simulations. The AWSM model predicted lower fatigue loading due to more local tracking of the induced velocity variations with the wind inflow conditions. The BEM model predicted an average 5% higher flapwise damage equivalent load along the length of the blade. The highest EQL was predicted at the root of the blade.
- The vortex wake model (AWSM) simulations come with a significantly high computational time. The simulation time in the case of the AWSM model is exponentially greater than that for the BEM model. To partially overcome this huge CPU time, different engineering improvements (for example- Wake reduction, Prescribed wake) were implemented. The reader can refer to Appendix A.5 for further details.

5.1.1. Concluding remarks

The wind turbine design and certification process are highly sensitive and critical. It requires high precision and accuracy. Therefore, these processes need to be robust, accurate and refined. The variations in the results obtained from both of the models have made a way further validation (experimental or CFD). Finally, it can be concluded that the calculation of the induced velocities play the most important role in the load calculation process. Thus, the aerodynamic model which predicts the induction factor accurately shall prove to be the most accurate.

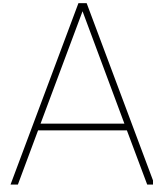
5.2. Recommendations

- The conclusions in the previous section clearly indicate a higher load prediction by the BEM model. Primarily, the wind energy sector should try to make a consensus among themselves to downsize the safety factors involved in the wind turbine design procedures. This step would certainly help in decreasing the LCOE for wind energy by curtailing the material cost.
- Most of the load cases prescribed in the IEC standard are not complex. It can be perceived from the thesis that, in the case of yaw misalignment and turbulence significant variations in the results obtained from both of the models are expected. Except for the DLC 3.3, the obliquity in the inflow angle is not more than $\pm 8^\circ$. Therefore, a few complicated load cases discussed in the thesis may be simulated with the vortex wake model and rest all of the load cases could be simulated with the BEM model. Specifically, the load cases with higher magnitude of the induced factor and with significant difference in the induced factor calculation by both of the models tend to show variations in the load calculations. Such load cases should be simulated with the vortex wake model. Therefore, a more robust wind turbine design and certification procedure with a reasonable computational effort could be achieved.
- The dissimilarity between the results obtained from the BEM and the AWSM calls for experimental analysis of the load cases. An experimental analysis could validate the results and hence would refine the wind turbine design process.
- Finally, the most important scope for the future study should be to analyze the cost reduction or increment due to usage of the vortex method. A significant reduction in the material costs is expected due to a lower loading involved in the vortex wake model.

Bibliography

- [1] AVATAR. URL <https://www.eera-avataar.eu/home/index.html>.
- [2] Hamidreza Abedi, Lars Davidson, and Spyros Voutsinas. Vortex method application for aerodynamic loads on rotor blades. (February):4–7, 2013.
- [3] Anderson. Fundamentals of Aerodynamics. 48(12):2983–2983, 2010. ISSN 0001-1452.
- [4] K Boorsma and M Caboni. ECN Aero-Module. page 74, 2018. doi: 21/12/2108.
- [5] K Boorsma, F Grasso, and J G Holierhoek. Enhanced approach for simulation of rotor aerodynamic loads. *EWEA Offshore 2011*, (FEBRUARY), 2011.
- [6] K. Boorsma, M. Hartvelt, and L. M. Orsi. Application of the lifting line vortex wake method to dynamic load case simulations. *Journal of Physics: Conference Series*, 753(2), 2016. ISSN 17426596.
- [7] Koen Boorsma, Luca Greco, and Gabriele Bedon. Rotor wake engineering models for aeroelastic applications. *Journal of Physics: Conference Series*, 1037(6), 2018. ISSN 17426596.
- [8] Arno J. Brand, Joachim Peinke, and Jakob Mann. Turbulence and wind turbines. *Journal of Physics: Conference Series*, 318(7), 2011. ISSN 17426596.
- [9] Tony Burton, David Sharpe, Nick Jenkins, and Ervin Bossanyi. Wind Energy Handbook. 2001.
- [10] DNV GL. DNVGL-ST-0437 Loads and site conditions for wind turbines. (November), 2016.
- [11] Horia Dumitrescu and Vladimir Cardos. Wind turbine aerodynamic performance by lifting line method. *International Journal of Rotating Machinery*, 4(3):141–149, 1998. ISSN 15423034.
- [12] Arne Van Garrel. Development of a Wind Turbine Aerodynamics Simulation Module. *ECN Wind Energy*, (August):106, 2003. ISSN 0040-5736.
- [13] Sandeep Gupta. Development of a Time-accurate viscous Lagrangian vortex wake model for wind turbine applications. 2006.
- [14] S. Hauptmann, M. Bülk, L. Schön, S. Erbslöh, K. Boorsma, F. Grasso, M. Kühn, and P. W. Cheng. Comparison of the lifting-line free vortex wake method and the blade-element-momentum theory regarding the simulated loads of multi-MW wind turbines. *Journal of Physics: Conference Series*, 555(1), 2014. ISSN 17426596.
- [15] H B Hendriks and B H Bulder. Fatigue Equivalent Load Cycle Method. (October):1–18, 1995.
- [16] IEC. IEC 61400-1 Ed.3 Wind turbines - Design requirements. 2005, 2010.
- [17] Christopher Jung, Dirk Schindler, Alexander Buchholz, and Jessica Laible. Global Gust Climate Evaluation and Its Influence on Wind Turbines. *Energies*, 10(10):1474, 2017. ISSN 1996-1073. URL <http://www.mdpi.com/1996-1073/10/10/1474>.
- [18] Christoph Kost, Shivenes Shammugam, Verena Jülch, Huyen-tran Nguyen, and Thomas Schlegl. Levelized Cost of Electricity- Renewable Energy Technologies. (March), 2018.
- [19] J Gordon Leishman, Glenn L Martin, Aiaa Aerospace, Sciences Meeting, and J Gordon Leishman. Proceedings and abstracts of the 22nd Annual West Coast Chromatin and Chromosomes Conference. Pacific Grove, California, USA. December 7-10, 2000. *Biochem Cell Biol*, 79(3):219–385, 2001. ISSN 08298211. URL <http://www.ncbi.nlm.nih.gov/pubmed/11803896>.
- [20] C Lindenburg. PHATAS Release " APR-2005 " USER ' S MANUAL Program for Horizontal Axis wind Turbine Analysis and Simulation. (May), 2005.

- [21] Iván Pineda and WindEurope Pierre Tardieu. Annual combined onshore and offshore wind energy statistics. 2018. ISSN 22107789. URL <https://windeurope.org/wp-content/uploads/files/about-wind/statistics/WindEurope-Annual-Statistics-2017.pdf>.
- [22] Gerard Schepers. Engineering models in wind energy aerodynamics: Development, implementation and analysis using dedicated aerodynamic measurements. (november), 2012. doi: 10.4233/uuid:92123c07-cc12-4945-973f-103bd744ec87.
- [23] J. G. Schepers and S. J. Schreck. Aerodynamic measurements on wind turbines. *Wiley Interdisciplinary Reviews: Energy and Environment*, (June 2018):1–25, 2018. ISSN 2041840X.
- [24] D. a. Simms, M. M. Hand, L. J. Fingersh, and D. W. Jager. Unsteady aerodynamics experiment phases II-IV test configurations and available data campaigns. *National Renewable Energy Laboratory, NREL/TP-500-25950, Golden, CO*, (July), 1999.
- [25] H. Snel and J.G. Schepers. Investigation and modelling of dynamic inflow effects. *Ecn*, 1993. URL <ftp://ftp.ecn.nl/pub/www/library/report/1993/rx93029.pdf><ftp://question.ecn.nl/pub/www/library/report/1993/rx93029.pdf><http://papers3://publication/uuid/B431F9AD-74D4-44AE-B87B-F5BD750673FF>.
- [26] H. Snel and J.G. Schepers. Joint Investigation of Dynamic Inflow Effects and Implementation of an Engineering Method. page 326, 1995.
- [27] H. Snel, J. G. Schepers, and B. Montgomerie. The MEXICO project (Model Experiments in Controlled Conditions): The database and first results of data processing and interpretation. *Journal of Physics: Conference Series*, 75(1), 2007. ISSN 17426596.
- [28] Ye Zhiquan, Chen Yan, and Zhang Feng. HAWT Aerodynamic Performance Prediction using a Semi-Rigid Wake Model Based on Vortex Theory. *Wind Engineering*, 24(5):349–359, 2000. ISSN 0309524X.
- [29] Ye Zhiquan, Chen Yan, and Zhang Feng. HAWT Aerodynamic Performance Prediction using a Semi-Rigid Wake Model Based on Vortex Theory. *Wind Engineering*, 24(5):349–359, 2000. ISSN 0309524X.



Appendix- A

A.1. DLC 2.3

In section 4.1.2 for DLC 23400, the plots appear to be deceiving. Specifically, the differences in the case of axial induction are not visible in the plot of angle of attack. Essentially, this occurs due to negligibly small variation in the trend of angle of attack. The variation is only visible on a micro scale.

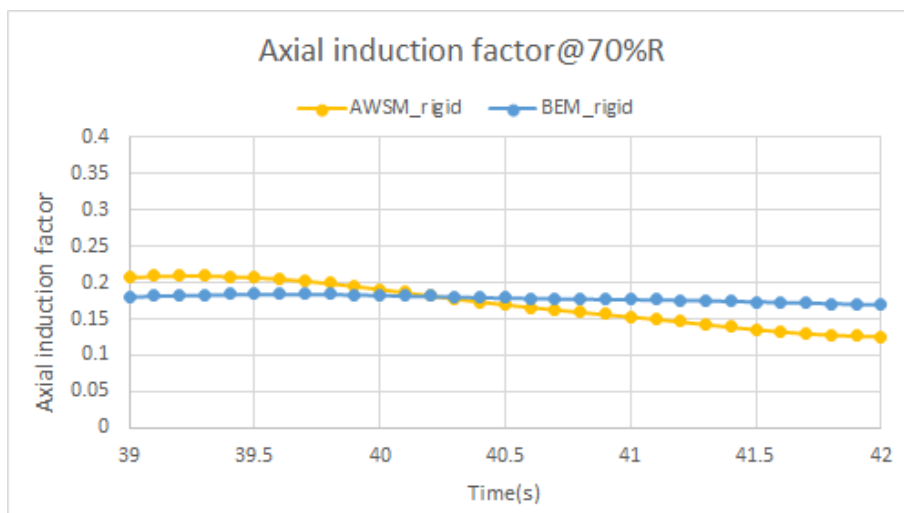


Figure A.1: Axially induced velocity

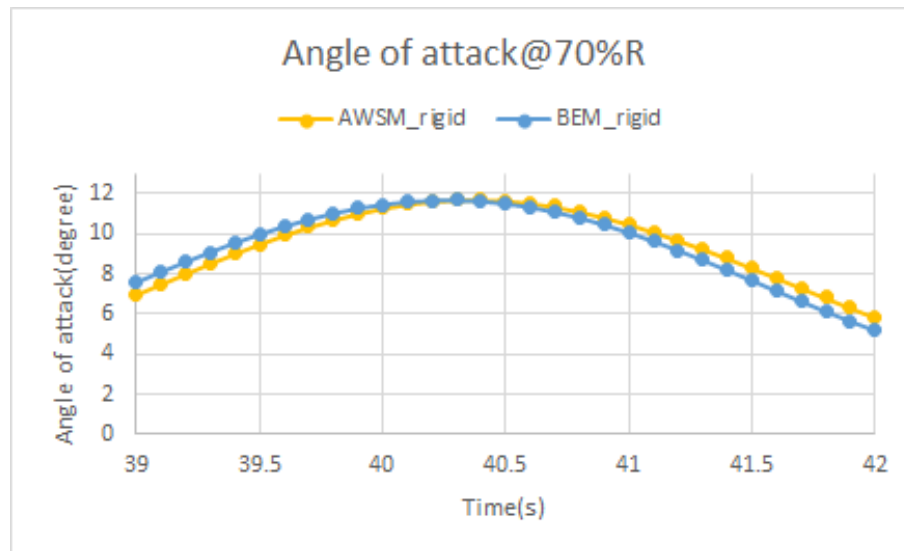


Figure A.2: Angle of attack

Figures A.1 and A.2 represent axially induced velocity and angle of attack on a micro scale.

A.2. DLC 3.3

The load case specifications are similar to those discussed in section 4.2.1.

Effect of pitch angle variation

In section 4.2.2, it was discovered that along the length of the blade the standard deviation of the normal force in the case of the AWSM model was higher than that in the case of the BEM model. The main cause of this variation was the variation in the prediction of the axial induction. In this section, the induction shall be varied by keeping the rotor speed constant and adding a pitch angle to the blade. The addition of the pitch angle to the velocity triangle shall lead to a variation in the angle of attack. Subsequently, this shall lead to a variation in the axial induction. The load case specifications and the wind velocity profile shall be maintained similar to that incorporated in section 4.2.2. In contrast to section 4.2.2, the pitch angle of 3° and 5° shall be added.

Axial induction

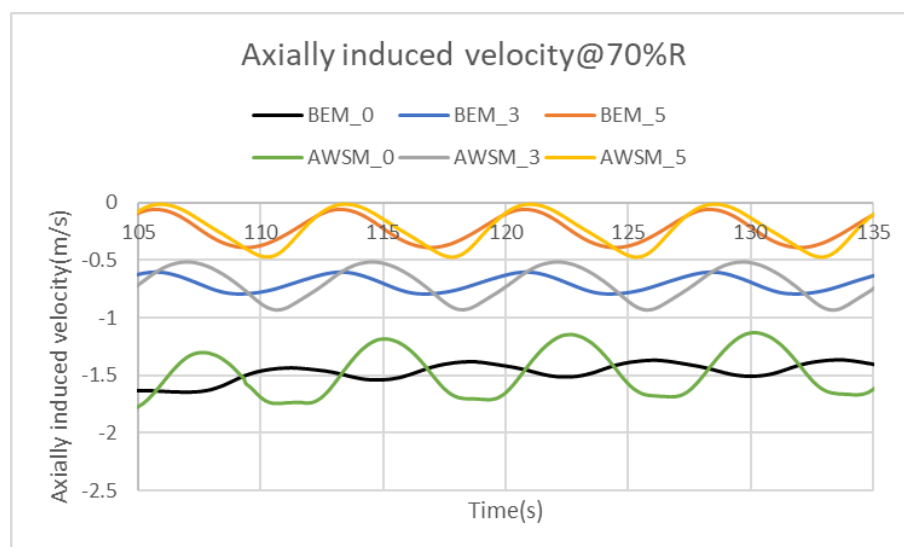


Figure A.3: Comparison of the axially induced velocity for various pitch angles.

In figure A.3, a comparison of the axially induced velocity for the pitch angle of 0°, 3° and 5° is presented. With increasing pitch angle the magnitude of the induced velocity decreases. Furthermore, it can also be observed that the variation in the induced velocity predicted by the BEM and the AWSM model decreases with increasing pitch angle.

Angle of attack and pitch angle

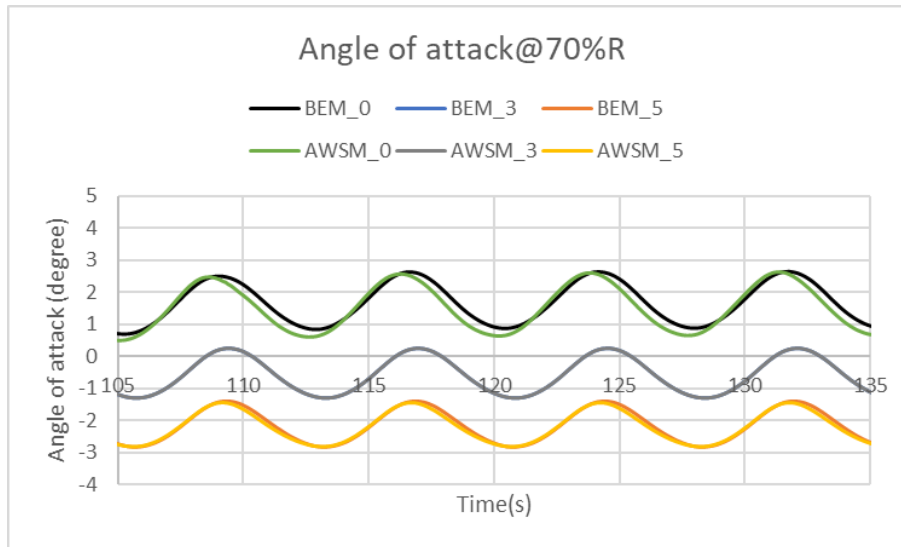


Figure A.4: Comparison of the angle of attack for various pitch angles

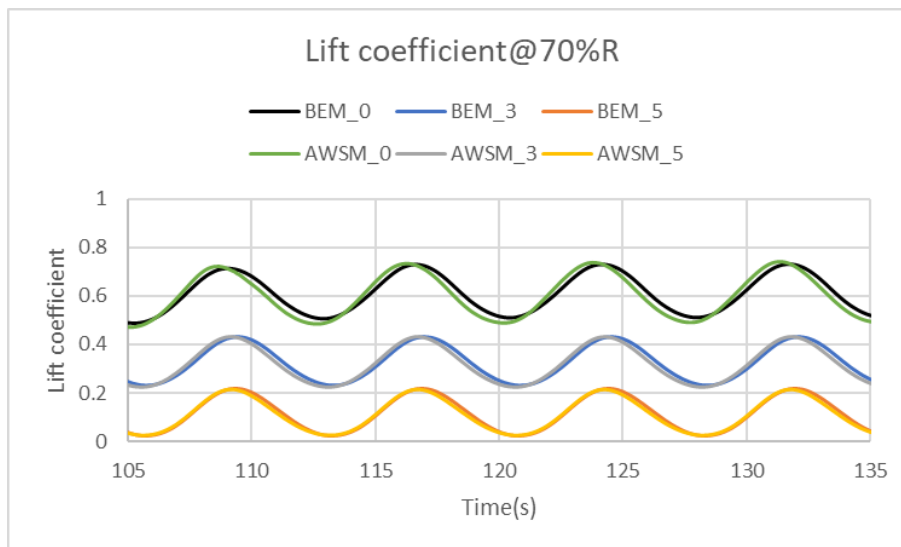


Figure A.5: Comparison of the lift coefficient for various pitch angles

In figures A.4 and A.5, the magnitude of the angle of attack and the lift coefficient for various pitch angles. Similar to the axially induced velocity, the variation in the prediction of the angle of attack (figure A.4) and the lift coefficient (figure A.5) by both of the aerodynamic load calculation models decreases with increasing pitch angle. This shows importance of the accuracy in the axial induction prediction.

Normal force

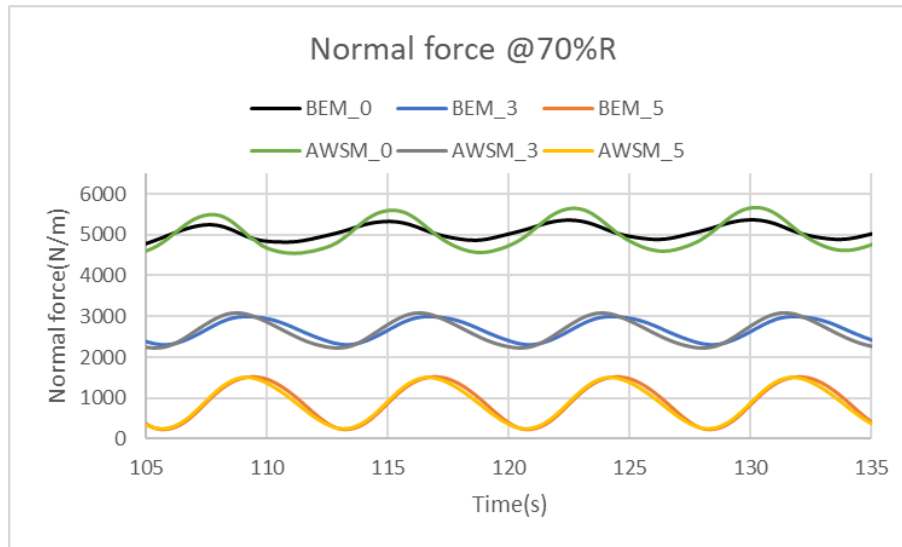


Figure A.6: Comparison of the normal force for various pitch angles

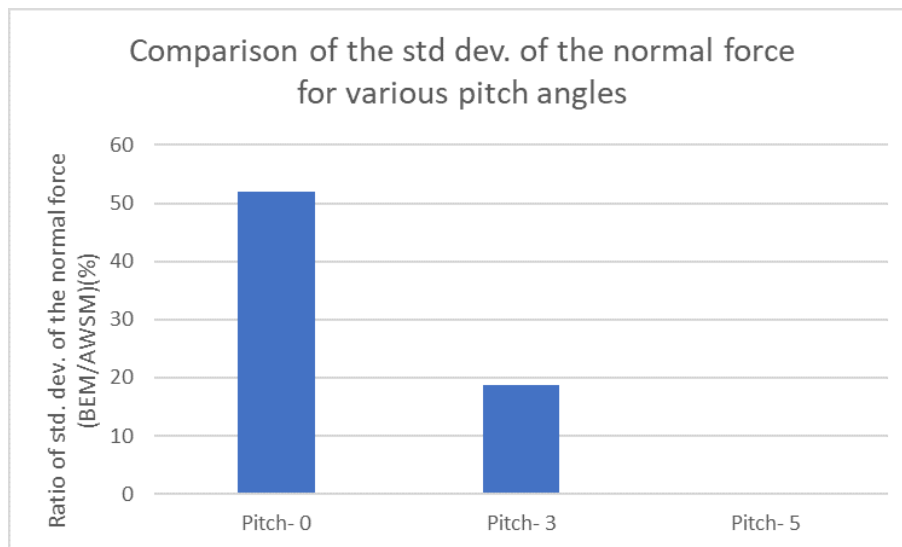


Figure A.7: Comparison of the ratio of the standard deviation of the normal force for various pitch angles

As we know that the normal force calculation is dominated by the lift coefficient, thus the trend of variation in the lift coefficient can also be observed in the normal force. In figure A.6, the magnitude of the normal force increases with decreasing pitch angle. It can be inferred from figure A.7 that the variation in the force prediction in the case of the BEM model and the AWSM model is least at the higher pitch angles. This certainly occurs due to negligible variation in the prediction of the axially induced velocity.

A.3. DLC 1.3

In section 4.3.2, the load case was discussed for the rigid rotor, however in actual the rotors are flexible and have various moments and the degrees of freedom. Therefore, in this section the results in the case of a flexible rotor are presented.

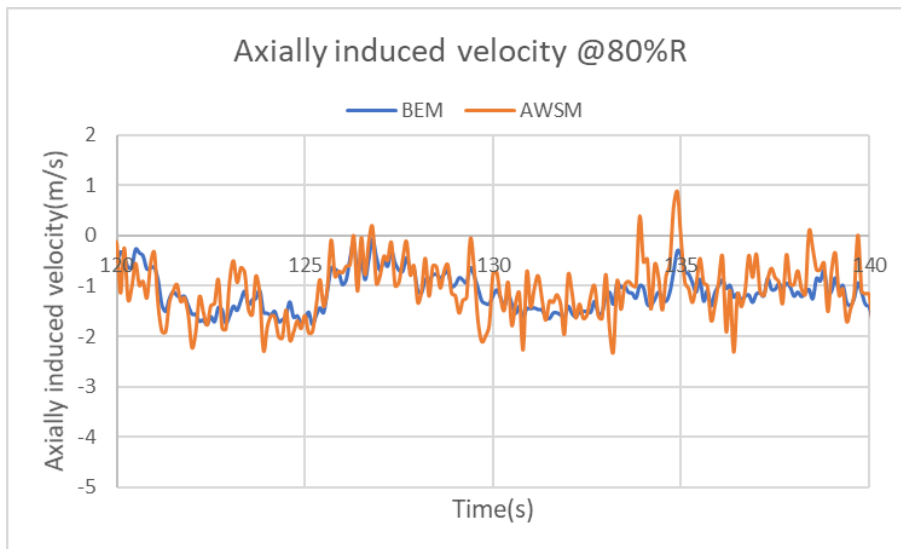


Figure A.8: Axially induced velocity in the case of a flexible rotor

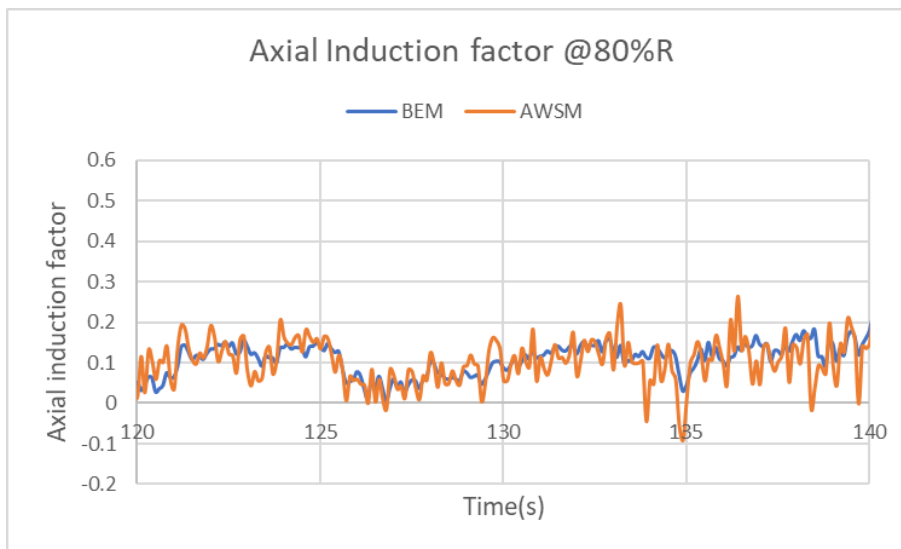


Figure A.9: Axial induction factor in the case of a flexible rotor

Figures A.8 and A.9, represent axially induced velocity and axial induction factor respectively. The figure A.10, represents the normal force in the case of a flexible rotor structure. A small delay can be observed in force calculation which occurs essentially due the blade and shaft flexibility.

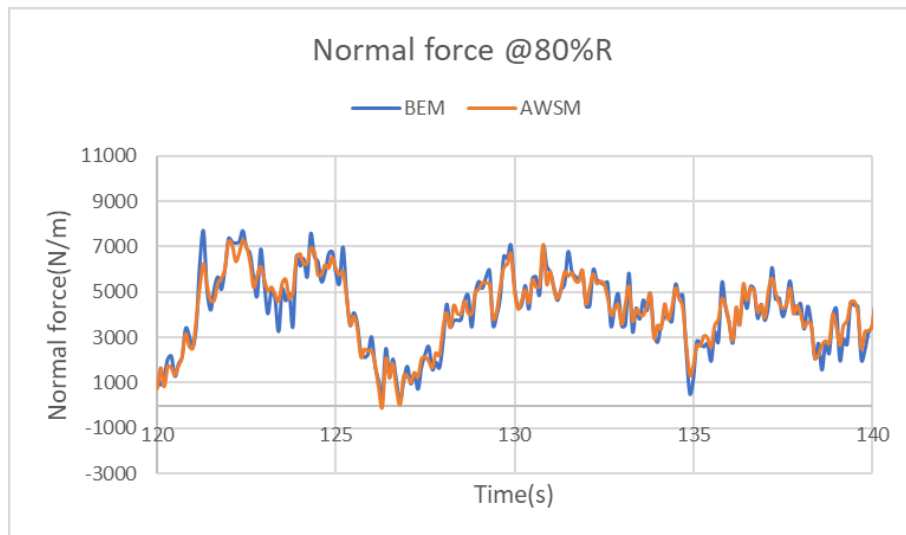


Figure A.10: Normal force in the case of a flexible rotor

A.4. DLC 1.2

In section 4.4, the load case was discussed for the rigid rotor, however in actual the rotors are flexible and have various moments and the degrees of freedom. Therefore, in this section the results in the case of a flexible rotor are presented.

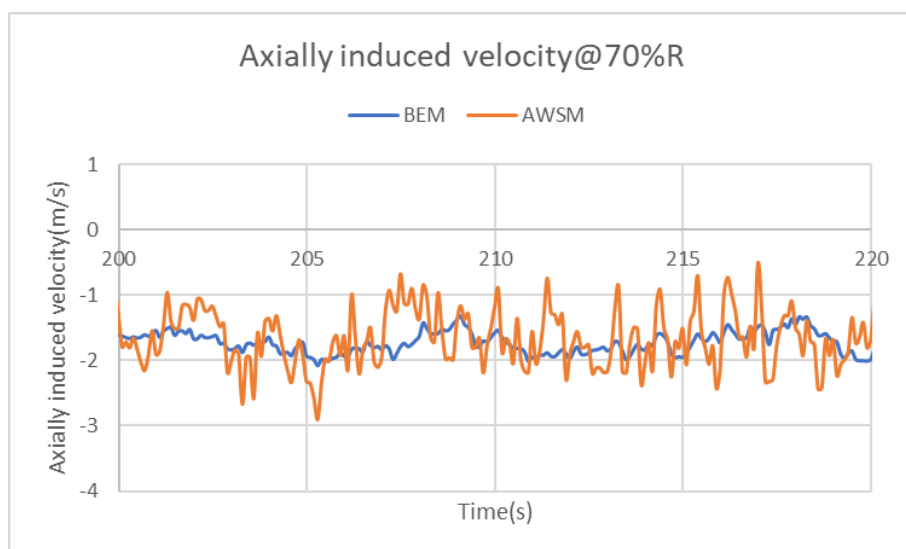


Figure A.11: Axially induced velocity in the case of a flexible rotor

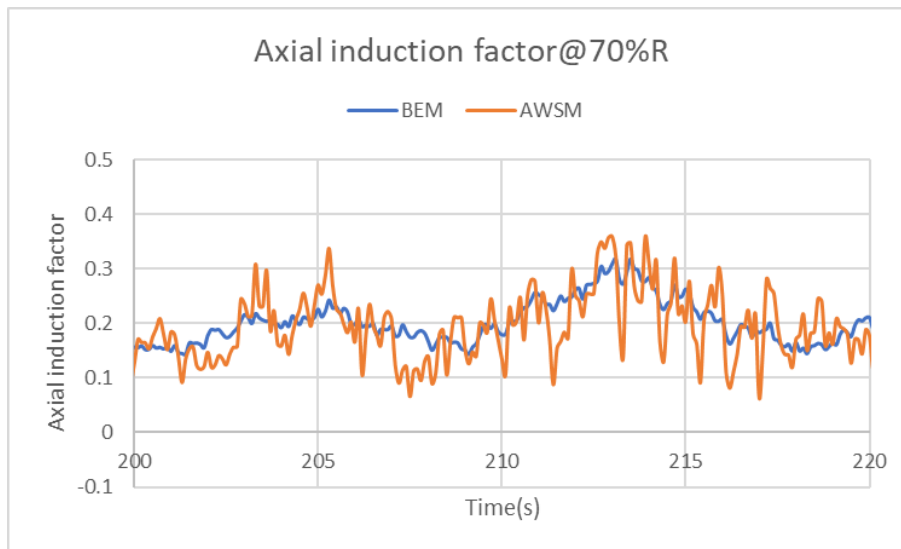


Figure A.12: Axial induction factor in the case of a flexible rotor

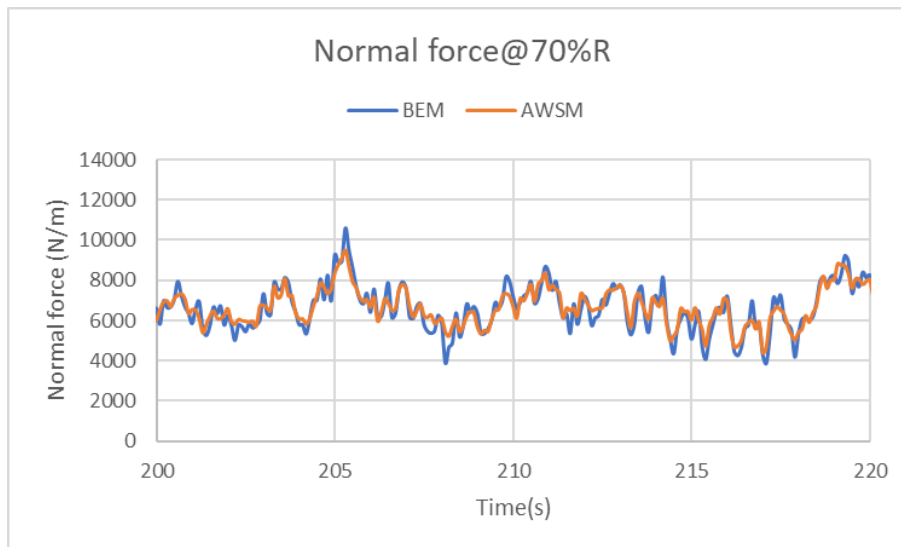


Figure A.13: Normal force in the case of a flexible rotor

Figures A.11 and A.12, represent axially induced velocity and axial induction factor respectively. The figure A.13, represents the normal force in the case of a flexible rotor structure. A small delay can be observed in force calculation which occurs essentially due the blade and shaft flexibility.

A.5. Wake reduction

As discussed in section 2.1.2, wake reduction is one of the method to reduce the simulation time involved in the vortex method. In this section a comparative study of the results obtained with and without wake reduction technique is presented.

A.5.1. Wake Reduction effect

The load case specifications are similar to those discussed in section 4.2.1. The implementation of wake reduction requires the defining of various keywords. Below are the keywords to be defined-

WAKEREDUCTIONSTART- The keyword defines the number of wake points after which the wake reduc-

tion routine shall be implemented.

$$WAKEREDUCTIONSTART = \frac{nD}{U_{\infty}(1-a)} \quad (A.1)$$

where, $0.5D$ = wake convection distance (based on the number of rotors)

Therefore, $WAKEREDUCTIONSTART= 102$

$WAKEREDUCTIONSkip$ - It defines number of wake points to be skipped. Assuming number of wake points to be skipped are 4.

Further number of streamwise wake points and freestream wake points are adjusted as per equation 2.7.

- Streamwise wake points(adjusted)= 245
- Free streamwise wake points(adjusted)= 128

Comparative analysis

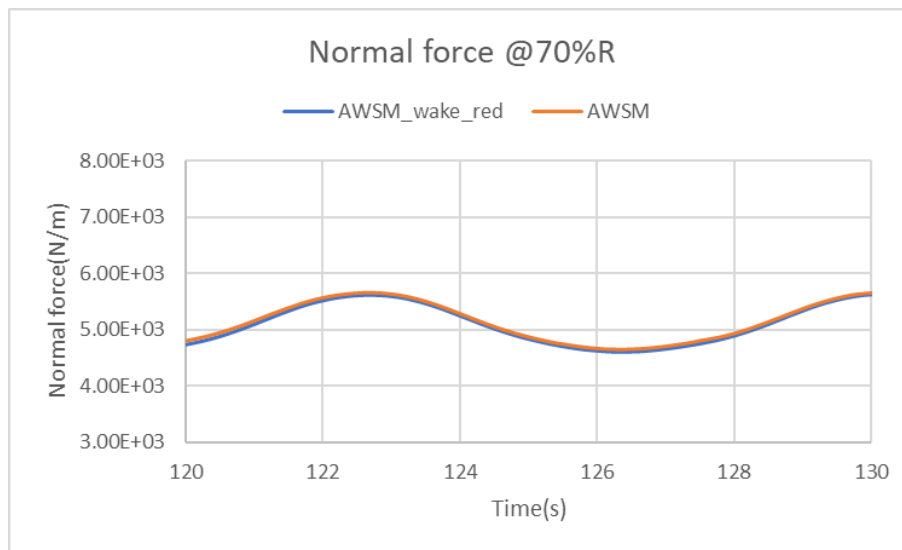


Figure A.14: Effect of wake reduction technique on the normal force

Figure A.14, represents the time series of the normal force with and without implementation of the wake reduction technique. It can be clearly seen the above figure that the differences in the maximum and minimum forces is negligible. However, the implementation of wake reduction technique leads to a curtailment of computation effort by 27%.